Helsinki University of Technology
Department of Electrical and Communications Engineering
Laboratory of Electronics Production Technology
Espoo 2006 TKK-EVT-16

INTERFACIAL REACTIONS BETWEEN SN-BASED SOLDERS AND COMMON METALLISATIONS USED IN ELECTRONICS

Vesa Vuorinen

Dissertation for the degree of Doctor of Science in Technology to be presented with due permission of the Department of Electrical and Communications Engineering, Helsinki University of Technology, for public examination and debate in Auditorium *Edison* at Helsinki University of Technology (Espoo, Finland) on the 8th of December, 2006, at 12 noon.

SUPERVISOR

Professor Jorma Kivilahti
Laboratory of Electronics Production Technology
Department of Electrical and Communications Engineering
Helsinki University of Technology, Finland

REVIEWERS

Dr. Mervi Paulasto-Kröckel
Director Packaging Automotive Power
Infineon Technologies AG
Neubiberg, Germany

Dr. Aleksander Kodentsov
Laboratory of Materials and Interface Chemistry,
Eindhoven University of Technology, The Netherlands

OPPONENTS

Professor Toivo Lepistö
Institute of Materials Science
Tampere University of Technology, Finland

Dr. Kari Rönkä
Senior Research Scientist, Micromodules
VTT Technical Research Centre of Finland

Distribution:
Helsinki University of Technology
Department of Electrical and Communications Engineering
Laboratory of Electronics Production Technology
P.O. Box 3000
FIN-02015 HUT, Finland
Tel: +358 (0)9 451 2716
Fax: +358 (0)9 451 5776
E-mail: Pia.Holmberg@tkk.fi
www.ept.tkk.fi

TKK-EVT-16
ISSN 1457-0440
ISBN 978-951-22-8526-6 (printed)
951-22-8526-6
ISBN 978-951-22-8527-3 (PDF)
951-22-8527-4
Otamedia Oy
Espoo 2006

ABSTRACT

During their lifetimes the electrical interconnections of portable electronic devices are subjected to high thermal, mechanical, chemical, and electrical loadings, and therefore the metallurgical compatibility between solder alloys and component pad metallisations has become ever more essential from the point of view of interconnection reliability. For this reason, the mechanisms of interfacial reactions are studied in this thesis by making use of thermodynamic calculations together with diffusion kinetic considerations and microstructural analyses. The formation of interfacial intermetallic compounds is investigated experimentally by using solid|liquid and solid|solid diffusion couples of several binary and ternary member systems. These systems include the most important metals used in electronics, tin (Sn), copper (Cu), nickel (Ni), silver (Ag), and gold (Au). The effects of additional elements such as P, Fe, Zn, and Ti on the growth kinetics and defect structures of interfacial intermetallics are also investigated. It is shown that the main factors affecting the thickness and morphology of interfacial intermetallic compounds in soldering are: i) the solubilities and, consequently, the dissolution rates of solid metals in liquid solders; ii) local equilibria and their changes as a function of time and temperature, and iii) the chemical reactions at the supersaturated liquid solder interfaces. The experimental results from isothermal aging at elevated temperatures demonstrate that alloying elements and impurities can change the microstructural evolution of solder interconnections drastically and thus diminish their mechanical integrity. The thermodynamic-kinetic approach, together with detailed microstructural observations, proved to be a very useful tool when studying the interfacial intermetallic reactions, as well as the evolution of solder interconnection microstructures, during long-term aging at elevated temperatures.

TIIVISTELMÄ

Kannettavat kulutuselektroniikkatuotteet joutuvat elinaikanaan kokemaan suuria termisiä, mekaanisia, kemiallisia sekä sähköisiä rasituksia. Siksi juotemateriaalien ja kontaktimetallointien välinen metallurginen yhteensopivuus on tullut yhä tärkeämmäksi tuotteiden luotettavuuden näkökulmasta. Tässä väitöskirjassa on tutkittu rajapintareaktioita termodynaamisten laskelmien, kineettisten tarkastelujen ja mikrorakennetutkimuksen avulla. Metallienvälisten rajapintayhdisteiden syntyä on kokeellisesti tutkittu sekä sula-kiinteä että kiinteä-kiinteä diffuusioparein useilla binäärisillä ja ternäärisillä systeemeillä. Nämä systeemit koostuvat tärkeimmistä elektroniikassa käytetyistä metalleista kuten tina (Sn), kupari (Cu), nikkelil (Ni), hopea (Ag) ja kulta (Au). Lisäksi työssä on tarkasteltu tyypillisten seosaineiden, kuten fosfori (P), rauta (Fe), sinkki (Zn) ja titaani (Ti), vaikutuksia sekä rajapintareaktioiden kinetiikkaan että virherakenteisiin. Työssä on osoitettu, että juotosprosessissa tärkeimmät metallienvälisten yhdisteiden paksuuteen ja morfologiaan vaikuttavat tekijät ovat: i) kontaktimetallien liukoisuus ja liukenemisnopeus sulaan juotteeseen; ii) paikallinen tasapaino ja sen muutokset lämpötilan ja ajan funktiona ja iii) juoterajapinnoilla ylikyllästeisessä sulassa tapahtuvat kemialliset reaktiot. Kokeelliset tulokset isotermisissä vanhennuskokeissa korotetussa lämpötilassa osoittavat, että seosatomeilla ja epäpuhtauksilla on voimakas vaikutus mikrorakenteiden käytönaikaisiin muutoksiin ja siten juoteliitosten luotettavuuteen. Työssä on osoitettu, että termodynaamis-kineettisen metodin käyttö yhdessä yksityiskohtaisen mikrorakenteellisen tarkastelun kanssa tarjoaa tehokkaan työvälineen juoteliitosten mikrorakenteiden muutosten tutkimukseen.

PREFACE

The work for this thesis was carried out in the Department of Electrical and Communications Engineering at the Helsinki University of Technology.

I am most grateful to my supervisor, Professor Jorma Kivilahti, for his guidance, time, and support.

I am grateful to all my co-workers for their contributions to the completion of this work. I wish to thank especially Dr. Tomi Laurila and Dr. Toni Mattila for their contribution to the research and willingness to enter into discussion at any time. D.Sc Kejun Zeng and D.Sc Hao Yu are acknowledged for their help in thermodynamic work. Mr Yoshioka is acknowledged for the transmission electron microscopy.

Finally, I would like to present my loving thanks to my family for their endless love and support. My parents deserve special thanks for providing continuous encouragement and support throughout my life.

Espoo, September 2006
Vesa Vuorinen

Contents Page

1. INTRODUCTION

During the last two decades surface mount technology (SMT) has become the dominant manufacturing technology for electronic products, mainly because of its cost-effective high-volume production capability. It has made possible the manufacturing of the highest density portable electronics of good quality and reliability. Recently, however, new technology drivers and environmental regulations have created new challenges on both the manufacturing and reliability of consumer electronics. On the one hand, the implementation of lead-free electronic materials has increased the complexity of interconnection metallurgies and on the other, the demands for higher functionality and performance are driving manufacturers to miniaturise their products, which tends to increase the mechanical and thermomechanical loadings of solder interconnections.

From the electronics manufacturing point of view, the most important solder interconnection systems include at least three elements. Tin is the major element practically in all solders, and contact metallisations are typically Cu, Ni, or Ni-based alloys with protective coatings such as Au or organic soldering preservatives (OSP). Therefore, Sn, Cu, and Ni constitute the most important metal alloy system in electronics. For example, when the most commonly used lead-free solder - a near-eutectic SnAgCu alloy - reacts with an electroless Ni(P)/Au surface finish on printed wiring board (PWB), the interconnection system contains six elements. Moreover, if the most prevalent impurities are included it is evident that the metallurgical complexity of solder interconnections is greatly increased.

Accordingly, the design for reliability of portable electronic products, in particular, has become very challenging, as the complex interfacial intermetallic layer structures of diminutive solder interconnections are more vulnerable to accidental mechanical shock loadings. For these reasons it is ever more important to have a better fundamental understanding of and control over the formation and evolution of microstructures in high-density solder interconnections. In this effort thermodynamic and kinetic modelling together with careful experimental work, which has proved to be so successful in

materials science and engineering, can be of great help. Their combined usage provides valuable information on the stabilities of interconnection microstructures, the driving forces for chemical reactions, and the growth rates of reaction products occurring in solder interconnections or metallisations during processing and testing or in the long-term use of electronic devices [1].

The purpose of this thesis is to study the formation and growth of interfacial intermetallic reactions and the microstructural evolution of bulk solders in lead-free solder interconnections, by utilising the thermodynamic-kinetic approach together with detailed microstructural investigations carried out with optical, scanning, and transmission electron microscopes. The fundamentals of the thermodynamic-kinetic method are presented in Chapter 2. The information available in the literature related to the formation and evolution of solder interconnection microstructures in the most relevant metal systems faced in solder interconnections is presented in Chapters 3 and 4. The sequence of events in the formation of intermetallic reaction layers during soldering is discussed in Chapter 6 by making use of experimental results from solid-liquid diffusion couple experiments. In addition, the evolution of interfacial microstructures under thermal aging, especially the effect of additional (or impurity) elements, is studied in Chapter 6.

Even though the failures of solder interconnections encountered in reliability testing as well as in use of products are strongly dependent on interconnection microstructures, the considerations of failure modes and mechanisms are not included in this thesis.

2. THERMODYNAMIC-KINETIC APPROACH

In order to have a better understanding of the mechanisms controlling the most common failures encountered in test vehicles, as well as in products in service, more attention should be paid to the metallurgical compatibility between new (lead-free) solder alloys, component metallisations, and board metal finishes. The thermodynamics of materials provides fundamental information both on the stability of phases and on the driving forces for chemical reactions and diffusion processes, even though complete phase equilibrium is hardly ever met in electronics applications. However, stable or metastable local equilibria are generally attained at interfaces, and this provides a feasible method - together with kinetic information - for analysing the interfacial reactions in solder interconnection systems. The approach which makes use of the available thermodynamic data is becoming even more important when studying interconnections under continuous microstructural evolution [1, 2]. For this purpose a special concept of the "local nominal composition" (LNC) in the effective joint region, utilising both thermodynamic and kinetic data, has been presented [3]. It is to be noted that assessed thermodynamic data from practically all binary systems and a few relevant ternary systems are available. However, the diffusion kinetic data, even in binary systems, are limited, especially at low ($T \leq 150°C$) temperatures.

2.1 Thermodynamic evaluation of phase equilibria

The phase equilibria in solder-substrate interconnection systems - as in any system - are computed by summing up all the Gibbs (free) energies of individual phases and then minimising - according to the second law of thermodynamics - the total Gibbs energy of the n-component system at constant temperature and pressure:

$$G_{tot} = \sum_{\phi} \sum_{i} (\mu_i^{\phi} n_i^{\phi}) = \sum_{\phi} y^{\phi} \sum_{i=1}^{n} (x_i \mu_i^{o} + RT \sum_{i}^{n} x_i \ln x_i + G_m^{E}) \qquad (1)$$

where y is the relative amount of a phase ϕ and x_i is a mole fraction of a component i in the system. The parameters μ_i^o in Equation (1) represent the partial molar Gibbs energies or chemical potentials of the pure components and are taken either from available databanks or from the literature. The total Gibbs energy of the system is expressed as a function of chemical potentials, which are related to the activities of the components as follows:

$$\mu_i^{\phi} \equiv \mu_i^0(T) + RT \ln a_i \qquad (2)$$

The chemical potential (or activity) of a component i will have the same value in all the phases that are in complete mutual equilibrium, and therefore the driving force for its diffusion will vanish in the system. However, in the case of the joining and bonding of dissimilar materials the equilibrium is attained only at the interfaces and, even though the activity of a component has the same value at the interface, there are activity gradients in the adjoining phases. These gradients, together with diffusivities, determine the diffusion of components in various phases of a joint region.

The equilibrium states to be considered within the framework of this thesis are: i) complete thermodynamic equilibrium; ii) local thermodynamic equilibrium, and iii) metastable equilibrium. It is to be noted that partial equilibrium, in which only some of the components fulfill the equilibrium condition, is also possible.

2.1.1 Complete equilibrium

As stated above, when the system is in complete equilibrium its Gibbs free energy has reached its minimum value and then the system is in mechanical, thermal, and chemical equilibrium with its surroundings [4]:

$$dG = 0 \text{ or}$$
$$\mu_i^{\alpha} = \mu_i^{\beta} = \ldots = \mu_i^{\phi} \qquad (3)$$

In other words, when complete equilibrium is obtained the activities of all components (i=A,B,C,…) are the same in all phases (α,β, …,ϕ) and there are no gradients inside the phases. Naturally, complete (or global) thermodynamic equilibrium is never met in electronic products or even in solder interconnections. However, the bulk solder material can be considered as a part of a system that tends to approach equilibrium. For example, the amount and composition of the phases formed during the cooling of a solder material can be analysed by making use of the thermodynamic description of the system in question. Figure 2.1 shows the relative amount of phases as a function of temperature, when SnAgCu solder with a nominal composition of Sn0.84Ag1.08Cu (at-%) is cooling from the upper reflow temperature.

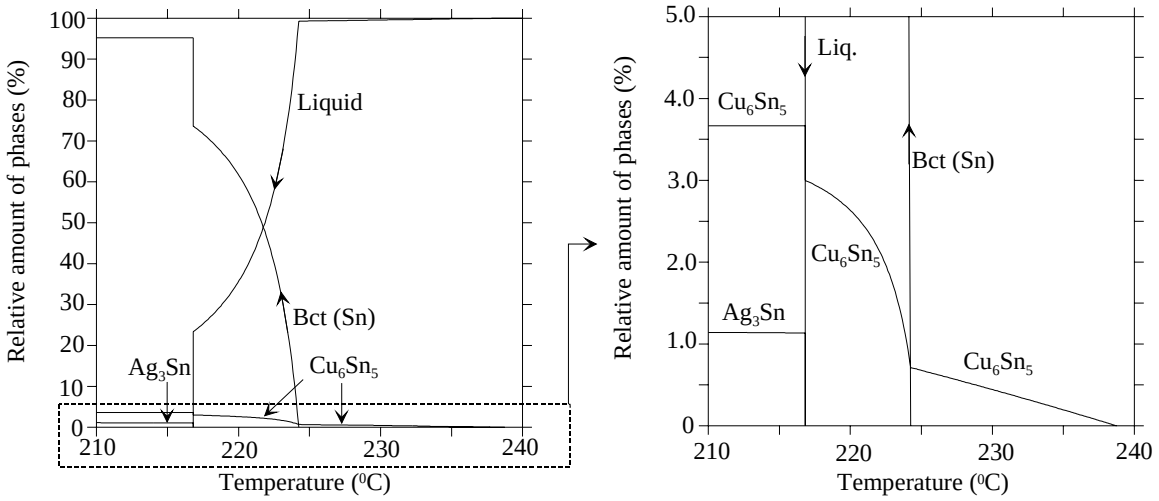

Figure 2.1: *Relative amount of phases as a function of temperature when solder nominal composition is Sn0.84Ag1.08Cu (at-%)[5].*

As can be seen from Figure 2.1, the solidification starts by the formation of primary Cu_6Sn_5 crystals at about 238°C. At 224°C the composition of the liquid meets the two-fold supersaturation curve and the primary tin starts to grow from the liquid, together with Cu_6Sn_5. The amount of β-Sn(bct) increases rapidly to about 75% when the temperature decreases to 217°C. The remaining liquid, which has a eutectic composition, solidifies at this temperature and the eutectic microstructure is formed between the β-Sn cells (or dendrite arms), as can be seen from Figure 2.2. Hence, the microstructure after

solidification is composed of primary (and secondary) Cu_6Sn_5 crystals and eutectic Cu_6Sn_5 +Ag_3Sn embedded in cellular β-Sn matrix. The total amounts of Cu_6Sn_5 (primary +eutectic) and Ag_3Sn are about 3.6% and 1.2% respectively. It is to be noted that the analysis above does not include the effects of either microsegregation or undercooling.

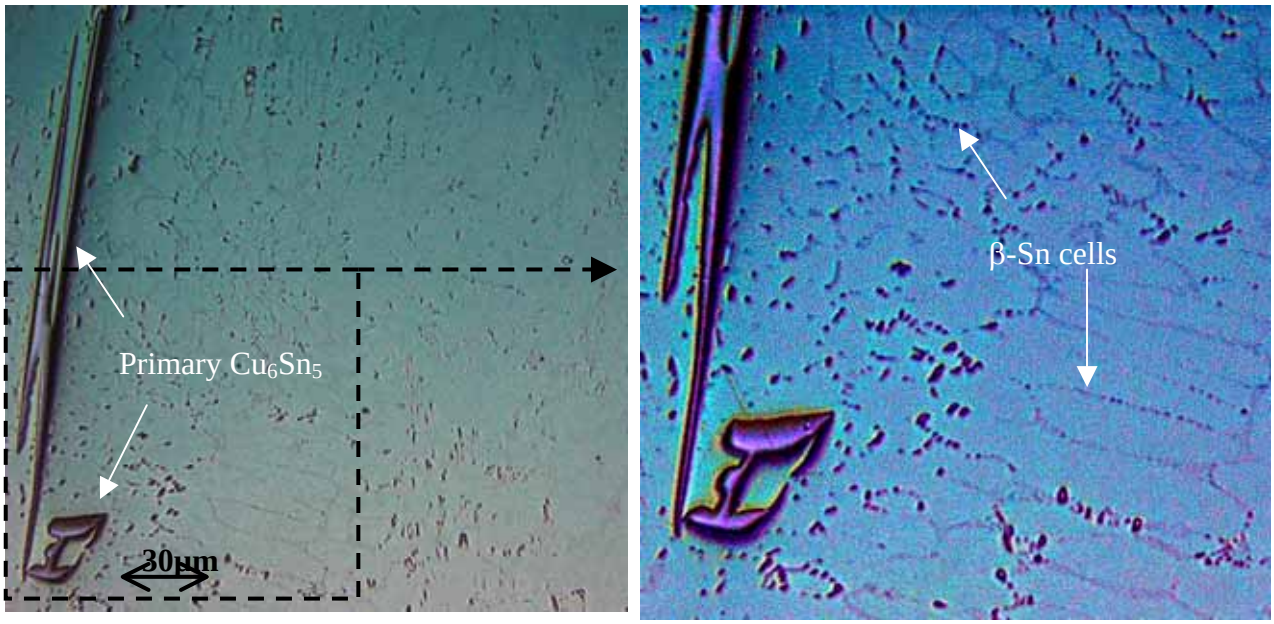

Figure 2.2: *Solidification structure of Sn0.84Ag1.08Cu (at-%)solder*

2.1.2 Local Equilibrium

By local equilibrium it is meant that the equilibrium exists only at the interfaces between different phases present in the system. The thermodynamic functions are continuous across the interfaces and the interfacial compositions can be obtained from the equilibrium phase diagrams. Therefore, the local equilibrium at the interphase between the α-phase and β-phase can be defined as [6]:

$$\begin{aligned} &\mu_i^{\alpha} = \mu_i^{\beta} \\ &\mu_i^{\alpha} = {}^0\mu_i^{\alpha} + RT\ln a_i^{\alpha} = {}^0\mu_i^{\alpha} + RT\ln x_i^{\alpha} + RT\ln \gamma_i^{\alpha} \\ &\mu_i^{\beta} = {}^0\mu_i^{\beta} + RT\ln a_i^{\beta} = {}^0\mu_i^{\beta} + RT\ln x_i^{\beta} + RT\ln \gamma_i^{\beta} \end{aligned} \qquad (4)$$

where ${}^{0}\mu_i$ is the chemical potential of pure *i* in the standard state, μ_i^j the chemical potential of component *i* in phase *j*, a_i^j the activity of component *i* in phase *j*, x_i^j the mole fraction of component *i* in phase *j*, γ_i^j the activity coefficient of component *i* in phase *j*, *R* is the gas constant, and *T* the temperature. The local equilibrium concept is especially important when analysing the interphasial reactions based on the so-called diffusion couple approach [7]. In a binary system the reaction products formed between components can be predicted by using the relevant phase diagram. After annealing at a certain temperature for a sufficiently long time, all the thermodynamically stable phases of the system at that particular temperature (and only them) will exist as layers between the end members. According to the phase rule, only single-phase regions can be formed and the interfaces between the phases have to be macroscopically planar. For example, when pure Cu is in contact with liquid Sn at 250°C the intermetallic compounds that are formed in the interphasial region can be derived from the phase diagram (see Fig 2.3, red contact line). From the critically assessed thermodynamic description of the system more information can be obtained by utilising the Gibbs free energy diagram (see Fig 2.4), where the molar Gibbs energy curves of the solution phases fcc (α), bct (β), and Liquid (Liq) are presented with solid green, blue, and red lines, respectively. The intermetallic compounds Cu_6Sn_5 (η) and Cu_3Sn (ε), which have a narrow homogeneity range, have been modelled as stoichiometric line compounds. The local equilibria at the interfaces I, II, and III, marked with dashed, dotted, and double-dashed lines, respectively, are: $\mu_{Sn}^{Liq} = \mu_{Sn}^{\eta}$ and $\mu_{Cu}^{Liq} = \mu_{Cu}^{\eta}$, $\mu_{Sn}^{\eta} = \mu_{Sn}^{\varepsilon}$ and $\mu_{Cu}^{\eta} = \mu_{Cu}^{\varepsilon}$ as well as $\mu_{Sn}^{\varepsilon} = \mu_{Sn}^{\alpha}$ and $\mu_{Cu}^{\varepsilon} = \mu_{Cu}^{\alpha}$. Both intermetallic phases [Cu_6Sn_5(η) and Cu_3Sn(ε)] can be observed after 64 min annealing as shown in Fig 2.5 (a). It is to be noted that the local equilibrium between Sn and Cu is, naturally, a function of temperature. If the temperature is raised to 500°C (see Fig 2.3, dotted blue contact line), Cu_6Sn_5 is not stable any more and liquid Sn comes into direct equilibrium with Cu_3Sn, which can also be experimentally verified (see Fig 2.5 (b) and (c)). Another phase (δ) becomes stable and can be observed between Cu_3Sn and Cu. The Gibbs free energy diagram at 500°C for the Cu-Sn system is presented in Figure 2.6. In addition to the interfacial compositions (such as $x_{Cu}^{Liq|\varepsilon}$ *and* $x_{Cu}^{\delta|\alpha}$), the driving forces for

diffusion can also be obtained from the Gibbs energy diagram. For example, $\Delta_r G^I_{Cu}$ represents the driving force for a pure Cu atom to diffuse through the δ- and ε-phases to the liquid|ε-interface to react with an Sn atom.

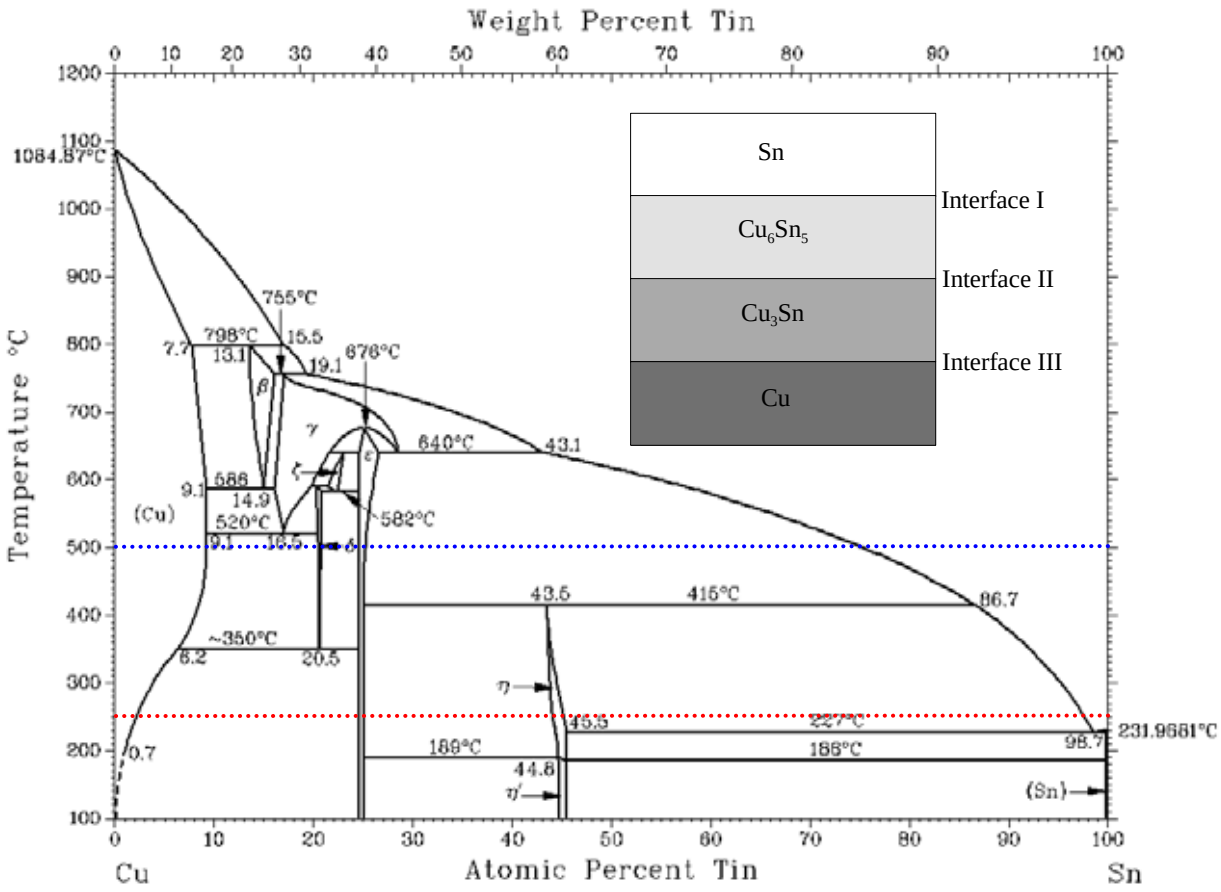

Figure 2.3: *Binary Cu-Sn phase diagram [8] together with superimposed reaction structure at 250 ℃, presented schematically.*

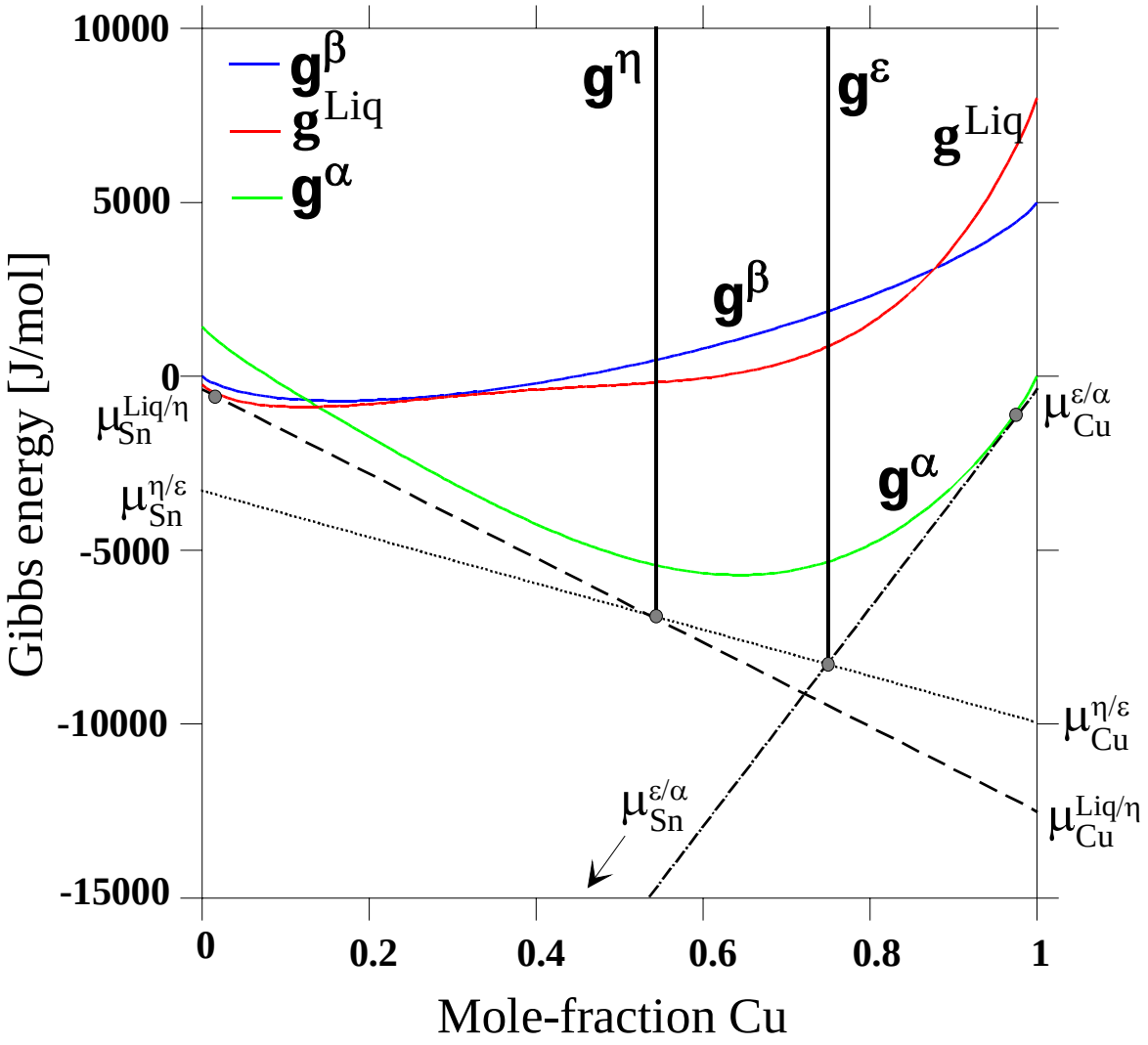

Figure 2.4: *Gibbs free energy diagram of the Sn-Cu system at 250 ℃* [5]

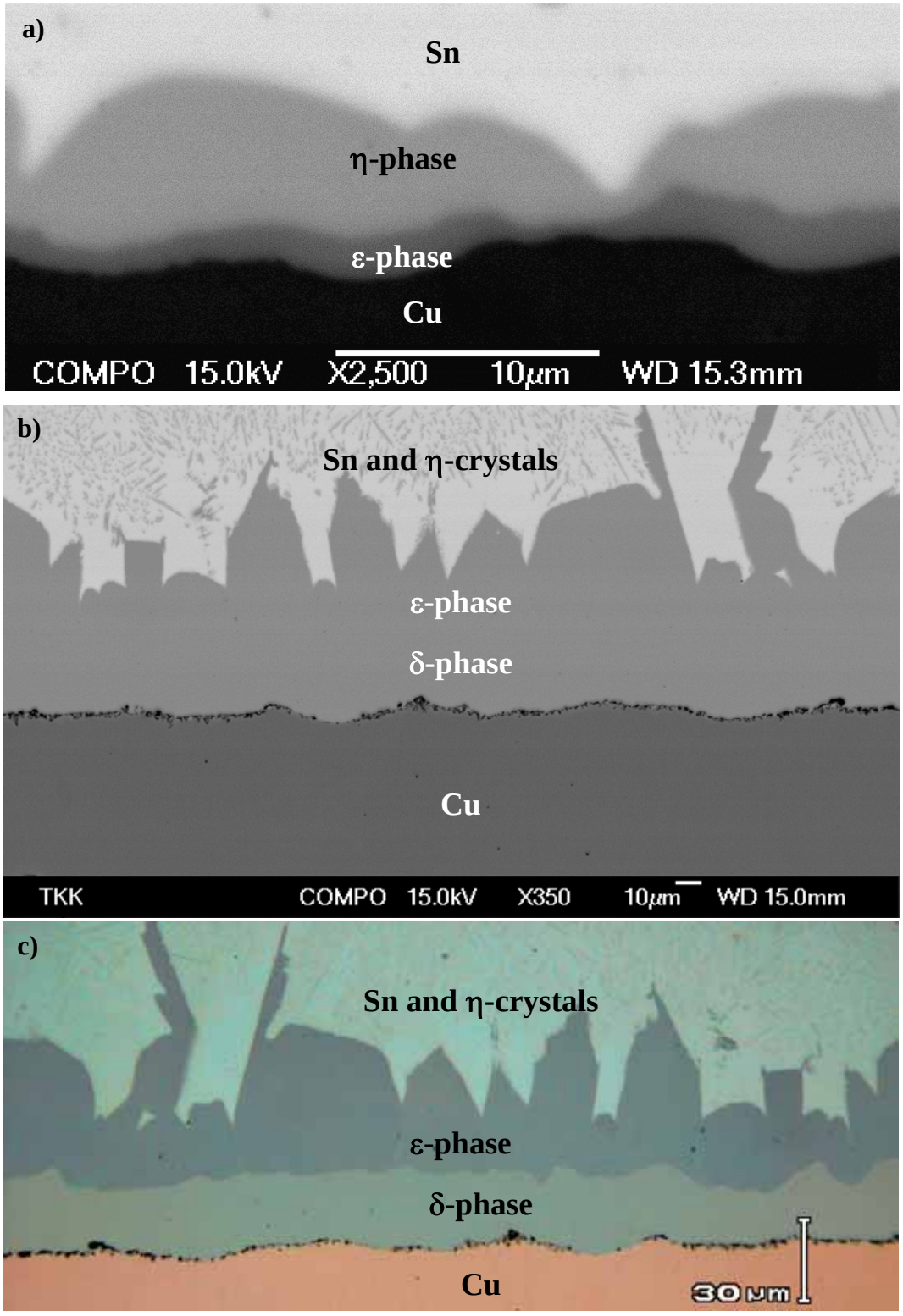

Figure 2.5: Cu|Sn diffusion couple annealed at (a) 250°C for 64 minutes, (b) and (c) 500°C for 120 minutes

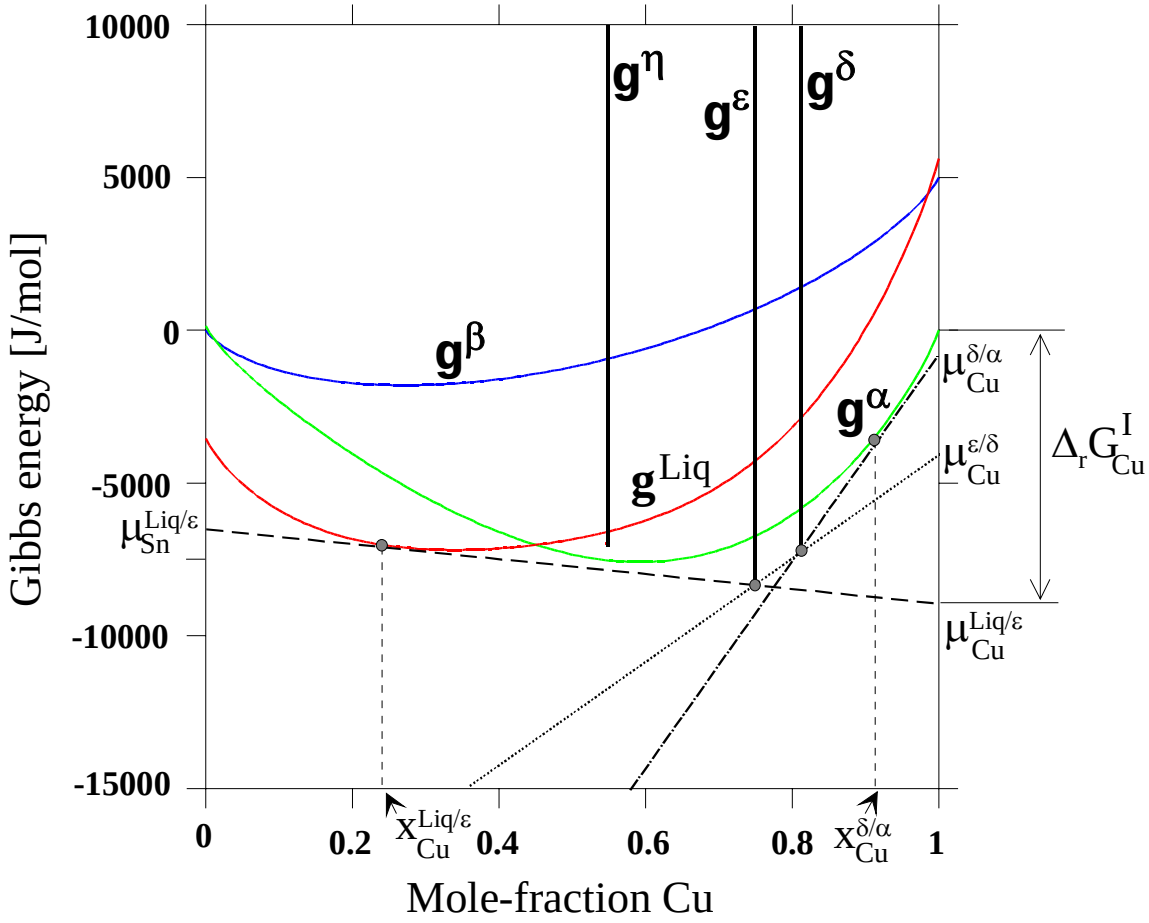

Figure 2.6: Gibbs free energy diagram of the Sn-Cu system at 500°C[5]

It is interesting to note that there are numerous small IMC crystallites embedded in the Sn matrix next to the interfacial intermetallic layer in Figure 2.5 (b). By performing an EDS analysis of these crystals it can be verified that they are Cu_6Sn_5 crystals. As can be seen from Figure 2.6, Cu_6Sn_5 is not thermodynamically stable at this temperature. Therefore these crystals must have grown during the cooling. Figure 2.6 shows that the composition of the liquid Sn in equilibrium with the ε-phase at 500°C is $x_{Cu}^{Liq|\varepsilon}$, denoting that the Cu content is as high as 24 at-%.

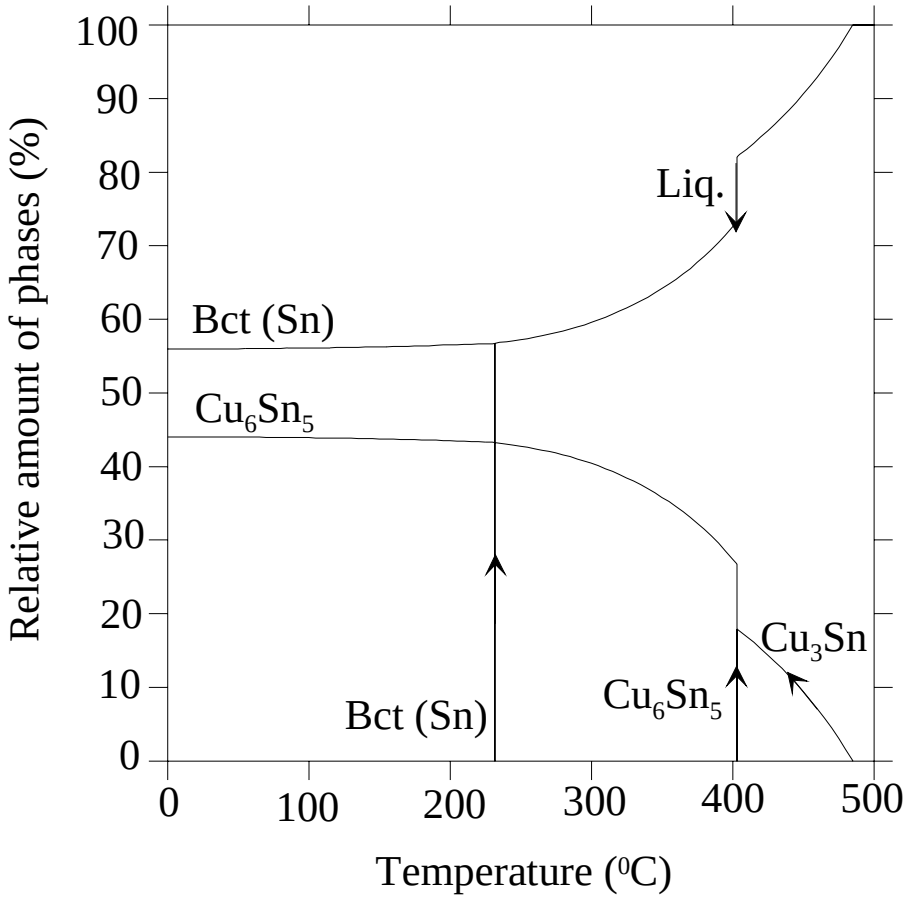

Figure 2.7: *Relative amount of phases as a function of temperature when the nominal composition is 76Sn24Cu (at-%)[5].*

The relative amount of phases as a function of temperature during cooling is presented in Figure 2.7. When the temperature has decreased to 415°C, peritectic Cu_6Sn_5 becomes in equilibrium with liquid Sn and Cu_3Sn. Therefore, the presence of Cu_6Sn_5 is obvious and with a closer look at the interface between ε and liquid a thin layer of Cu_6Sn_5 can also be seen there. As the composition difference between the ε- and δ-phases is very small, it is difficult to observe any contrast difference between these phases in a backscattered electron image (BEI, 2.5(b)), but these phases can easily be distinguished with an optical image (Fig 2.5 (c)). There are also a large number of voids at the interface between the Cu and the δ-phase.

2.1.3 Metastable equilibrium

Metastable equilibrium can be defined as a local minimum of the total Gibbs energy of the system. Therefore, in order to obtain the global stable equilibrium some activation (e.g. thermal energy) must be brought into the system. It is to be noted that metastable equilibrium can also be global, local, or partial; out of these the local metastable equilibrium concept will be used frequently in the following chapters. Very often one or more intermetallic compounds, which should be thermodynamically stable at a particular temperature, are not observed between two materials and then these interfaces are in local metastable equilibrium. Another situation where it is commonly encountered is in rapid interfacial reactions when one of the reacting materials is in a liquid state. Then, during the few first seconds, the solid material is in local metastable equilibrium with the liquid containing dissolved atoms, before the intermetallic compound(s) is formed at the interface.

2.1.4 Driving force for chemical reaction

A chemical reaction taking place at a constant temperature and pressure can be represented by:

$$aA + bB + ... \leftrightarrow cC + dD + ... \tag{5}$$

where *A, B, C, etc.* are species (reactants and products) in the reaction and *a, b, c, etc.* are the number of moles of the species in question. The Gibbs free energy change $(\Delta_r G)$ of the reaction is given by the difference in the chemical potentials of the reactants and the products and is defined as [6]:

$$\Delta_r G = (c\mu_C + d\mu_D + ...) - (a\mu_A + b\mu_B + ...) \tag{6}$$

If the change in the Gibbs free energy of the reaction is negative, the reaction can proceed spontaneously unless there are kinetic barriers that hinder the reaction. By giving the

Gibbs free energies with respect to the standard states of the species (i.e. $G=G^0+RT\ln a$), Equation 8 can be rewritten as:

$$\Delta_r G - \Delta_r G^o = (c\mu_C + d\mu_D + ...) - (a\mu_A + b\mu_B + ...) \quad (7)$$

where $\Delta_r G^o$ is the change in the standard Gibbs free energy of the reaction and $\mu_{A,B,C,D...}$ are the chemical potentials of the species *A, B, C, D*.... Furthermore, Equation 7 can be rewritten with the help of Equation 2 as:

$$\Delta_r G - \Delta_r G^o = RT \ln\left[\frac{a_C^c a_D^d ...}{a_A^a a_B^b ...}\right] \quad (8)$$

At equilibrium $\Delta_r G = 0$. Equation 8 is also valid in non-equilibrium conditions. For example, it is applicable when chemical reactions occur in supersaturated metastable liquid solder. In the Sn-Cu-Ni system the chemical reactions to form the IMCs that can be in local equilibrium with the liquid Sn at soldering temperatures are:

$$\begin{aligned} (6-y)Cu + yNi + 5Sn &\Rightarrow (Cu,Ni)_6 Sn_5 \\ (3-y)Ni + yCu + 4Sn &\Rightarrow (Ni,Cu)_3 Sn_4 \end{aligned} \quad (9)$$

where y is the fraction of Ni atoms in the Cu sublattice in Cu_6Sn_5 and the fraction of Cu atoms in the Ni sublattice in Ni_3Sn_4, respectively. In order to calculate the effect of the activities of dissolved Cu and Ni on the stabilities of the intermetallics, the following equations for the Gibbs energy change of the chemical reactions can be derived:

$$\begin{aligned} \Delta G^{(Cu,Ni)_6 Sn_5} &= (1-y)\times\Delta^0 G^{Cu_6Sn_5} + y\times\Delta^0 G^{Ni_6Sn_5} + RT\ln\left(\frac{a_{(Cu,Ni)_6 Sn_5}}{a_{Sn}^5 \times a_{Cu}^{6-y} \times a_{Ni}^y}\right) \\ \Delta G^{(Ni,Cu)_3 Sn_4} &= (1-z)\times\Delta^0 G^{Ni_3Sn_4} + z\times\Delta^0 G^{Cu_3Sn_4} + RT\ln\left(\frac{a_{(Ni,Cu)_3 Sn_4}}{a_{Sn}^4 \times a_{Ni}^{3-z} \times a_{Cu}^z}\right) \end{aligned} \quad (10)$$

From these equations it can be seen that if the activity of one reactant is very small in the liquid solder and if the activity of IMC is assumed to be 1, the value in brackets becomes large and thus the driving force for the reaction becomes smaller (or even vanishes).

2.2 Kinetic considerations

Thermodynamics provides the basis for analysing chemical reactions between different materials. However, one cannot predict the time frame of chemical reactions on the basis of thermodynamics alone. Therefore, diffusion kinetics, which, because of the lack of data is, unfortunately, often qualitative in nature, must then be brought into the analysis. In this chapter the basics of the kinetic analysis utilised in the thermodynamic-kinetic approach are presented in a very concise form. The reasons for the formation of Kirkendall voids are also considered briefly.

2.2.1 General

The driving force for interdiffusion is the difference in concentration (or more precisely in chemical potential or activity). Typically, diffusion kinetic analyses are based on the standard solutions of Fick's laws under certain boundary conditions. In the case of the steady state materials flow, i.e. when the concentration remains constant with time, Fick's first law states that the flux of element i (J_i) is directly proportional to the product of the diffusion coefficient (D_i) and the concentration gradient of an element i [9]:

$$J_i = -D_i \frac{\partial c_i}{\partial x} \tag{11}$$

For non-steady state diffusion, in which the concentration varies with distance and time, Fick's second law is applied [9]:

$$\frac{\partial c_i}{\partial t} = -\frac{\partial J_i}{\partial x} = \frac{\partial}{\partial x}\left(D_i \frac{\partial c_i}{\partial x} \right) \tag{12}$$

Thus, at constant temperature the rate of change of concentration is equal to the diffusivity times the rate of change of the concentration gradient. The utilisation of Equation 12 requires there to be a significant (measurable) composition difference within a phase. Then the diffusion coefficients can be obtained by using either Bolzmann-Matano or Sauer-Freise analysis [7]. However, if the system includes phases that have narrow homogeneity ranges (like many intermetallic compounds in solder interconnections), the above-mentioned analyses are not applicable and the method derived by Wagner needs to be used [10].

From the fundamental point of view Fick's laws have a limited validity, as the diffusion of an element i between two phases can occur, even if the concentration of i is equal in both phases (i.e. $c_i^{\alpha} = c_i^{\beta}$). This is due to the fact that the diffusion of matter takes place in such a manner that the system is changing to a state of energy minimum. Therefore, instead of the concentration gradient the chemical potential gradient $\left(\frac{d\mu_i}{dx}\right)$ should be used as a driving force. By using the well-known Nernst-Einstein relation, the flux for component i is [9]:

$$J_i = c_i \frac{D_i}{kT} \frac{d\mu_i}{dx} = c_i M_i \frac{d\mu_i}{dx} \qquad (13)$$

where M_i is the mobility of component i. Unfortunately, there is not much in the way of reliable diffusion kinetic data (diffusion coefficients) concerning even the most common intermetallic compounds formed at the interfaces of solder interconnections. Additionally, data on the effect of additional elements on the intrinsic diffusion coefficients, i.e. how the dissolved Ni affects the diffusion of Sn and Cu atoms through the $(Cu,Ni)_6Sn_5$ layer, are generally unavailable.

2.2.2 Kirkendall effect

In general the different elements move in phases with different rates, i.e. the intrinsic diffusion coefficients are not equal and the concentration gradients of elements 1 and 2 are equal but of opposite signs (in binary systems). Therefore, it is obvious that in the lattice system more material will diffuse out of one side of a couple than diffuses in. As the number of lattice sites is fixed in regions without vacancy sources or sinks, and the sum of the fluxes of atoms and vacancies in the lattice coordinate system is zero,

$$J_V + J_1 + J_2 = 0 \tag{14}$$

Clearly (in such a case) the vacancy flux $J_v\left[= -\left(J_1 + J_2\right)\right]$ will not be zero. Therefore vacancies must be created on one side of the couple and annihilated on the other side; otherwise, the accumulation of vacancies can give rise to so-called Kirkendall voids [9].

3. COMMON METAL SYSTEMS IN ELECTRONICS

Tin is the major solder component, which reacts with the most commonly used contact metals (i.e. Cu, Ni, Au, and Pd) on the component as well as on the printed wiring board side. After the implementation of lead-free materials the most important alloying elements used in Sn-rich solders are Ag, Cu, Ni, and Bi. Hence, because the interconnection metal systems are presently in most cases multicomponent, the metallurgical considerations of such complex systems require them to be divided into binary and ternary subsystems. In the following sections the most important systems will be reviewed by placing the emphasis on interfacial intermetallic formation.

3.1 Formation of microstructures in Sn|Cu reaction couples

At temperatures typical for the soldering processes, i.e. below 260°C, Cu_6Sn_5 (= η-phase) is the first phase to form at the liquid Sn/Cu conductor interface. When Cu comes into contact with molten Sn it starts to dissolve rapidly and after saturation Cu_6Sn_5 crystallites can form very fast as a result of heterogeneous nucleation and growth at the Cu/liquid interface [11]. The fast formation of Cu_6Sn_5 has also been observed experimentally [12]. Gagliano et al. carried out an investigation concerning the nucleation of the η-phase at liquid Sn/solid Cu interfaces at temperatures of 240-300°C [12]. They found out with a scanning electron microscope (SEM) that after a Cu strip had been dipped into molten pure Sn for even one second, the surface was covered with η-crystallites. At each temperature the morphology of the η-crystallites was the same, i.e. hemispherical or rounded morphology with some apparent faceting. They also found out that each crystallite appeared to grow independently from the adjacent ones. Further, the state of the surface (or the roughness) was found to have an effect on the formation of the η-crystallites. The rougher the surface, the more crystallites will be formed per unit area. They also monitored the growth of the crystallites and observed that even after the 1-second dip, there had been substantial growth of the crystallites. The growth rate was obviously very fast at the beginning and slowed down as the intermetallic that formed

reduced the dissolution of Cu into the molten Sn. As no ε-phase was detected, this investigation supports the general understanding that in the very early stages of a reaction the η-phase is the only compound forming at the Cu/liquid Sn interface. In addition to a more or less uniform scallop-type Cu_6Sn_5 layer (uniphase), the (Cu_6Sn_5 + Sn) two-phase layer can form next to the uniphase layer, most probably enhanced by the local constitutional supercooling of the liquid. Concentration profiles in front of the Cu/liquid interface are not necessarily very uniform and therefore there are areas where not all the Cu atoms are used in the formation of Cu_6Sn_5 uniphase. These surplus Cu atoms can form relatively long Cu_6Sn_5 tubes (primary Cu_6Sn_5), as well as bunches of Cu_6Sn_5 fibres in the eutectic (Cu_6Sn_5 + Sn) structure [13]. Fig. 3.1 presents such Cu_6Sn_5 tubes and fibres that appear when the tin matrix has been selectively etched away.

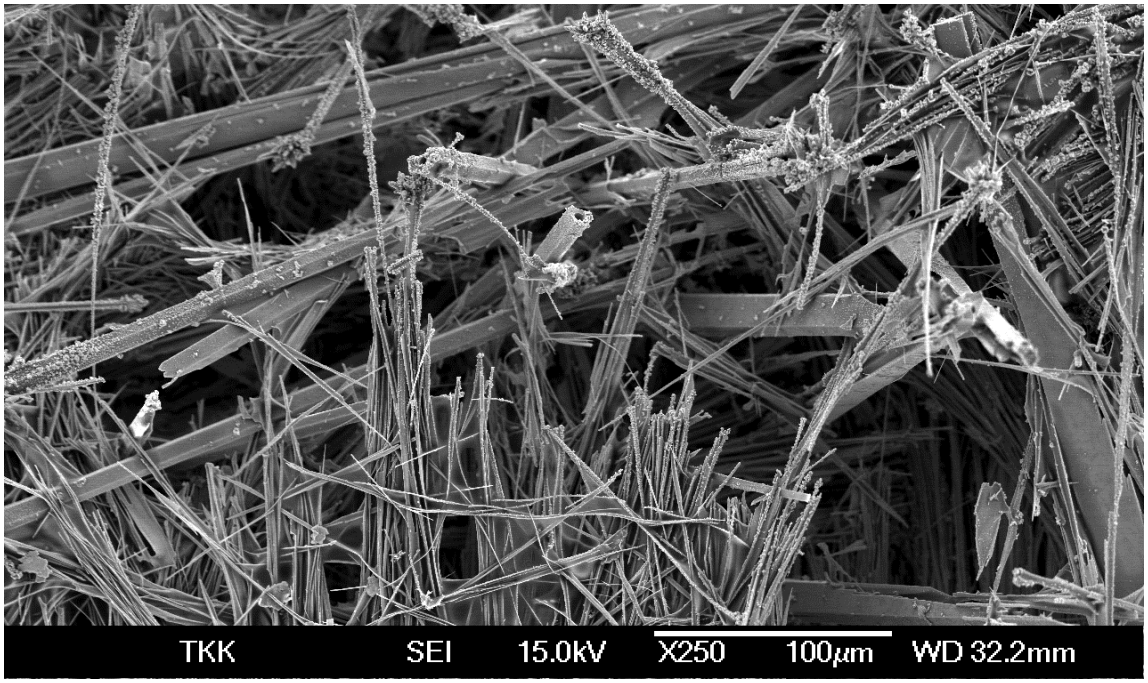

Figure 3.1: *SEM micrograph from an etched (selective Sn etch) Sn/Cu sample showing long Cu_6Sn_5 tubes.*

It is to be emphasised that these kinds of interfacial microstructures are generally observed in the binary Sn-Cu system (or ternary system where the third element is non-reactive, such as Pb or Bi) only after prolonged liquid state reactions. However, in ternary systems these kinds of two-phase reaction layers are more common, as will be shown

later on. Thermodynamically, there should be a Cu_3Sn layer between the Cu and Cu_6Sn_5 and it has been observed experimentally to form even during short soldering times [14]. However, since the growth of the Cu_3Sn requires solid-state diffusion the thickness of the layer remains much smaller than that of the Cu_6Sn_5 after soldering.

Kao [15] and Hayashi et al. [16] investigated the interfacial reaction at temperatures of 240-275°C between solid Cu and liquid Sn, with and without the addition of Cu. They found out that the morphology of the reaction layers was different if Sn was saturated with Cu or if it was pure Sn. In the case of a reaction in an Sn bath saturated with Cu, η- and ε-phases formed with layered structures. When Cu reacted with Sn in the pure Sn bath, the ε-layer was very thin and the η-layer was thick and irregular. The highly non-planar morphology of the reaction layer was not unambiguously explained in the study. It is possible that the dissolution rate of Cu is faster along the grain boundaries or along the specific direction of the Cu substrate. As the grain structure of the Cu plates used was not identified in the study, it is quite difficult to quantify the importance of this effect.

It should be emphasised that Cu_6Sn_5 has two structural forms in solid state. At room temperature, the stable form is η', the ordered long-period superlattice (LPS), which is based on the NiAs-type structure [17-20]. During soldering and subsequent cooling the available time for the transformation into this low-temperature structure is not sufficient and so high-temperature Cu_6Sn_5 (η) (the conventional NiAs structure) remains as a metastable phase. The equilibrium transformation temperature of Cu_6Sn_5 is 186°C. This means that during subsequent use of the device, transformation to η' should take place. However, if the temperature is near room temperature, transformation does not occur within a reasonable time, because of kinetic constraints. Nevertheless, when the structure is subjected to relatively high temperatures (e.g. around 150°C), the time required for the transformation is significantly shortened. Such high temperatures can readily be reached during use in novel electronic devices, because of the strong local heating of power components. If the temperature is somewhat higher still, the transformation time will be reduced even more drastically. In fact, we have been able to detect the transformation starting after 6 min at 175°C with differential scanning calorimeter (DSC) measurements.

Another question still practically unanswered is the effect of dissolved (impurity, or alloying) elements on the crystal structure of Cu_6Sn_5 and especially the equilibrium transformation temperature between η and η'. It has also been reported that Cu_3Sn (ε) has a long-period superstructure [14], but the ordering temperature is not as well-defined as that of the η-phase.

The interfacial reactions between solid Cu and Sn are of special interest and have been investigated thoroughly during recent decades. However, the results are not entirely in agreement and some of them even contradict each other. In the case of the Cu-Sn system, adequate diffusion data are not available for the temperatures of interest, *i.e.* from room temperature up to 200°C. In particular, the main diffusing species in the different IMCs of interest, *e.g.* η and ε, differs from one investigation to another. Quite an extensive summary of the available results has been published recently [21] and therefore only a short recapitulation is given below.

Tu [22, 23] and Tu and Thompson [24] stated that at room temperature, the η'-phase is first to form and the reaction is controlled by the release of Cu atoms from the Cu lattice. The main diffusing species at room temperature is Cu. Cu_3Sn (ε) does not form until the Cu/Cu_6Sn_5 couple is annealed at temperatures above 50-60°C and then it grows at the expense (at least partly) of Cu_6Sn_5. They also suggested that ε-phase did not form in the Cu/Sn and in the Cu/Cu_6Sn_5 diffusion couples as a result of the nucleation difficulties. No further evidence than the extrapolated reduction rate of Cu_6Sn_5 was provided to support this statement. According to the investigation of Bhedwar et al. [25], instead of Cu, Sn is the main diffusing species at 200°C during the formation of Cu_6Sn_5 and the growth kinetics is parabolic and not linear. This is in contrast to the more rapid grain boundary and interstitial diffusion of Cu in Cu_6Sn_5 and Sn, respectively, at room temperature. This is expected because at high temperatures, the volume diffusion is usually predominant in metals, whereas at relatively low temperatures with respect to the melting points of the corresponding materials (with metals 0.3-0.5 T_m), short-circuit diffusion (5 to 6 orders of magnitude faster than the volume diffusion at 0.5 T_m) becomes an important mechanism. The change in diffusion mechanism is also reflected in the results of Revay [26], where it

was observed that the activation energy of the combined growth of ε- and η-phases is reduced at temperatures below ~ 120°C. At this lower temperature regime grain boundary and interstitial diffusion mechanisms are expected to dominate over vacancy-mediated diffusion. The earlier results of Onishi and Fujibuchi [27] further support the analysis of Bhedwar et al. [25] that Sn atoms diffuse more rapidly than Cu atoms during the growth of the intermetallic layers (both Cu_6Sn_5 and Cu_3Sn). Onishi and Fujibuchi [27] also carried out experiments with markers at temperatures between 190 and 220°C. The direction of the marker movement was always towards the Sn side and the markers were found inside the Cu_6Sn_5 layer. The conclusions of the study by Mei et al. [28] were also concurrent with the analysis of Onishi and Fujibuchi [27]. An extensive diffusion study of the Cu-Sn system has been carried out by Oh in his thesis [28]. On this basis it can be stated that several factors influence the growth of ε- and η-phases at ~ 200°C. The first one is the diffusion flux of Sn in the η-phase. The second one is the decomposition rate of the η as the ε grows. The third one is the change in the relative magnitudes of Sn and Cu fluxes in the ε-phase. It appears that at higher temperatures of ~ 220°C, the first factor dominates and the η-phase grows fastest. However, as the temperature decreases the other two factors start to influence the growth of the intermetallic layers. The change in the ε/η ratio as the temperature decreases can be explained by the more rapid decrease of Sn flux with temperature in the η-phase (because the activation energy is higher) than fluxes of Cu and Sn in ε-phase. Oh [29] also observed the formation of Kirkendall voids inside Cu_3Sn during the annealing of Cu/Cu_6Sn_5 diffusion couples. Recently, other investigators have observed the same kind of behaviour in both SnPb and SnAgCu solder interconnections with Cu [30]. We have also detected the formation of Kirkendall voids during the solid-state annealing of Cu of different “quality” (electrochemically deposited coppers, Cu laminate with chemical Cu deposition and alloyed Cu substrates) both with pure Sn and SnAgCu solder at temperatures as low as 125°C, as will be shown in Chapter 6.

3.2 Formation of microstructures in Sn|Ni reaction couples

The Sn-Ni system is well characterised [8, 31]. There are three IMCs that are stable at the temperatures of interest *i.e.* below 260°C (see Fig. 3.2).

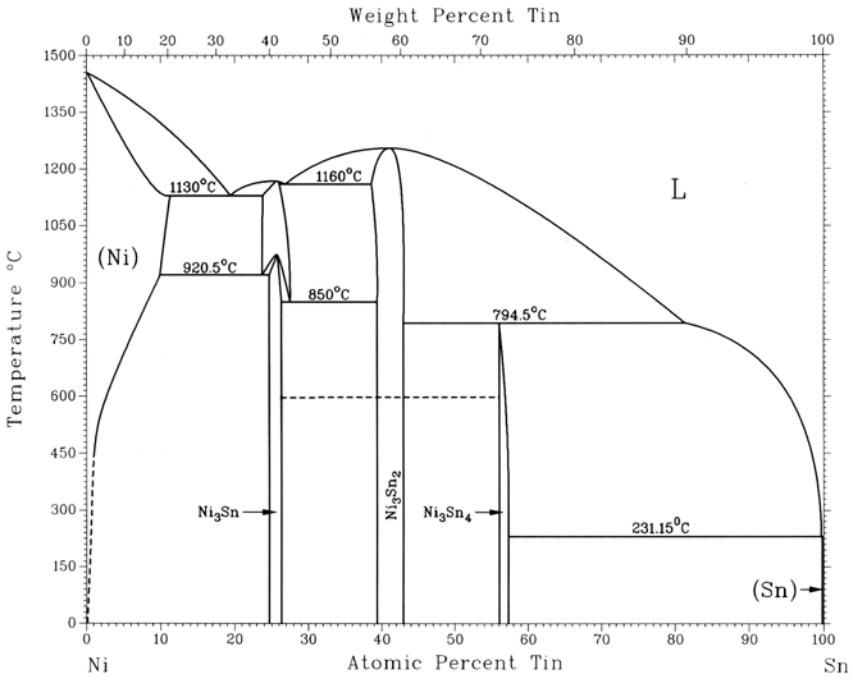

Figure 3.2: *Binary Ni-Sn phase diagram [8].*

Ni_3Sn has two structures, a low-temperature hexagonal form and a high-temperature cubic form. Ni_3Sn_2 also has two structures, a hexagonal NiAs-based structure below 600°C and a simple hexagonal one at temperatures above that. Ni_3Sn_4 has only one monoclinic structure. It has been reported that the Ni_3Sn_4 phase or metastable phases form during soldering in preference to Ni_3Sn or Ni_3Sn_2 at low temperatures [32], even though Ni_3Sn_4 is the least stable compound thermodynamically and it possesses the most complicated structure of all the Ni-Sn compounds [8, 31]. The Sn-Ni system was first thermodynamically assessed by Ghosh [33] and later modified by Miettinen [34]. The latter description has been widely adopted, despite the fact that the extrapolated liquid/fcc equilibrium is abnormal. This is not critical for those applications on the Ni-rich side but inappropriate in studying soldering metallurgy. Liu et al. [35] managed to correct this

problem and presented a new description of the Sn-Ni system. It has been slightly modified for two reasons: 1) the calculated metastable solubility of Ni in liquid is still high, considering the generally acknowledged rule that metastable solubility is normally 2-3 times the stable solubility in metallic systems [4]; 2) the models for some phases, especially Ni_3Sn_2 and Ni_3Sn_4, needed to be changed so that they would be consistent with the models in the ternary Sn-Cu-Ni system [36, 37]. The equilibrium solubility of Ni in liquid Sn is much less than that of Cu. Further, Ni-Sn IMCs are more stable than the corresponding Cu-Sn IMCs.

To study the growth of Ni_3Sn and Ni_3Sn_2 IMCs, Bader et al [32] also carried out solid-state diffusion experiments with Ni/Ni_3Sn_4 couples. At 240°C and 300°C only the Ni_3Sn_2 phase appeared as a layer with thin, long, columnar grains. At 400°C the Ni_3Sn phase also appeared in the couples with a similar grain morphology. They concluded that Ni_3Sn had difficulties in nucleating when the Ni/Sn interface was clean. However, when the Ni/Sn interface was contaminated, the nucleation of Ni_3Sn was enhanced. This was suggested on the basis of the results with single crystal experiments, where Ni_3Sn appeared even at lower temperatures. They proposed that because single crystal samples were fabricated by evaporating Sn onto an Ni substrate, the Ni substrates had come into contact with air before the evaporation of the Sn and there were some oxygen-based contaminants at the Ni/Sn interface. Both phases exhibited non-parabolic time dependence for growth with the exponent n less than 0.5. This indicates that the grain boundary diffusion of Ni in Ni_3Sn_2 and Ni_3Sn phases dominated the phase growth at the temperatures under investigation [32]. This was due to the grain coarsening, which reduced the effective diffusion coefficient with time.

Gur and Bamberger [38] investigated the isothermal solidification of three types of Ni-Sn samples at temperatures between 235-500°C. They observed with SEM that during solidification the Ni_3Sn_4 phase was the only intermetallic to grow. However, detailed TEM investigations revealed that contrary to the results of Bader et al. [32], the Ni_3Sn layer also existed in these samples. Nevertheless, it should be noted that the experimental conditions, especially temperature, in these two investigations were different. Gur and

Bamberger [38] concluded that Ni dissolution and reactive isothermal solidification, controlled by the diffusion of Ni in liquid, are the main reaction mechanisms in the formation of Ni_3Sn_4.

Haimovich [39] studied the growth of IMCs in solid Sn/Ni diffusion couples made by plating Sn or Sn-Pb over Ni. The growth rates of the stable Ni-Sn IMCs were quite slow and out of them only Ni_3Sn_4 was detected. However, together with this slowly growing stable IMC, a very fast-growing metastable $NiSn_3$ compound was also detected. Oh [29] studied interfacial reactions between solid Sn and Ni at 200°C. Despite the existence of three equilibrium phases in the Sn-Ni system (Ni_3Sn, Ni_3Sn_2, and Ni_3Sn_4), he also found that only Ni_3Sn_4 was present after annealing for as long as 918 hours. The growth kinetics of the Ni_3Sn_4 phase appeared to be parabolic and thus diffusion-controlled. The absence of the equilibrium phases Ni_3Sn and Ni_3Sn_2 was also observed when the Ni/Ni_3Sn_4 diffusion couple was used. The probable reasons for the absence of the two equilibrium phases are difficult nucleation and/or slow diffusion behaviour in the missing phases. Some information is available from the literature that either surface roughness or contaminants can help the nucleation of Ni_3Sn and Ni_3Sn_2 [29, 32]. It is also known that Ni is the predominant diffusing species during the formation of Ni_3Sn and Ni_3Sn_2 [29]. It should be emphasised that no diffusion of Ni has been observed to take place via an interstitial mechanism in Sn, as is the case with Cu, Au, and Ag.

In conclusion, on the basis of the results discussed above, it can be stated that at the temperatures of interest, Ni_3Sn_4 is the first phase to form and to grow into observable thickness in a solid Ni/liquid Sn reaction couple. After the formation of continuous Ni_3Sn_4, further growth occurs as a result of the diffusion of Sn through the intermetallic layer. The kinetics for this growth has been observed to be non-parabolic, thus indicating that short-circuit diffusion mechanisms are operating during the growth. The other two equilibrium Ni IMCs (Ni_3Sn_2 and Ni_3Sn) grow with much slower kinetics and Ni_3Sn especially seems to have difficulties in nucleating at the Ni/Sn interface. In both Ni_3Sn and Ni_3Sn_2 the main diffusing species during the growth is Ni.

3.3 Sn-Ag, Sn-Au, and Sn-Pd systems

Au, Ag, and Pd coatings have been used for a long time to protect conductor surfaces from oxidation and thereby to promote solderability. Ag is also an essential component in Pb-free solders, which are mostly based on the binary Sn-Ag system. In addition, in the IC industry solutions based on Ag interconnections have been explored because of its superior electrical conductivity. The ternary Sn-Pb-Au and Sn-Bi-Au systems are also included in this frame of reference, although Au can form intermetallic compounds with Pb and Bi. Typically, only Sn-Au intermetallics are observed.

The Sn-Au system (Fig. 3.3) resembles that of the Cu-Sn system. It is also characterised by a series of peritectic reactions and several intermediate phases exist in the system. The intermetallic phases of interest are hexagonal NiAs-type AuSn, showing a very small homogeneity range between 50.0 and 50.5 at-% Sn, orthorhombic $AuSn_2$, and $PtSn_4$-type orthorhombic $AuSn_4$.

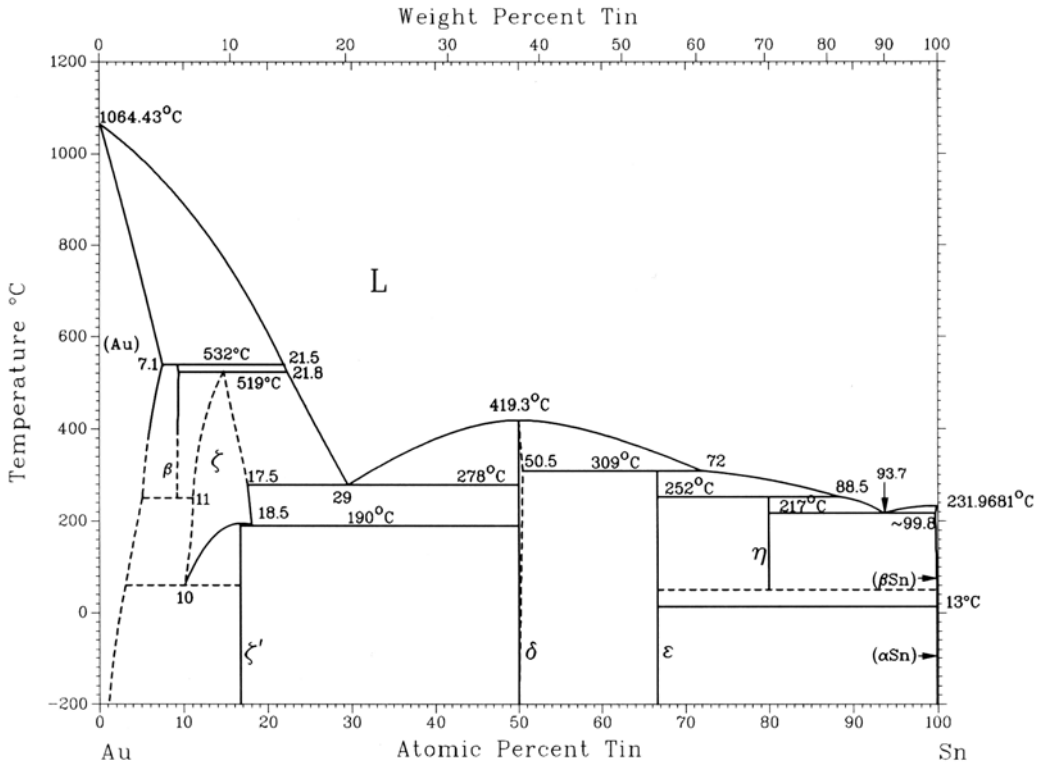

Figure 3.3: *Binary Au-Sn system [8].*

$AuSn_4$ is usually the phase observed when using SnPb or Sn-based Pb-free solders on conductor metals with a thin Au coating [40-44]. However, when using bulk Au wires (1 mm diameter), results from solderability experiments with SnPb and SnBi solders show that other intermetallics can form (see Fig. 3.4).

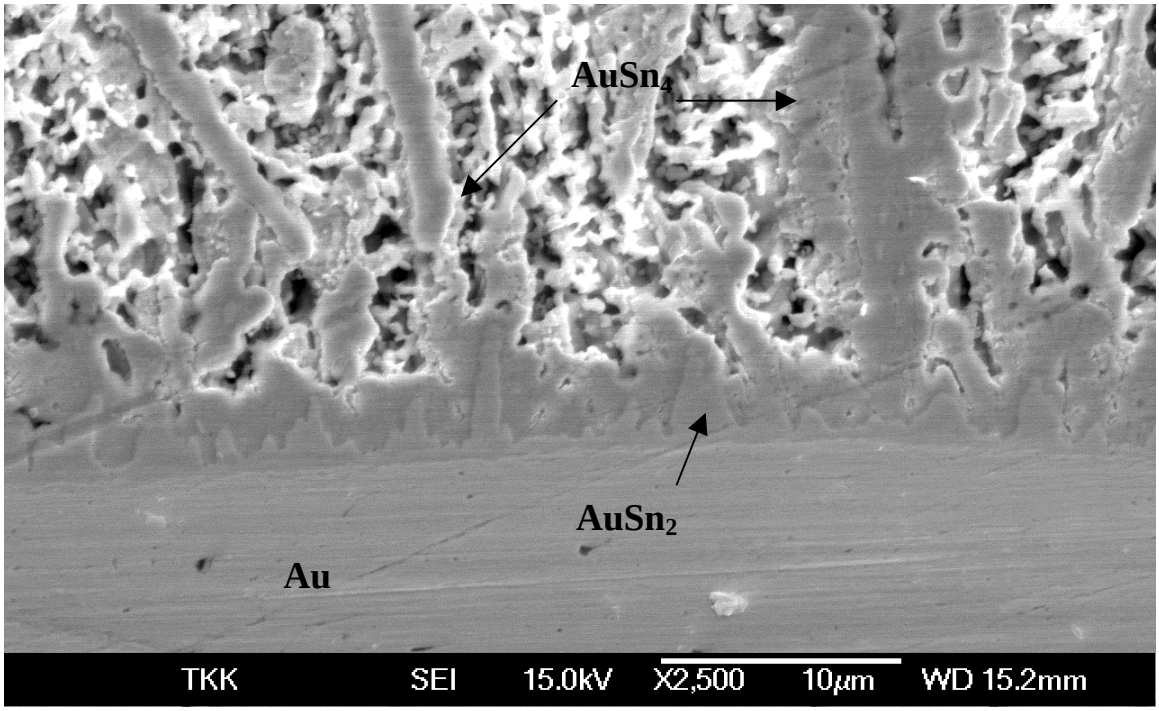

Figure 3.4: *SEM micrograph from an etched (selective Sn etch) Sn26Pb /Au sample after 100s at 230℃.*

On the other hand, it was observed that the dissolution of the gold wire continued throughout the experiment, regardless of the formation of intermetallic layers. The average dissolution rate during immersion for 100s in eutectic Sn26Pb solder at 230°C was 2.5 µm/s, which is in agreement with previous results [45]. However, the thickness of the ($AuSn_4$ + Pb) two-phase layer remained relatively unchanged, i.e. $AuSn_4$ was equally thick after 10 seconds and 100 seconds. Kim and Tu [46] also studied the time dependence of the reaction between SnPb and Au. They discovered that at 200°C $AuSn_4$ had already formed after 2 seconds. In this system the (Au-Sn-IMC + Sn) two-phase layer tends to be very thick with respect to the uniphase IMC layer. This is most probably related to the high metastable solubility of Au in liquid Sn, which in turn indicates a high

dissolution rate. The same kinds of observations have also been made with pure Sn and Au. For example, Au wire reacted with liquid Sn for 10 seconds at 245°C showed a very thick $AuSn_4$ layer, together with a thin $AuSn_2$ layer [47]. Sn-rich areas were also present, partly embedded inside the irregular $AuSn_4$ layer [47]. It is unlikely that the dissolution of Au would continue so fast after the formation of the $AuSn_4$ and $AuSn_2$ layers. Therefore, it is more likely that the IMC layers are formed mainly during the cooling of the sample and so the dissolution of the Au wire can continue throughout the whole immersion time. In another investigation Kim and Tu [44] studied the wetting behaviour of several Pb-containing and Pb-free solders on an Au thin film coating. They found out that the dissolution rate of Au was highest for the 95Pb-5Sn solder. After dissolution the interface was sunken and showed double (positive and negative) curvature. A pure Au/Sn couple showed less dissolution than the lead-rich solder and 96Sn-4Ag. The latter two solders still had sunken interfaces. The only solder that formed a relatively flat interface with Au was eutectic SnBi, which also showed relatively slow intermetallic compound formation. Our own experimental results confirm this (see Fig. 3.5).

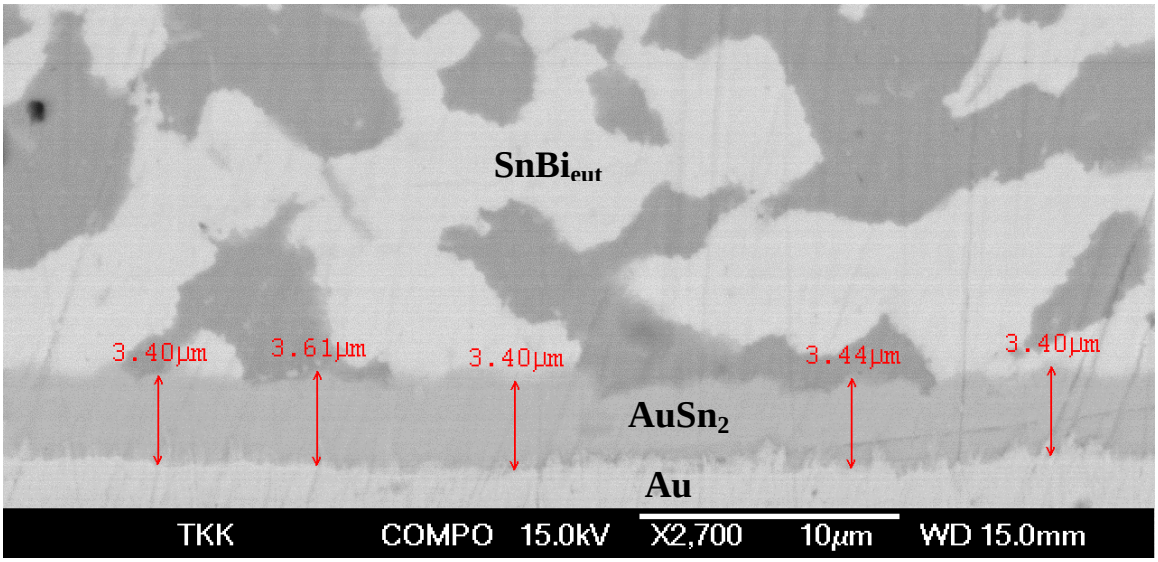

Figure 3.5: *SEM micrograph from $SnBi_{eut}$ /Au sample after 100s at 180℃.*

It is interesting to note that in this system the interfacial intermetallic compound is $AuSn_2$ rather than $AuSn_4$. In fact, the explanation here is more straightforward than that in the case of the Sn-Pb/Au diffusion couple. Figure 3.6 shows the isotermal section from the

Sn-Bi-Au system at 180°C, as well as the isothermal sections from the Sn-Pb-Au system at 180°C and 235°C. From Fig. 3.6 (a) it can be seen that $AuSn_2$ is in equilibrium with the eutectic solder at 180°C. Therefore, the diffusion path marked with a blue dotted line is expected. On the other hand, a similar diffusion path can also be expected for the $SnPb_{eut}$/Au diffusion couple [see Fig. 3.6 (b)] at 235°C. The apparent difference is the much higher solubility of Au in the liquid. However, as can be seen from Fig. 3.6 (c), the equilibrium phase with liquid changes from $AuSn_2$ to $AuSn_4$ during cooling, which necessitates the formation of $AuSn_4$. More detailed discussion of this matter has been given by Zeng and Kivilahti [48].

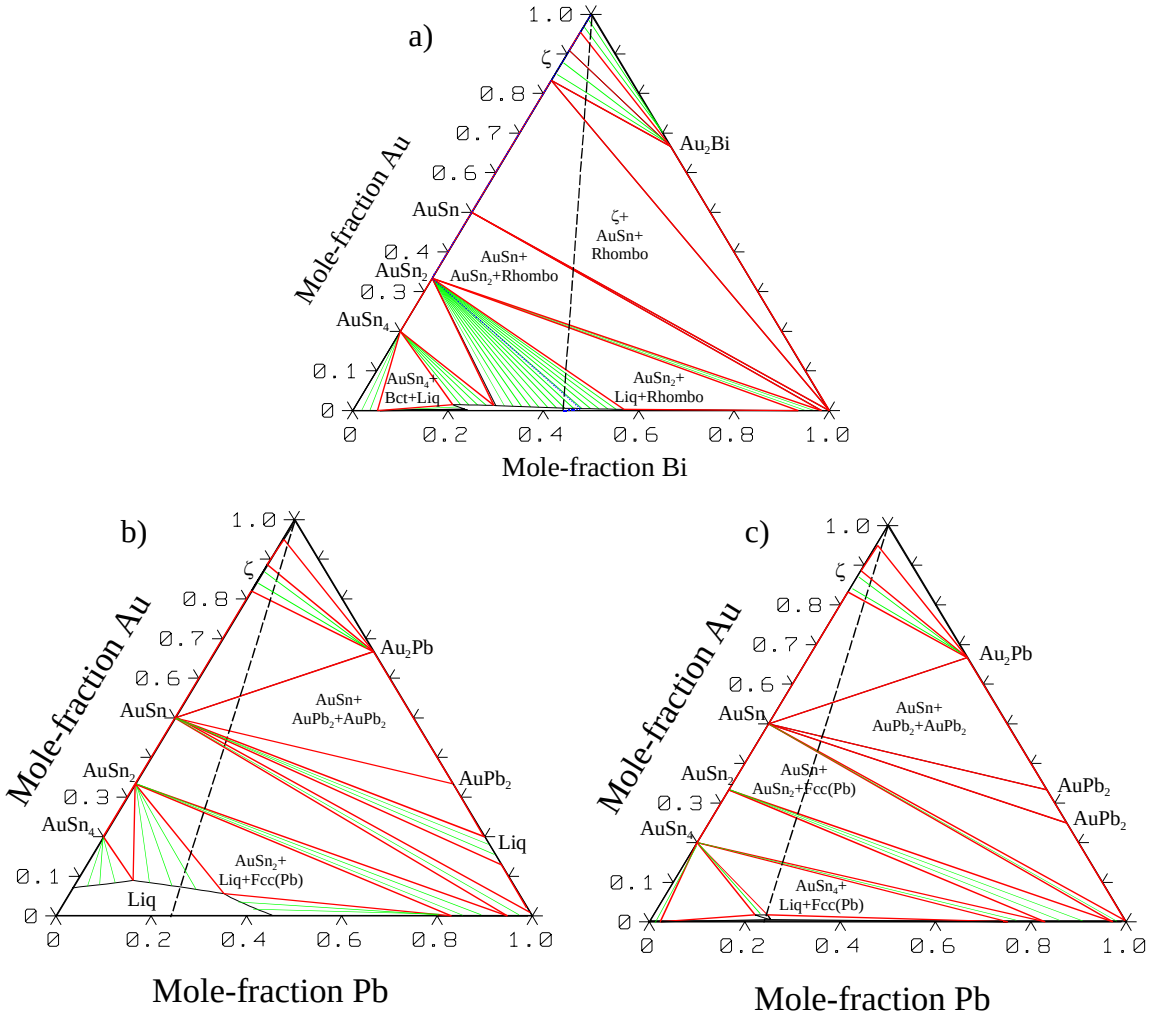

Figure 3.6: *Isothermal sections from the (a) Sn-Bi-Au system at 180℃, Sn-Pb-Au system at (b) 235℃ and (c) 180℃[5].*

Generally, it seems that the temperature and duration of the soldering process have only a minor effect on the morphology of the compound. However, the solder composition and especially the amount of Au (original Au thickness and solubility) are important. The uniphase IMC layer (actually consisting of $AuSn_2$ and/or AuSn4) formed in the Au-Sn system is quite thin in comparison to the ($AuSn_4$ + Sn) two-phase layer.

Solid-state interfacial reactions in the Au-Sn system have been extensively investigated, especially in thin-film diffusion couples [49-56]. A detailed review is available in [21] and thus only a short summary is given here. The first phase to form in the reaction between solid Sn and Au is $AuSn_4$, by the rapid interstitial diffusion of Au into Sn. Almost simultaneously, the formation of AuSn takes place, with slightly slower kinetics. The formation of either Sn- or Au-rich phases takes place as a result of the decomposition of the AuSn and $AuSn_4$ phases initially formed, depending on the amount of Au and Sn present. The AuSn structure provides a good "platform" for these kinds of structural modifications. Diffusion in the Au-Sn system exhibits very strong concentration dependence. In Au-rich regions the diffusivities of both Sn and Au are very small. In the rest of the concentration range the diffusivities seem to be relatively high. In particular, the diffusivity of Au in an Sn-rich area is high [56]. The large difference in diffusivities between the Au-rich and Sn-rich ends of the system is a consequence of different atomic diffusion mechanisms, as in Au-rich solutions Au (and Sn) can diffuse only by a vacancy-mediated mechanism, whereas at the Sn-rich end Au can diffuse interstitially.

In the Ag-Sn system there exist only two intermetallic compounds. One of them is the disordered cph-phase ζ and the other is the orthorhombic short-range ordered $Ag_3Sn(\varepsilon)$. Sn exhibits considerable solid solubility in Ag, with a maximum value of 11.5 at-% at 724°C (Fig. 3.7).

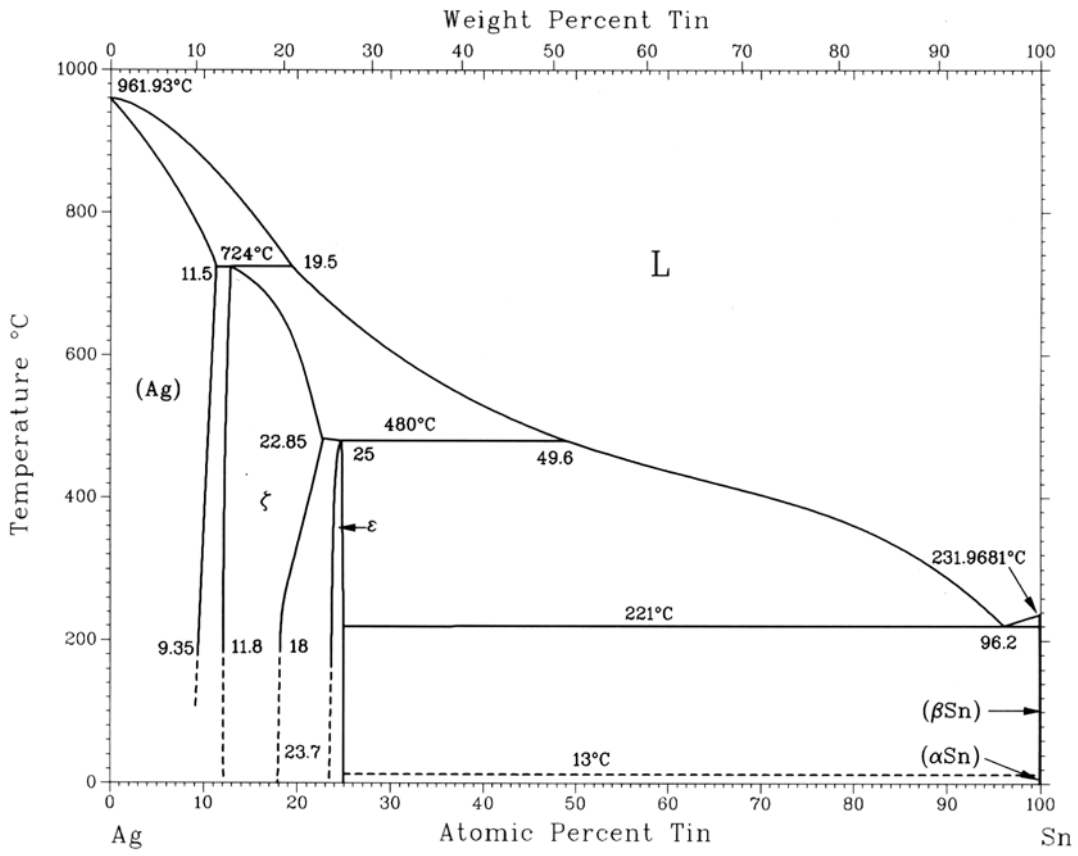

Figure 3.7: *Binary Ag-Sn system [8].*

The intermetallic phase that has been observed to form when Ag metallisations are soldered with Sn-based solders is orthorhombic Ag_3Sn [57-59]. If the Ag substrate is thick enough, the intermetallic compound forms a continuous layer on top of the original surface. However, as Ag (like Au) is usually used as a surface finish in electronics [60], it quickly dissolves to liquid solder and forms the Ag_3Sn intermetallic compound inside the bulk solder during cooling. The morphology of the Ag_3Sn resembles that of $AuSn_4$. The Ag-IMCs are in the form of relatively large flakes and can therefore cause reliability problems with a relatively low concentration. On the basis of the investigation by Brunson and Gerl [61], the diffusion of Ag in liquid Sn is a little faster than that of Sn and experiences a stronger increase with rising temperature. According to the same investigation, the diffusion of Au in liquid Sn is still faster (~ 1.5-2 times) than that of Ag or Sn [61]. This observation is quite interesting as it can, together with the high

metastable solubility of Au in liquid Sn, give some indication as to why the reaction between Au and liquid Sn produces such thick two-layer reaction product layers. A frequently used method to prevent excess Ag leaching, in addition to adding Ag to the solder, is to use AgPd metallisations. These alloys exhibit smaller dissolution rates and are frequently used as thin and thick film metallisations.

The solid-state reactions in the Ag-Sn system have been investigated much less than those in the very similar Au-Sn system. The two systems resemble each other in that both are so-called fast diffuser systems, where partially interstitial diffusion of solute atoms (i.e. Au, Ag, and Cu) in the host matrix (for example Sn) has been observed to take place [61]. As Sn has a tetragonal structure, bulk diffusion studies of both Ag and Au in single-crystal Sn show asymmetry [62]. In thin film structures the polycrystalline character of the films add new processes to diffusion study in the form of grain-boundary diffusion, as has already been seen in the case of the Au-Sn system [55]. Sen et al. [63] carried out a study of interfacial reactions in Ag-Sn thin film diffusion couples. It was found out that reactions started even at room temperature (during the evaporation of Sn) by interdiffusion between the thin films. The phase formed during the interdiffusion was identified as Ag_3Sn. The subsequent room-temperature annealing showed that the reaction had already reached completion at such a low temperature. The diffusion behaviour in the system was twofold: grain boundary diffusion of Sn into Ag and interstitial bulk diffusion of Ag into Sn. Marinkovic and Simic [64] also studied the reactions between Ag and Sn at room temperature. Consistent with other investigations, Ag_3Sn was the only compound formed during the reaction. Hence, the only phase to grow to detectable thickness in the reaction between solid Ag and Sn is Ag_3Sn.

In the Pd-Sn system there exist several intermetallic compounds (see Fig. 3.8), of which the most relevant from the soldering point of view are the Sn-rich orthorhombic $PdSn_4$ and $PdSn_3$ [65, 66].

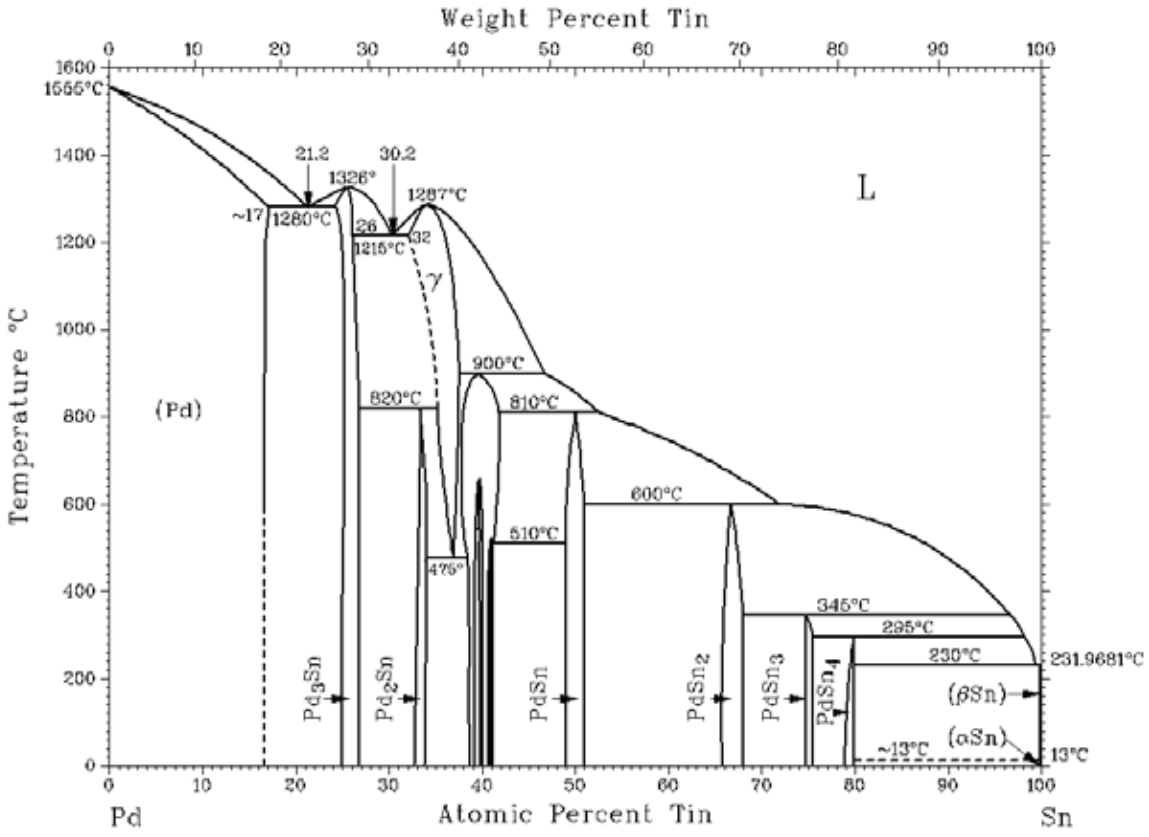

Figure 3.8: Binary Pd-Sn system [8].

After reflow soldering only $PdSn_4$, which has a similar two-phase morphology to $AuSn_4$, has been observed at the interface with both SnPb and SnAgCu solders [65]. Figure 3.9 shows the $SnPb_{eut}$/Pd interfacial microstructure after 100s at 230°C, together with the EDS element maps. It is clearly seen that the two-phase layer is composed of $PdSn_4$ and lead, which is left between the $PdSn_4$ grains during the chemical reaction.

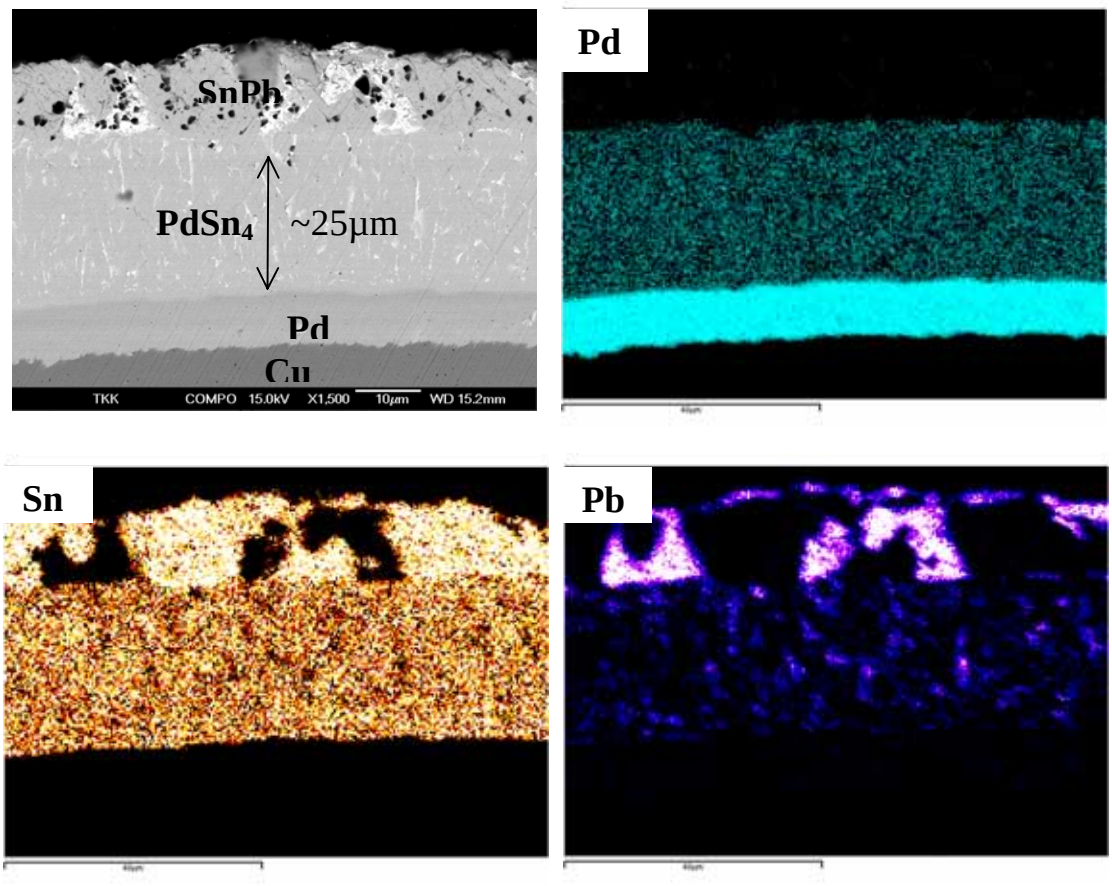

Figure 3.9: *SEM micrograph from $SnPb_{eut}$ /Pd sample after 100s at 230℃ together with the EDS element maps.*

The reaction between $SnBi_{eut}$ solder and Pd results in a similar interfacial microstructure to that with Au. As can be seen from Figure 3.10, two intermetallics are present at the interface after 100s at 180°C. The morphology of $PdSn_4$ is dense and it does not contain Pb precipitates inside. Therefore it is likely that the formation mechanism is different when using SnPb or SnBi solders. Unfortunately, no assessed Sn-Bi-Pd system is currently available. Therefore, it is not possible to carry out a similar thermodynamic analysis to that presented above in relation to Au. However, is seems evident that the lower solubility of Pd in $SnBi_{eut}$ than $SnPb_{eut}$, as well as the changes in local equilibria between liquid and IMCs during cooling, are the dominating factors.

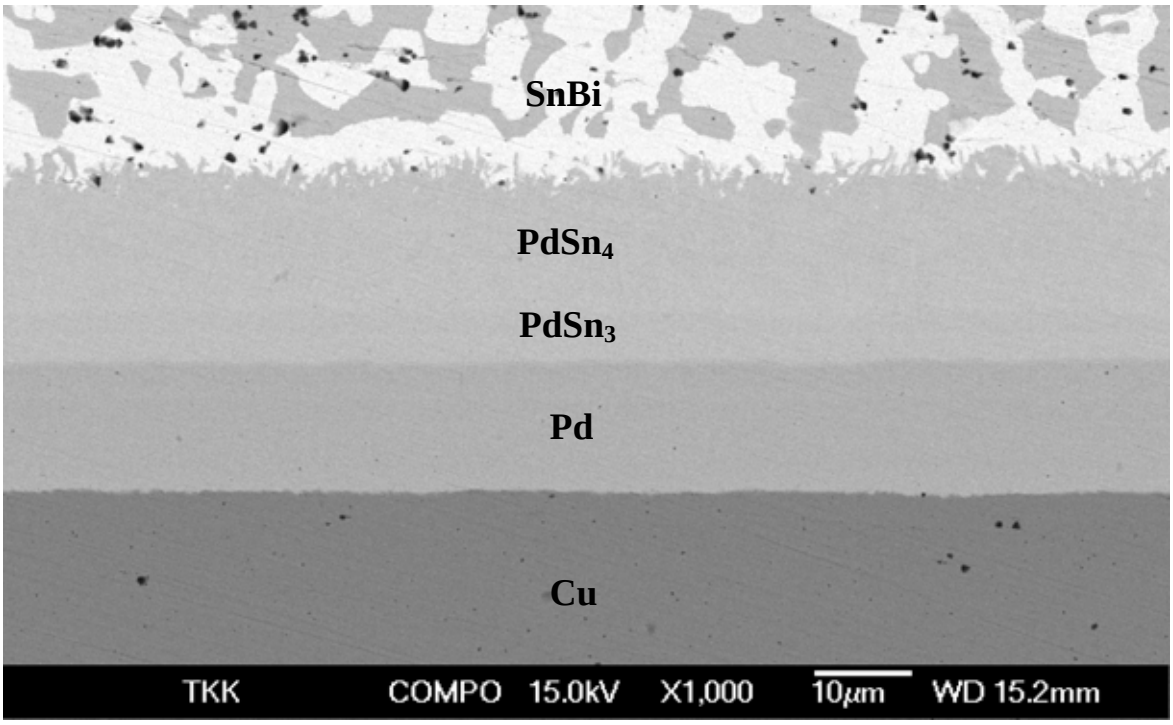

Figure 3.10: *SEM micrograph from $SnBi_{eut}$ /Pd sample after 100s at 180℃*

4. FORMATION OF SOLDER INTERCONNECTION MICROSTRUCTURES IN MULTICOMPONENT SYSTEMS

The purpose of this chapter is to introduce concisely the most essential aspects related to the formation of solder interconnections in multicomponent systems. The component board assembly process typically involves mounting components on a printed wiring board (PWB) and soldering their leads, solder balls, or contact pads to that board [66]. From the metallurgical point of view there are four major issues related to the modern surface mount assembly process. First, there are many commercial solders that have somewhat different chemical compositions. Most of them are high (>90%) Sn solders alloyed with Cu, Ag, Bi, In, etc. Second, the number of different metallisations and contact finishes has increased markedly, leading to more complex interconnection systems. Third, the dissolution of the contact materials can change the nominal composition of the bulk solder material and thus the physical and chemical properties are also altered. Finally, the solidification structures of solder interconnections are not stable under typical operating conditions but undergo continuous structural evolution during their lifetimes [67-69].

As already stated, the Sn-Cu-Ni system is probably the most important and widely investigated ternary system involved in lead-free soldering metallurgy. Even though experimental observations on this system have been reported in the literature, quantitative theoretical analyses of the results are not yet available, mainly because they need to be based on reliable thermodynamic and diffusion-kinetic descriptions of the system. The phase relations in the Sn-Cu-Ni system have been studied experimentally at soldering temperatures by Oberndorff [47], as well as by Lin et al. [70]. Their phase diagrams differ to some degree in regard to the solubility of a third element (i.e. Cu or Ni) in the binary intermetallics, as well as to the existence of the ternary intermetallic compound 44Sn27Cu29Ni [47]. Some experimental information concerning the quaternary Sn-Ag-Cu-Ni system has also been published [71]. In many recent publications the formation of intermetallic layers between Cu-bearing lead-free solders and Ni substrate or between Ni-bearing lead-free solders and Cu substrate has been explained by making use of the

diagram proposed by Lin et al. [72-78]. On the other hand, Hsu et al. [79] and Wang and Liu [80] have used an earlier preliminary version of the Sn-Cu-Ni isothermal section [5, 81, 82] to explain the formation of $(Cu,Ni)_6Sn_5$ in soldering reactions between Cu-alloyed SnAg solders and Ni substrate, as well as in the Ni/Sn3.5Ag/Cu sandwich structure. However, the authors did not consider either the supersaturation of the solders with dissolved Cu and Ni atoms or the existence of the metastable solubility limits. In addition, the effect of temperature change on local equilibria at the interfaces was not taken into account. The published results [72-78] show slightly different values related to the minimum amount of Cu in Sn-based solders which is required to change the primary intermetallic compound from $(Ni,Cu)_3Sn_4$ to $(Cu,Ni)_6Sn_5$ between the solders and Ni metallisation. Alam et al. state that after 20 minutes' annealing of Sn3.5Ag0.5Cu (wt-%) on Ni/Au metallisation at 240°C the Cu content of the liquid has decreased to 0.2 wt-%, and that is the reason why $(Ni,Cu)_3Sn_4$ starts to form between Ni and $(Cu,Ni)_6Sn_5$ [83]. However, this explanation is not easy to agree with, since $(Cu,Ni)_6Sn_5$ cannot be in local equilibrium with pure Ni. So it is more likely that the absence of $(Ni,Cu)_3Sn_4$ with shorter soldering times is due to the kinetic constraints (or difficulties in its nucleation). This issue is addressed in more detail later on. Hsu et al. annealed binary SnCu solders on Ni/Ti thin film metallisation at 250°C for different periods of time up to 20 minutes [79]. They reported that after 30 seconds a layer of $(Ni,Cu)_3Sn_4$ had already formed at the interface when using Sn0.6Cu (wt-%) solder and the higher Cu contents resulted in the formation of $(Cu,Ni)_6Sn_5$ [79]. Wu et al. reported the formation of $(Cu,Ni)_6Sn_5$ when Ni/Au metallisation was soldered with Sn3.0Ag0.5Cu wt-% using a reflow (peak temperature 250°C) time of 75 seconds [74]. Ho et al. studied the reactions between Ni and SnAgCu solders at 250°C [73]. The Ag content was fixed to 3.9 wt-%, the Cu content varied between 0.0 - 3.0 wt-%, and the soldering times used were from 10 minutes to 25 hours. They found out that with a low Cu content $\leq$ 0.2 wt-% $(Ni,Cu)_3Sn_4$ and with a high $\geq$ 0.6 wt-% $(Cu,Ni)_6Sn_5$ were the only phases to form. When the Cu content was 0.4 wt-%, a continuous $(Ni,Cu)_3Sn_4$ was formed, on the top of which was a small amount of discontinuous $(Cu,Ni)_6Sn_5$ particles. With Sn3.9Ag0.5Cu wt-% both intermetallics were formed as continuous layers, but the $(Ni,Cu)_3Sn_4$ was very thin [73]. They also reported that $(Cu,Ni)_6Sn_5$ had two different morphologies (and Ni contents), of

which the one in contact with the solder exhibited the tendency to detach (spalling) from the other. They confirmed this result in later publications and the explanation is based on the so-called “Cu concentration effect”, by which they mean the changes in Cu content as a function of time as a result of the small solder volume (i.e. a limited amount of Cu is consumed by IMC reactions and therefore the composition of the solder has changed accordingly) [76, 78]. Chen et al. studied interfacial reactions between binary SnCu solders and Ni at 250°C for 10 min and 25 hours [72]. The Cu contents used were 0.2, 0.4, 0.7, and 1 wt-%. The results were similar to those that Ho et al. found. With Sn0.2Cu solder $(Ni,Cu)_3Sn_4$ and with Sn0.7Cu and Sn1.0Cu $(Cu,Ni)_6Sn_5$ were the only phases to form. When the Sn0.4Cu was used as solder both intermetallic layers were formed [72]. Tsai et al. studied the reactions between Cu and SnAg solder doped with a small amount of Ni [75]. The Ag concentration was fixed at 3.5 wt-% and the Ni concentrations used were 0, 0.1, 0.5, and 1.0 wt-%. The temperature used was 240°C and the reaction times ranged from 20 sec to 9 hours. $(Cu,Ni)_6Sn_5$ was the only phase observed at the interface in all samples, but the Ni concentration affected the reaction kinetics, as well as the morphology of the intermetallic compound [75]. The effects of the addition of Ni to SnAg or SnAgCu solder on the interfacial reactions on Cu substrate have recently been studied by M. Amagai, H. Nishikawa et al., F. Gao et al., M. Tanaka, and I. Sousa et al. [84-88]. Ohriner [89] has carried out an extensive investigation of reactions between various Cu-based alloys and solders containing Sn at temperatures between 150 and 250°C. The substrates were exposed to liquid solder for 5 s (at a temperature 30°C above the liquidus temperature of the solder) and subsequently annealed in solid state at different temperatures from 150-225°C [89]. He observed interesting behaviour when Cu alloys containing Ni were soldered with 95Sn-5Ag, 95Sn-5Sb, and Sn-Pb solders. The rate of intermetallic formation was found to be dependent on solder composition and temperature, as well as Ni concentration. The maximum growth rate was always around 6-9 at-% of Ni in Cu [89]. A. Paul [90] recently made another interesting observation when studying solid-state reactions (T = 225°C) between pure Sn and Cu conductor metal alloyed with 5-15 at-% Ni. He also detected a significant increase in the growth rate of $(Cu,Ni)_6Sn_5$ within this concentration range, as well as the absence of Cu_3Sn. What is interesting is that when he etched the Sn away to reveal the $(Cu,Ni)_6Sn_5$, he observed that

when the Cu was alloyed with 5-15 at-% of Ni, the grain size of the $(Cu,Ni)_6Sn_5$ was more than one order of magnitude smaller than in the case of pure Cu [90]. Moreover, high diffusion flux in $(Cu,Ni)_6Sn_5$ could suppress the detectable growth of Cu_3Sn, as will be discussed later on. Recently, some investigators have observed the formation of pores (claimed to be Kirkendall voids) in Cu_3Sn or at the Cu/Cu_3Sn interface with both SnPb and SnAgCu solder interconnections with Cu [30]. In relation to the formation of Kirkendall pores, Paul [90] has shown that Kirkendall planes in a given reaction couple can be multiple, stable, unstable, or virtual. He used an approach based on the so-called Kirkendall velocity plot [91, 92] to explain and predict Kirkendall plane formation. This velocity plot can be constructed from the available experimental kinetic data [90-92]. On the basis of the calculations made by Paul [90], in an Sn/pure Cu system no stable Kirkendall plane should form inside the Cu_3Sn phase. The word "pure" is important, since the results from the velocity construction are heavily dependent, among other factors, on the compositions of the end-members of the diffusion couple [90]. In fact, Paul [90] detected extensive porosity inside Cu_3Sn when the Cu layer in the Cu/Sn diffusion couple contained 1 at-% of Ni.

During recent years, reliability problems have been reported when using Ni/Au coatings with Sn-based solders. Problems have appeared especially when using the electroless Ni/immersion Au finish [93-101]. In the electroless deposition process Ni is coated on Cu together with phosphorus, because hypophosphate is used as a reducing agent in the plating bath. The presence of phosphorus in the finishing layer has been observed to be associated with reliability problems. Although wetting has occurred properly and a chemical reaction between Sn and Ni is evident, the adhesion of the interface is inadequate. This weak interface readily fractures under stress even during cooling, leaving behind an open circuit. The root cause for the brittle fracture has been discussed in many papers concerning the reactions between electroless Ni and both lead-free and SnPb solders [102-112]. The formation mechanism of the interfacial reaction products that causes the reliability problems has not yet been identified with certainty. However, what has been found out is that the as-reflowed BGA joints generally fracture at the $Ni_3Sn_4/Ni(P)$ interface. It has been claimed that the segregation of phosphorus on the

PWB side of the fractured surface is responsible for the failure [100]. Jang et al. detected phosphorus enrichment in the $Si/SiO_2/Al/Ni(P)/63Sn37Pb$ multilayer structure after reflow and suggested that the formation mechanism of the interfacial reaction layers is related to the so-called solder reaction-assisted crystallisation [113]. The mechanism is based on the preferential dissolution of Ni from the Ni(P) layer and an increase in the phosphorus content of the upper part of the Ni(P) layer and the subsequent formation of Ni_3P [113].

There also exist claims that the brittle fracture is related to the redeposition of $AuSn_4$ at the interface after high-temperature annealing if the amount of Au (the thickness of the Au coating) is high [100, 101, 113-118]. Typically, the amount of gold present in soldering systems is usually quite small because Au is generally used in electronics as a thin protective surface-finishing layer to ensure solderability. However, the behaviour of these small amounts of Au with other metals is theoretically interesting and is of great importance in soldering applications. Mei et al. [100] have revealed a problem that is peculiar to Ni/Au metallisation with SnPb solders. They discovered that after prolonged aging (150°C for 2 weeks) the $AuSn_4$ intermetallic compound which had formed during the soldering in the bulk solder redeposited at the solder/substrate interface. The reconstituted interface was significantly weakened and failed by brittle fracture along the surface between the redeposited $AuSn_4$ and the Ni_3Sn_4 layer formed during the reflow. Minor and Morris [118] studied the mechanism of the redeposition of the $AuSn_4$ intermetallic compound. They used Cu substrates with electrodeposited Ni (7 μm) followed by Au deposition (1.5 μm). After soldering (peak temperature about 220°C), the samples were aged at 150°C for various times ranging from 3 to 504 hours. The as-solidified solder interconnections contained dense distributions of small needle-like $AuSn_4$ particles evenly distributed throughout the bulk solder. The interface between the Ni and the bulk solder consisted of a layer of Ni_3Sn_4 that contained a very small amount of Au. A coarse intermetallic layer developed above the Ni metallisation during the aging. It thickened roughly as $t^{0.5}$, i.e. indicating that the growth was diffusion-controlled. The simultaneous depletion of $AuSn_4$ needles from the bulk occurred. The redeposited intermetallic compound in the aged samples appeared to have a composition close to

$AuSn_4$. Hence, it seemed that the availability of Ni at the interface was the reason for the redeposition process. Ho et al. [119] investigated how the addition of small amounts of Cu to SnPb solder influences the redeposition behaviour of $AuSn_4$. They used solder balls with two compositions: 37Pb-63Sn (wt-%) and 36.8Pb-62.7Sn-0.5Cu. The Au layer was about 1 μm and the Ni layer about 7 μm thick in the Au/Ni/Cu metallisation. After the reflow, the samples were aged at 160°C for periods of time up to 2000 hours. Again, after the reflow, gold was completely absent from the interface and all the $(Au_{1-x},Ni_x)Sn_4$ intermetallic particles were evenly distributed throughout the bulk solder. At the Ni/solder interface, a Ni_3Sn_4 layer was formed, except in the sample where the solder included Cu. In this case, the interfacial reaction layer was not Ni_3Sn_4 but an Au-bearing $(Cu_{1-p-q}Au_pNi_q)_6Sn_5$ quaternary compound. The addition of 0.5 wt-% of Cu to the SnPb solder completely inhibited the redeposition of $(Au_{1-x},Ni_x)Sn_4$. Only a layer of $(Cu_{1-p-q}Au_pNi_q)_6Sn_5$ was detected at the interface, and it reduced the consumption rate of Ni in the reaction. No thermodynamic explanation for the effect of Cu on the interfacial reactions was offered in the publication. Shiau et al. [120] carried out a study of reactions between lead-free Sn-Ag-Cu solder and an Au/Ni finish in order to find out whether the redeposition of $AuSn_4$ intermetallic compound would also take place in this lead-free system. Three solders were used: Sn3.5Ag, Sn4Ag0.5Cu, and Sn3.5Ag0.75Cu. The Au and Ni layers were electroplated and were 1 and 7 μm in thickness, respectively. The soldering was carried out in a hot-air reflow oven. The peak temperature was 240°C, and the reflow time was about 2 min. After soldering, the samples were aged at 180°C for periods of time up to 500 hours. With the Sn3.5Ag alloy, a thin layer of Ni_3Sn_4 formed at the interface, while with the Sn3.5Ag0.75Cu a layer of $(Cu_{1-p-q}Au_pNi_q)_6Sn_5$ formed. With the Sn4Ag0.5Cu solder, both Ni_3Sn_4 and $(Cu_{1-p-q}Au_pNi_q)_6Sn_5$ were present near the interface. The $(Cu_{1-p-q}Au_pNi_q)_6Sn_5$ was, however, detached from the interface and there was a layer of solder between the intermetallic layers. No explanation for this interesting observation was offered. In the case of the Cu-free solder, minor redeposition of $(Au,Ni)Sn_4$ was observed at the interface.

5. EXPERIMENTAL PROCEDURES

The formation of intermetallic compounds has been investigated experimentally in several systems. The alloys used were manufactured from either commercially pure or high-purity metals by melting them in quartz ampoules containing an inert atmosphere or a vacuum at temperatures clearly above the liquidus temperatures. In order to avoid any inhomogenities the liquid alloys were occasionally mixed. Commercial electrochemical Cu and electroless Ni[P]+Au platings were also used. The solid|liquid reactions were carried out by immersing the metal strips for specific periods of time in a large volume of liquid Sn (or Sn-based solder) heated up in stainless steel crucibles. As solder interconnections are formed by melting the solder material, the solder-metallisation interface is subjected to at least one solid|liquid reaction cycle. Hence, the evolution of solder microstructures in solid state starts from a situation where the bulk solder material has a solidification structure and the interfaces have a relatively thick intermetallic layer (or layers) present. Therefore, prior to solid-state annealing at elevated temperatures the soldering was performed under an air atmosphere in a Heraus Ewos 5.1 production-scale reflow furnace to achieve as realistic an initial state as possible. Regardless of this difference from any “classical” definition, these samples are referred as solid-state diffusion couples in this thesis because of the fact that local equilibria can generally be assumed at the interfaces.

The cross-sectional samples were manufactured according to standard metallographic methods [121]. Some of the samples were slightly etched in a dilute solution of CH_3OH+HCL. The samples were studied by means of optical microscopy (Olympus BX60), also utilising polarised light and scanning electron microscopy (SEM, Jeol 6335F), together with energy-dispersive x-ray spectroscopy (EDS, Oxford INCA) [121]. Some of the interfacial reaction products were also characterised with transmission electron microscopy (TEM, Jeol 2000FX) by using bright field images and selected area diffraction patterns [122]. Because of the difficulties involved in manufacturing the TEM samples the imaging was done by Jeol Hightech co, Japan. The thermodynamic calculations were carried out with Thermo-Calc software [123].

6. RESULTS AND DISCUSSION

In this chapter the emphasis is placed on the formation and evolution of interfacial intermetallic compounds in the Sn-Cu-Ni system. The studies are carried out by utilizing both solid|liquid and solid|solid reaction couples. The effects of typical additional or impurity elements, the source of which can be either the bulk solder material (solder paste) or contact pad metallisations on the component as well as the PCB side, on the interfacial reactions are studied both experimentally and theoretically. The additional elements included here are Ag, Au, P, Fe, Zn, and Ti, which were alloyed to Sn and/or Cu. Detailed discussions are also given on the formation mechanisms of intermetallic compounds in soldering processes.

6. 1 Dissolution and intermetallic compound formation in liquid|solid diffusion couples

Differing markedly from solid-solid diffusion couples, where the growth of an intermetallic layer is slow, the formation of reaction layers can be very rapid if one of the contact materials is in a liquid state. In the latter case the dissolution rate of a solid metal in liquid solder has a significant effect on the growth kinetics of intermetallic compounds. In some liquid solder/conductor systems the intermetallic layers have been observed to build up within seconds [12], and thus the nucleation and growth of intermetallic compounds has to occur by some other mechanism than those that are operative in solid state diffusion. Therefore, the formation mechanisms of intermetallic compounds are discussed first. Then the ternary Sn-Ag-Cu system is presented and experimental results and discussions on the Sn-Cu-Ni system are provided. Finally, the effects of additional elements on the interfacial reactions are covered. Even though there are some characteristic differences between the systems dealt with in this thesis, the intermetallic reaction layers are formed, in principle, in three consecutive stages: dissolution, chemical reaction, and solidification, although the relative importance of each stage varies between the systems, depending mainly on the solubility of the conductor metal in liquid Sn.

6.1.1 Formation mechanisms of intermetallic compounds

The general sequence of events during a soldering operation can be described as follows. Immediately after the flux has removed the oxides (except in the case of Au) and permits metallurgical contact between the solder and the conductor metal, the contacted metal starts to dissolve into the molten solder. Initially, the rate of dissolution is high, particularly if the solder is not alloyed with the metal in question and therefore high (non-equilibrium) concentrations of solute elements can be realised locally. After a short period of time, the layer of molten solder that is adjacent to the contacted metal becomes supersaturated with the dissolved metal throughout the interface. Thermodynamically, at the local (metastable) equilibrium solubility, the solid IMC starts to form in this part of the solder [1]. The thickness of the IMC at this stage varies considerably between different systems. After the formation of the (first) IMC layer, the growth of the layer, as well as the formation of additional layers, occurs via solid-state diffusion. This sequence of events is presented in Fig. 6.1 by utilising the Sn-Cu system as an example. When the solid Cu surface becomes covered with liquid Sn, the dissolution of the Cu starts and the solid|liquid interface moves from its original position. The dissolution rate is high at this stage [57, 58]. The dissolved Cu atoms form a concentration profile in the liquid Sn, as shown with the hatched area in Fig. 6.1 (a). The dissolution continues until the Cu content at the interface has increased to the metastable solubility limit ($^{m}x_{Cu}^{L}$), which in the Sn-Cu system at 240°C is about 3.5 at-%. The stable solubility of Cu at this temperature is about 1.9 at-% and therefore a certain volume (dependent on the mobility of Cu in liquid Sn) of liquid is supersaturated [the double-hatched area in Fig. 6.1 (b)] and the chemical reaction between Cu and Sn atoms builds up the Cu_6Sn_5 layer. After the formation of a continuous layer of Cu_6Sn_5 (T_{mp}=415°C) at the interface, further growth and the formation of Cu_3Sn occur via solid-state diffusion [see Fig. 6.1 (c)]. It is to be noted that the analysis presented above is based on the assumption of the temperature being constant. However, the temperature varies as a function of time during reflow soldering. Since the solubility of Cu is a function of temperature (and thus also time), the formation mechanism is extremely complex. It has been pointed out that in most binary systems the growth kinetics of the intermetallic compounds (that form first at the

solid|liquid interface) is directly proportional to the dissolution rate of the solid metal in the liquid [124, 125]. On the other hand, the dissolution rate is proportional to the solubility and therefore those metals that have high solubility in liquid Sn (such as Au and Ag) dissolve rapidly and form a relatively thick intermetallic layer within a few seconds (Table VI.I).

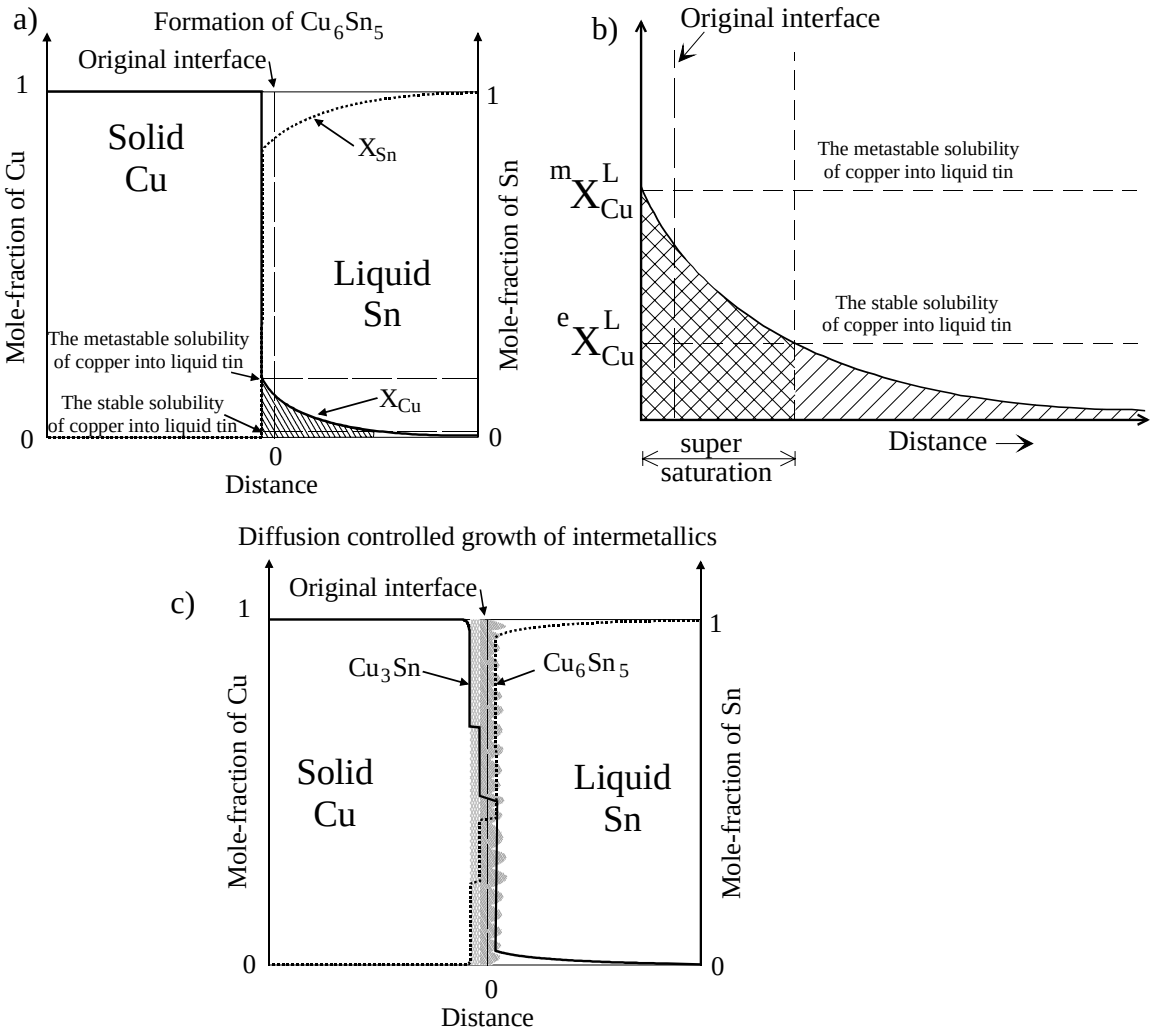

Figure 6.1: *The formation and growth of Cu_6Sn_5 and Cu_3Sn.*

On the contrary, the IMC thickness after reflow is extremely thin after the reflow process in those systems (such as Ni-Sn) in which the solubility (and dissolution rate) is small [45]. Unfortunately, apart from the data presented by R. J. Klein Wassink [see Fig. 6.2 (a)], experimentally measured dissolution rates are not widely available [45]. Therefore, the modelling of the dissolution process suggested by K. J. Rönkä can make use of the

knowledge of the phase diagram (stable or metastable solubilities) of a solder/conductor system for predicting the relative qualitative dissolution rates as a function of temperature and solder composition, despite the limited kinetic data available [125]. As can be seen from Fig 6.2 (b), the calculated dissolution rates (dots) are in good agreement with the experimental values (solid lines).

Table VI.I: *The layer thickness of the intermetallics formed by immersing pure conductor metals in eutectic Sn26Pb solder at 230°C for 10 and 100 seconds under RMA flux.*

Conductor metal	Intermetallic	Thickness / μm	
		10 s	100 s
Ni	Ni_3Sn_4	Indistinguishable	Indistinguishable
Cu	Cu_6Sn_5	0.5	1.0
Au	$AuSn_4$ (+Pb)	~10	~10

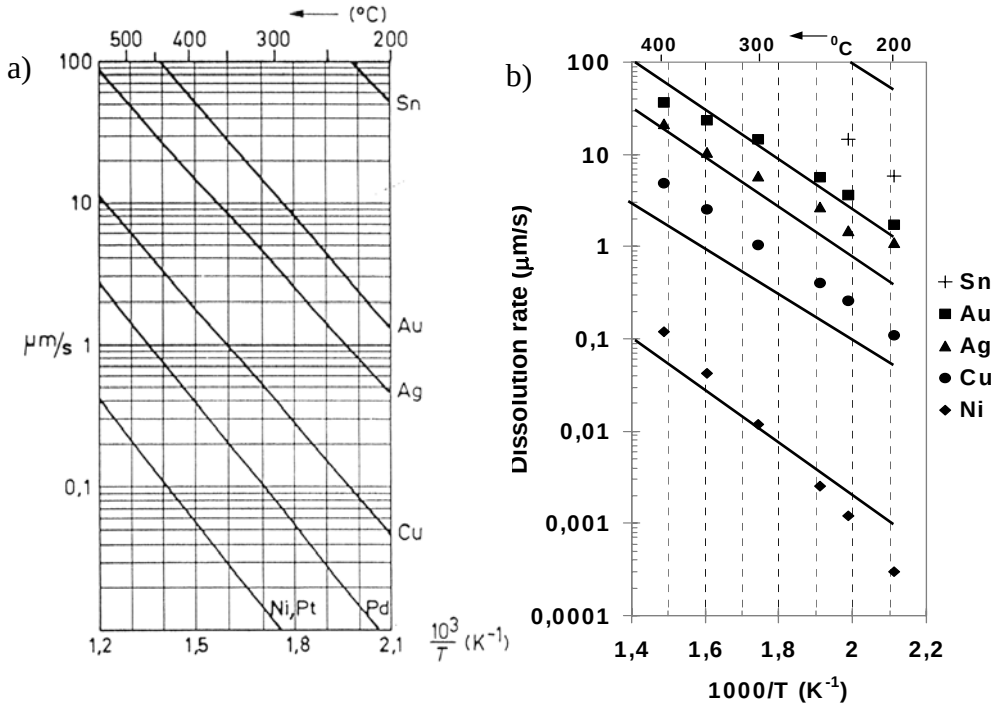

Figure 6.2: *(a) Dissolution rate of various metals in SnPb solder as a function of temperature [45] (b) Calculated dissolution rates of tin, gold, silver, copper, and nickel in SnPb solder as a function of temperature [125] compared with the data of Klein Wassink.*

There is some information available in the literature about the dissolution kinetics of common metallisations in Sn-based lead-free solders [126-129]]. Harris and Chaggar measured the IMC thickness and the thickness of dissolved Cu as a function of time and temperature in Sn37Pb, Sn0.7Cu, and Sn3.5Ag (wt-%) solders [129]. They found out that during the first few seconds the dissolution rate of Cu is high (~0.5-1µm/s) and that it slows down to 0.1-0.2 µm/s during the first minute, regardless of the solder. However, the dissolution rate was clearly fastest with Sn3.5Ag and slowest with Sn0.7Cu solder. This is reasonable, as the solubilities are higher in Sn3.5Ag than Sn37Pb (see Fig. 6.3.) and, on the other hand, the Cu alloying reduces the driving force for Cu dissolution to Sn0.7Cu solder [5]. In spite of the slowest dissolution rate, the observed IMC thickness was greatest with Sn0.7Cu solder.

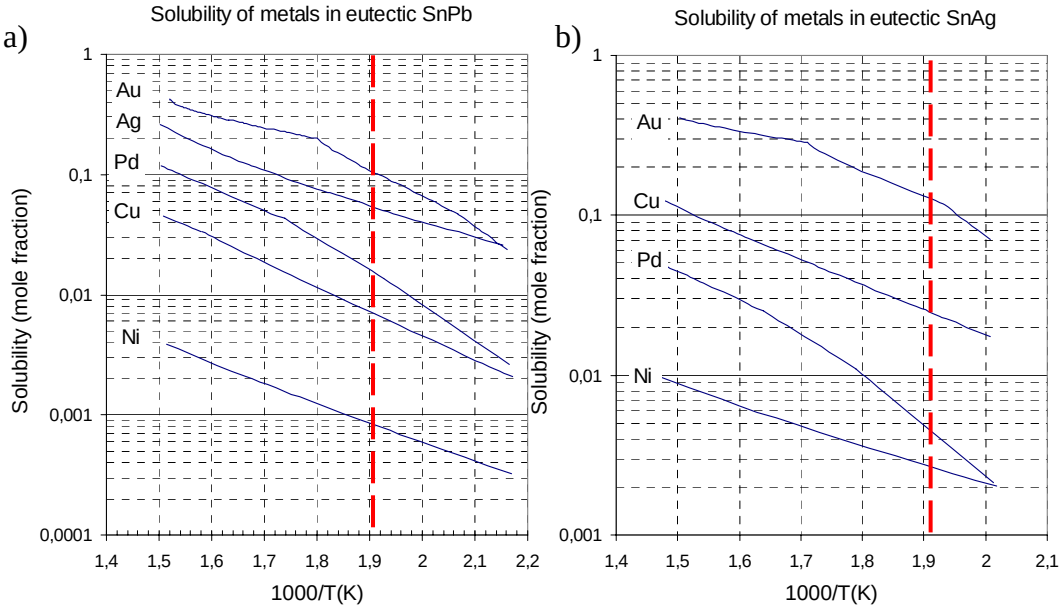

Figure 6.3: *Solubility of metals in (a) eutectic SnPb solder and (b) eutectic SnAg solder. T=250℃ marked with dashed red line. [5]*

The experimental observations in several conductor metal/solder systems where relatively thick intermetallic layers are formed during short bonding times cannot be explained by the nucleation and growth mechanisms operating in solid state [3, 130, 131]. For example, when copper wire is immersed in the eutectic Sn26Pb solder, the formation

of intermetallic compounds, η-Cu_6Sn_5 and/or ε-Cu_3Sn, directly from the solder is so fast that mechanisms other than those in the solid state must play a role. Therefore, it is expected that a thin layer of Cu_6Sn_5 (or Cu_3Sn, depending on the composition of the liquid solder) is formed rapidly via chemical reaction from the supersaturated melt at the Cu/liquid interface, as presented above. On the other hand, the solidification conditions are not easy to control in detail and they can vary even between the interconnections at different locations in a single component. This makes reliability predictions under different operating conditions difficult to carry out. In this chapter the intermetallic reactions between liquid Sn and a few typically used pure metallisations (Cu, Ni, Au, Ag) are discussed.

6.1.2 Sn-Ag-Cu and Sn-Cu-Ni systems

Currently, SnAgCu solders with near-eutectic compositions are considered the most promising candidates for the general-purpose replacement of tin-lead in SMT reflow processes [69]. It is well known that Ni/Au finishes are often utilised in both printed wiring boards (PWB) coatings and under bump metallisations (UBM) of components. Recently, Ni has also been used as an alloying element in solder pastes in an attempt to improve their reliability [132, 133]. Therefore, it is of interest to study the solid-liquid reactions where: i) tin is in local equilibrium with pure Cu or Ni, as well as with CuNi alloys of different Ni-to-Cu ratios; ii) Cu-alloyed Sn (or SnAg) reacts with pure Ni, and iii) Ni-alloyed Sn (or SnAg) reacts with pure Cu.

Sn-Cu-Ag system

The most promising lead-free alloys are primarily based on the Sn-Ag system [2]. In order to reduce the dissolution rate of metallisations and slightly reduce the melting temperature, SnAg solders are typically alloyed with small amounts (<0.7 wt-%) of copper [69]. The near-eutectic SnAgCu alloys, with an Ag content less than 4 wt-% and Cu content less than 1 wt-%, have a fatigue strength 3-4 times higher than $SnPb_{eut}$ alloys because of the interspersed Ag_3Sn and Cu_6Sn_5 particles providing resistance to dislocation movement [69].

The Sn-rich corner of the Sn-Ag-Cu system is characterised by the strong dependence of liquidus temperatures on the alloy composition. As can be seen from Fig. 6.4, even a slight increase in either the Ag or Cu content, resulting from, for example, dissolution increases the liquidus temperatures drastically. Figure 6.4 (b) shows the relative amount of phases as a function of temperature when the nominal composition is Sn 4.7Ag 1.7Cu (wt-%). It can be seen that the primary Cu_6Sn_5 crystals start to form at 265°C and Ag_3Sn at 245°C.

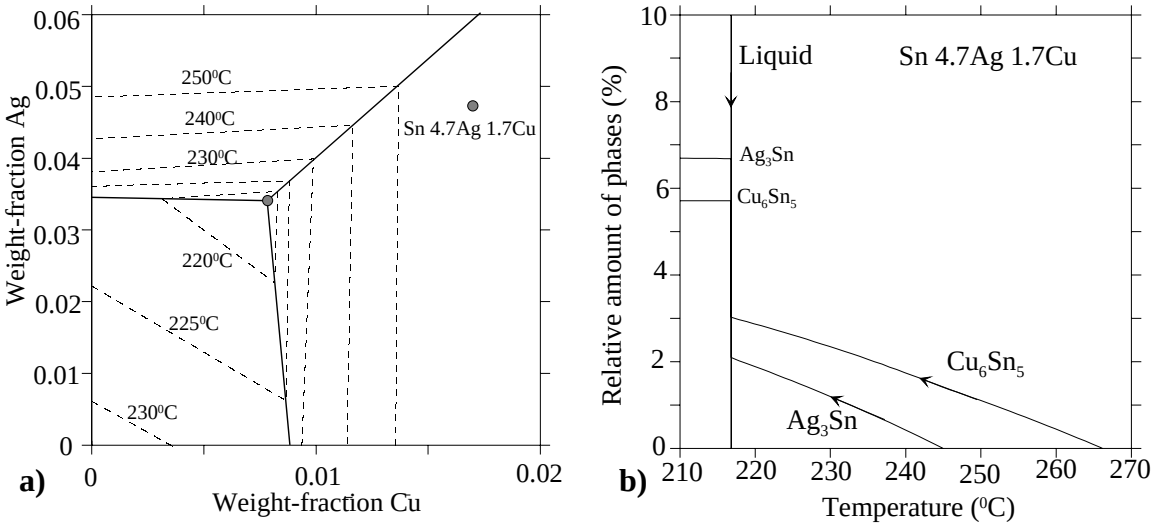

Figure 6.4: *a) Liquidus projections in the Sn-Ag-Cu system and b) Amount of phases as a function of temperature when the nominal composition is Sn 4.7Ag 1.7Cu (wt-%)[5].*

On the Phase Equilibria in the Sn-Cu-Ni System

Thermodynamic description of the Sn-rich part of the Sn-Cu-Ni system was carried out by using the assessed data of the binary systems: Ni-Cu[134], Sn-Cu [135], and Sn-Ni [136], as well as the published experimental isothermal sections at 235°C and 240°C [47, 70]. To obtain the additional data needed for evaluating the phase equilibria, several ternary Sn-Cu-Ni alloys and Sn|Cu, Sn|Ni and Sn|$NiCu_x$ diffusion couples were prepared. For the diffusion couple experiments, CuNi alloys were placed into quartz tubes with about 100 g solder for the annealing treatment. The diffusion couples and the ternary alloys were annealed at 240°C for different periods of time (up to 13,000 hours).

The two-phase equilibrium between liquid tin and the intermetallic compound Cu_6Sn_5 is of great technological interest in solder-substrate systems. It can be computed thermodynamically from the assessment of the ternary systems. Even though more complicated models are usually used in the calculations, simple thermodynamic models can be used to show how the calculation is performed and what are effective factors. The lattice ratio of Cu_6Sn_5 is practically constant. If we assume that the Ni atoms occupy the Cu sublattice sites randomly, the ternary intermetallic compound can be regarded as a binary regular solution phase $(Cu,Ni)_6Sn_5$ composed of Cu_6Sn_5 and Ni_6Sn_5 components. Then the molar Gibbs energy of the $(Cu,Ni)_6Sn_5$ (= IMC) will be

$$\begin{aligned} G_m^{IMC} &= (1-y)G^o_{Cu6Sn5} + yG^o_{Ni6Sn5} + \\ &aRT\left[y\ln y + (1-y)\ln(1-y)\right] + ay(1-y)I^{IMC}_{Cu,Ni} \end{aligned} \quad , \qquad (15)$$

where y is the site fraction of Ni atoms in the Cu sublattice, G^o_{Cu6Sn5} is the standard molar Gibbs energy of Cu_6Sn_5, G^o_{Ni6Sn5} is the standard molar Gibbs energy of the hypothetical component Ni_6Sn_5, a (= $x_{Cu} + x_{Ni} \equiv 6/11$) is the number of substitutional sites in the Cu sublattice, and $I^{IMC}_{Cu,Ni}$ is the interaction parameter, which can depend on composition and temperature. The chemical potential of the Cu_6Sn_5 and Ni_6Sn_5 components in $(Cu,Ni)_6Sn_5$ is therefore presented as

$$\begin{aligned} G_{Cu6Sn5} &= G^o_{Cu6Sn5} + aRT\ln(1-y) + aI^{IMC}_{Cu,Ni}y^2 \quad and \\ G_{Ni6Sn5} &= G^o_{Ni6Sn5} + aRT\ln y + aI^{IMC}_{Cu,Ni}(1-y)^2 \end{aligned} \qquad (16)$$

The condition for the two-phase equilibrium between Sn-rich liquid and $(Cu,Ni)_6Sn_5$ is

$$\begin{aligned} a\mu^L_{Cu} + (1-a)\mu^L_{Sn} &= G_{Cu6Sn5} \quad and \\ a\mu^L_{Ni} + (1-a)\mu^L_{Sn} &= G_{Ni6Sn5} \end{aligned} \qquad (17)$$

Because the solubility of both Cu and Ni in liquid Sn is limited, Sn-rich liquid is dilute ($x_{Sn}^{L} \approx 1,\ 1-x_{Cu}^{L} \approx 1,\ 1-x_{Ni}^{L} \approx 1$) and can be described by a regular solution model, and therefore the chemical potentials in Equation (17) can be calculated as

$$\begin{aligned} \mu_{Cu}^{L} &\approx \mu_{Cu}^{o,L} + RT\ln x_{Cu}^{L} + I_{Sn,Cu}^{L} \quad \textit{and} \\ \mu_{Ni}^{L} &\approx \mu_{Ni}^{o,L} + RT\ln x_{Ni}^{L} + I_{Sn,Ni}^{L} \end{aligned} \tag{18}$$

where $\mu_{Cu}^{o,L}$ and $\mu_{Ni}^{o,L}$ are the standard chemical potentials of pure liquid Cu and Ni, $I_{Sn,Cu}^{L}$ and $I_{Sn,Cu}^{L}$ are the interaction parameters in liquid. By assuming that all the interaction parameters are constant, Equations (15)-(18) will lead to the distribution coefficient of Ni between liquid solder and Cu_6Sn_5

$$\begin{aligned} k_{Ni}^{L/IMC} &= \frac{x_{Ni}^{L}/x_{Cu}^{L}}{x_{Ni}^{IMC}/x_{Cu}^{IMC}} = \frac{(1-y)x_{Ni}^{L}}{yx_{Cu}^{L}} = \exp\left(\frac{Q}{aRT}\right) \quad \text{where} \\ Q &\approx \left(G_{Cu6Sn5}^{o} - G_{Ni6Sn5}^{o}\right) - a\left(\mu_{Cu}^{o,L} - \mu_{Ni}^{o,L}\right) - \left(I_{Sn,Cu}^{L} - I_{Sn,Ni}^{L}\right) + aI_{Cu,Ni}^{IMC}(2y-1) \end{aligned} \tag{19}$$

The values of the variables in the equations given above can be obtained by fitting the regular models (both $(Cu,Ni)_6Sn_5$ and liquid) with the calculated Gibbs energies in certain composition and temperature ranges, which are provided by the thermodynamic assessment of the Sn-Cu-Ni system.

Reactions between pure Sn and CuNi alloys

When studying the formation of intermetallic compounds with the help of Sn|$CuNi_x$ alloy diffusion couples, microstructurally and kinetically interesting behaviour was observed. Fig. 6.5 shows how the average thickness of the reaction layer varies as a function of the Ni content of the binary substrate alloy immersed in molten Sn for 10 minutes at 240°C. The alloys with an Ni content of about 10 at-% exhibit the fastest reaction rate, which is many times higher than those obtained with pure copper or nickel. In addition, the reaction zone is composed of two different morphologies. A continuous uniform layer of the intermetallic compound (uniphase) can be observed in contact with the CuNi alloy.

On the top of the uniphase layer there is a two-phase layer containing IMC tubes and fibres, which are embedded in the tin matrix. The thickness of the two-phase layer is strongly dependent on the composition of the alloy (i.e. Cu-to-Ni ratio). In the samples with a high reaction rate the reaction layer is mainly composed of the two-phase layer and the thickness varies considerably.

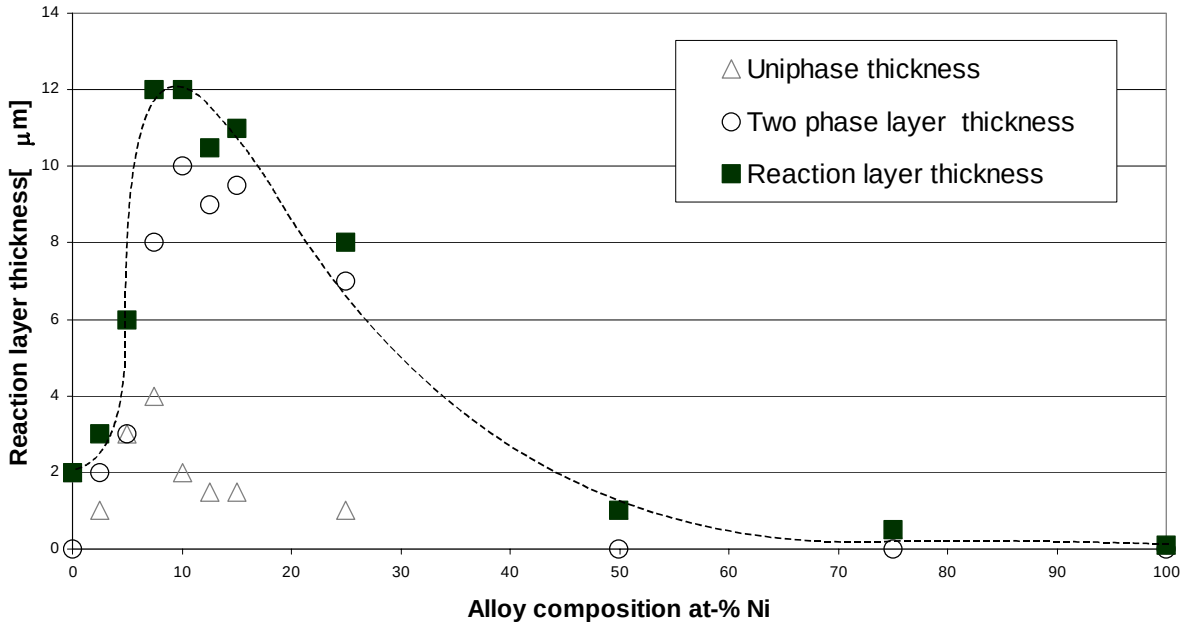

Figure 6.5: *Reaction layer thickness of different Sn|Cu-Ni diffusion couples at 240℃ for 10 min.*

Figure 6.6 (a-d) shows the typical microstructures of the reaction layers when high-purity Cu, CuNi alloys with two different Ni contents (2.5 and 15 at-%), and high-purity Ni were immersed in molten Sn for 10 minutes at 240°C. In the case of the 97,5Cu2,5Ni alloy [see Fig. 6.6(b)], the thickness of the intermetallic layer is relatively small but the morphology differs slightly from that normally observed in the Sn-Cu system [see Fig. 6.6(a)]. As can be seen from Fig. 6.6(d), the thickness of the $(Ni,Cu)_3Sn_4$ is very small. On the other hand, in the case of the 85Cu15Ni alloy the thickness of the layer is remarkably large and the morphology of the intermetallic layer differs from the typical scallop-like appearance of Cu_6Sn_5. The layer clearly exhibits two different morphologies: a uniphase Cu_6Sn_5 layer next to the substrate followed by a two-phase zone.

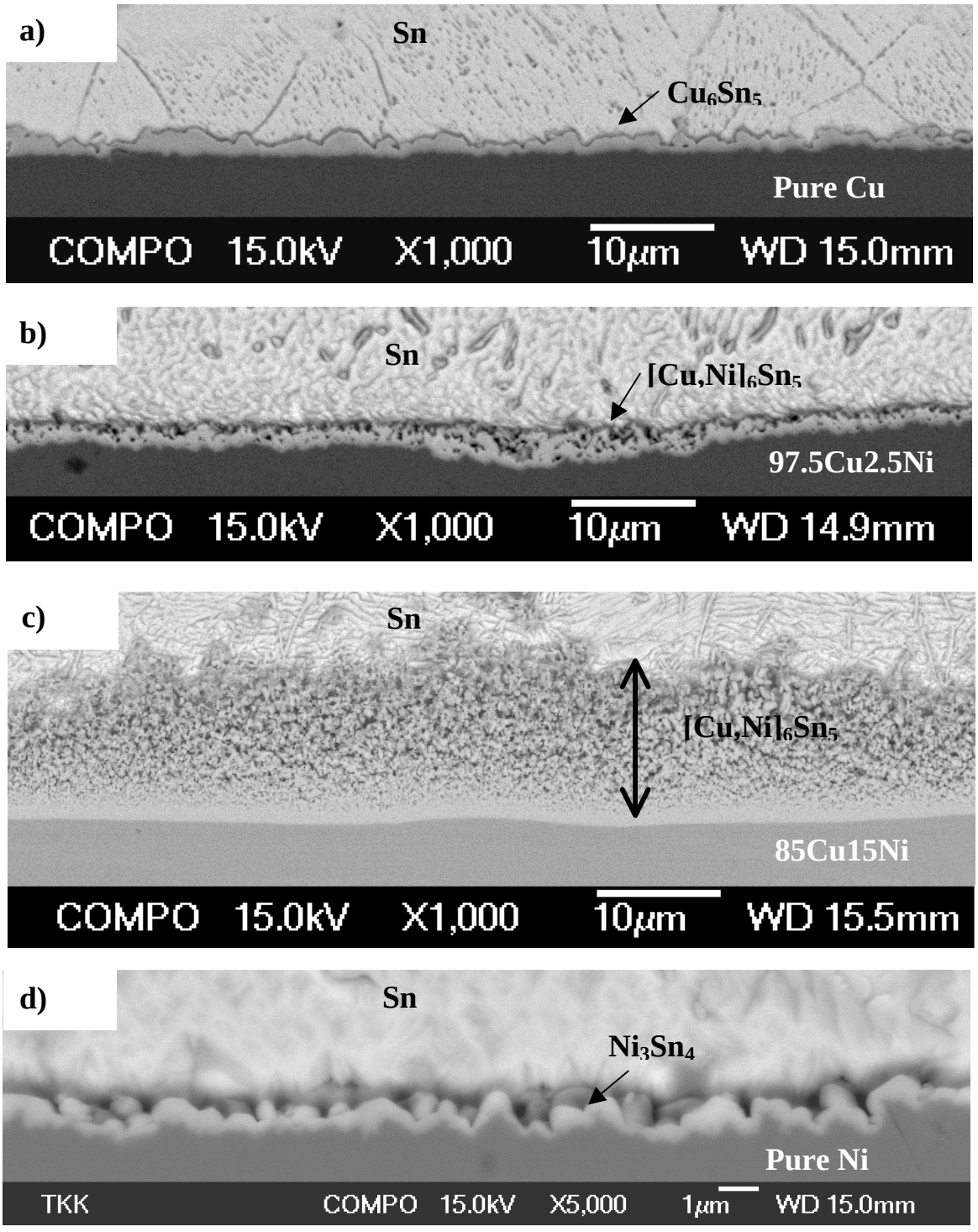

Figure 6.6: *(a) Pure Cu/Sn, (b) 97.5Cu2.5Ni/Sn, (c) 85Cu15Ni/Sn, and (d) Pure Ni/Sn (higher magnification) diffusion couples annealed at 240℃ for 10 min.*

More detailed SEM/EDS observations revealed that the second layer is composed of the Cu_6Sn_5 tubes embedded in the tin matrix [see Fig. 6.7, which is from the same sample as in Fig. 6.6 (c) but more heavily etched]. The corresponding microstructures containing the same features, i.e. hexagonal tubes or fibres filled with solder alloy, have also been reported elsewhere [47].

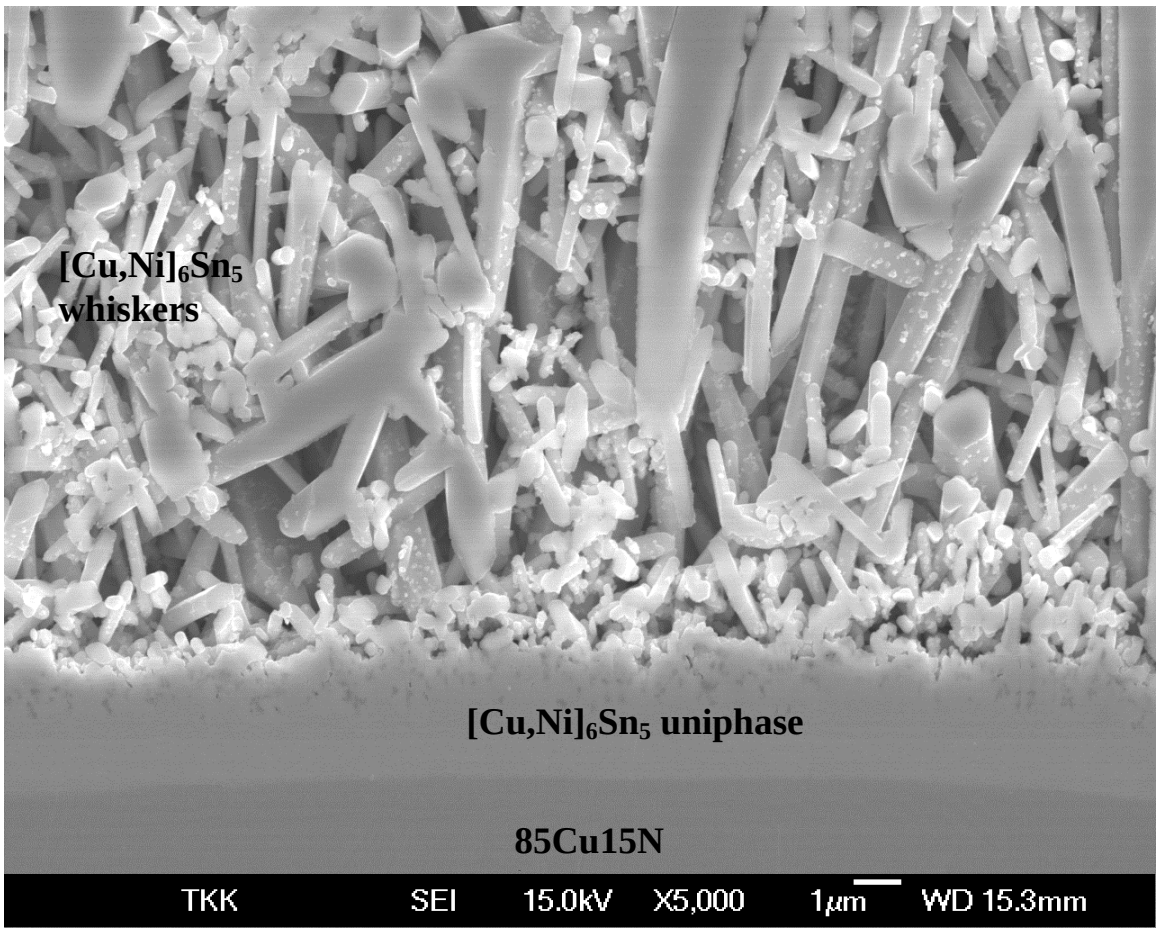

Figure 6.7: *85Cu15Ni/Sn diffusion couple annealed at 240℃ for 10 min. More heavily etched than Fig. 6.6 (c).*

The two-phase structure can be seen more clearly in Fig. 6.8 (b), where the sample was annealed at 240°C for 60 minutes. The uniphase layer is of the same thickness as after 10 minutes' immersion. However, the thickness of the two-phase layer has increased markedly. On the other hand, when the sample was annealed for only 1 minute at 240°C [see Fig. 6.8(a)], the uniphase is clearly observable but the two-phase layer is very thin.

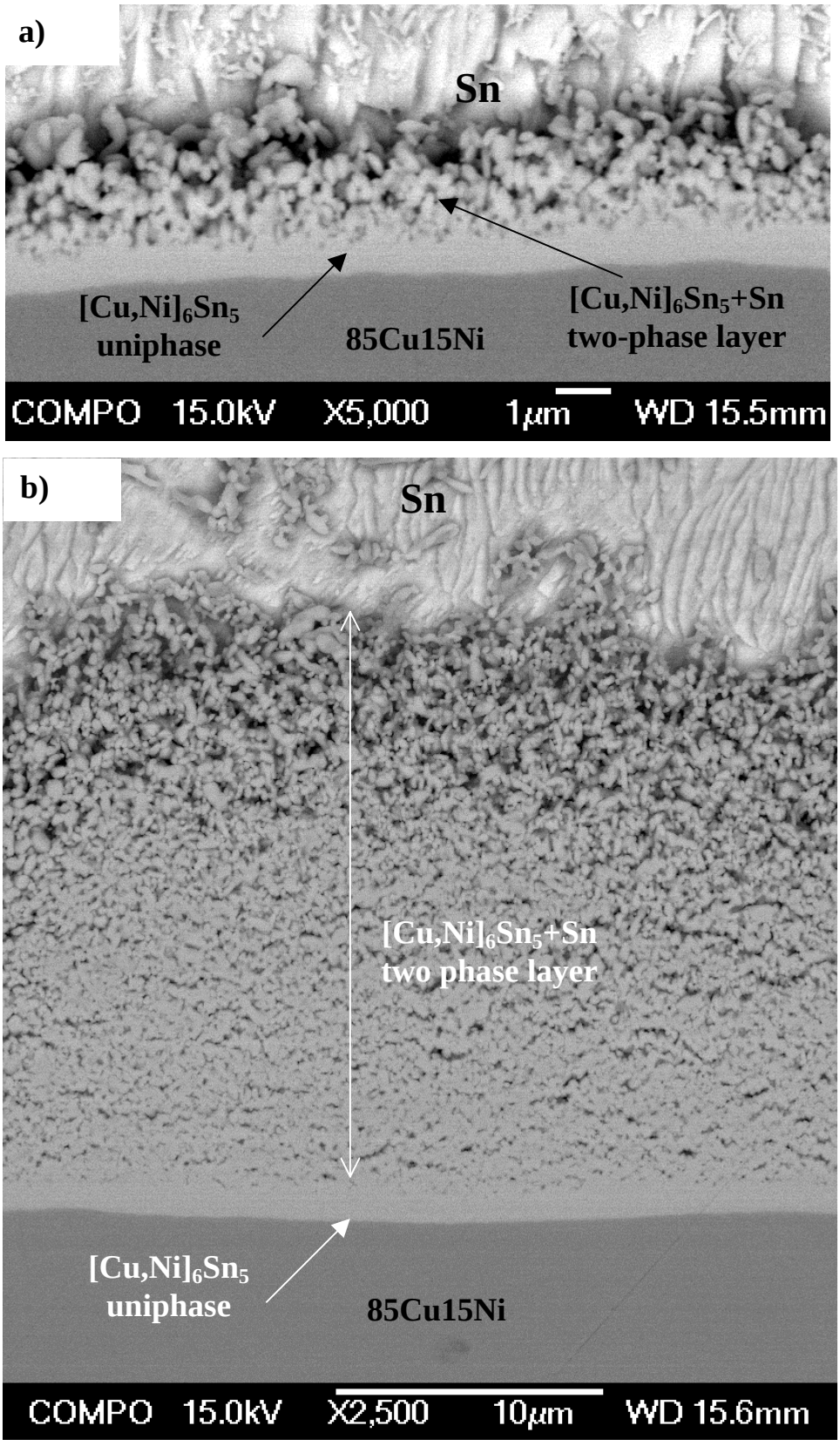

Figure 6.8: *85Cu15Ni/Sn diffusion couple annealed at 240℃ for (a) 1 min and (b) 60min.*

The chemical microanalyses of the reaction layers in the Sn|$CuNi_x$ diffusion couples reveal that the intermetallic phase (both the uniphase and the IMC needles in the two-phase layer) is $(Cu,Ni)_6Sn_5$. The structure of this phase corresponds to the binary Cu_6Sn_5 compound where Ni atoms have substituted some of the Cu atoms, as also reported by other authors [73, 137-139]. There are some variations in the Cu-to-Ni ratio of the intermetallic compounds with the different substrates studied. Typically, the Cu-to-Ni ratio was close to (or slightly more Ni than) that of the base alloy. The existence of the $(Cu,Ni)_6Sn_5$ compound and solubility even up to 50 at-% of Ni in the Cu sublattice at 220°C has also been reported earlier [29]. Similar results were obtained when the $(Cu,Ni)_6Sn_5$ layer was formed in the reaction between Sn-rich solders and SnCuNi alloys [89]. Moreover, a ternary 44Sn27Cu29Ni phase has also been identified at 240°C [47]. However, the growth kinetics of the suggested 44Sn27Cu29Ni compound is very slow and therefore during the relatively short periods of time used in soldering only metastable $(Cu,Ni)_6Sn_5$ compounds of different Cu-to-Ni ratios can form.

On the basis of the above-mentioned results, together with the results from the long-term diffusion couple experiments, as well as other published information [29, 47, 70, 89, 140], a metastable isothermal section (Fig. 6.9) of the Sn-Cu-Ni system can be constructed at 240°C. This metastable diagram does not include either the solid miscibility gap in the binary Cu-Ni system or the ternary 44Sn27Cu29Ni compound (τ) observed at this temperature. The phase equilibria on the CuNi-rich side of the system at temperatures below 300°C are not well known because of the extremely low diffusion and reaction kinetics [29, 47]. The phase separation between Cu_3Sn and Ni_3Sn has been observed at higher temperatures [34, 141] and the thermodynamic assessment shows that the high-temperature phases can be stable at these temperatures in the ternary region [36, 37]. However, these compounds were not observed in the diffusion couples, except when very long (> 1000 hours) annealing times were used. Therefore, the phase equilibria in this area are drawn with dashed lines. The $(Cu,Ni)_6Sn_5$ and $(Ni,Cu)_3Sn_4$ intermetallics can be considered line compounds, since they exist in narrow composition ranges in the binary systems. The results presented by Lin et al. indicate that the solubility of Cu in

Ni_3Sn_4 and Ni_3Sn_2 is 10 and 36.5 at-%, respectively [70]. On the other hand, Oberndorff has reported smaller solubility values, which are 7 and 11-17 at-% [47].

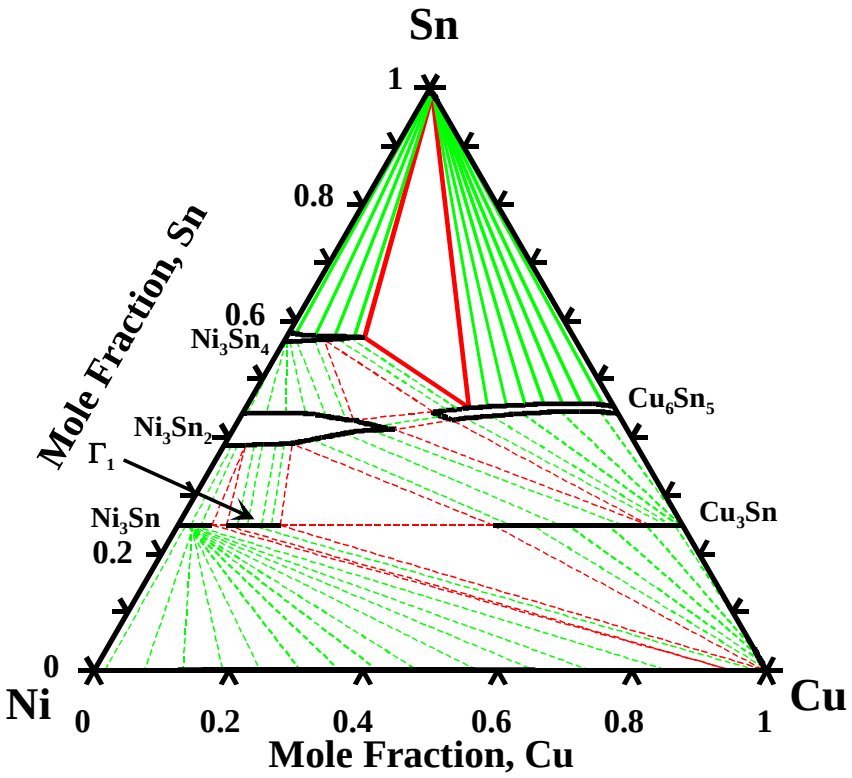

Figure 6.9: *Calculated metastable equilibria of the Sn-Cu-Ni system at 240°C[5].*

The metastable diagrams are best applicable to predicting the reactions, which occur during soldering, because of the short periods of time used. But even during accelerated testing or in the use of soldered assemblies, the ternary compound or the Ni-rich compounds are not likely to form. Hence, in order to explain the sequence of interfacial reactions between Cu-containing solders on Ni metallisations, as well as Ni-containing solder reactions in contact with Cu during soldering, detailed information on the phase equilibria, i.e. the activities of the components in tin-rich liquid solutions, is needed. What is especially important is the position of the apex of the three-phase triangle [$(Ni,Cu)_3Sn_4$ + $(Cu,Ni)_6Sn_5$ + Liquid] as a function of temperature. The Sn-rich corner of the isothermal section of the Sn-Cu-Ni phase diagram at 240°C is presented in Figure 6.10.

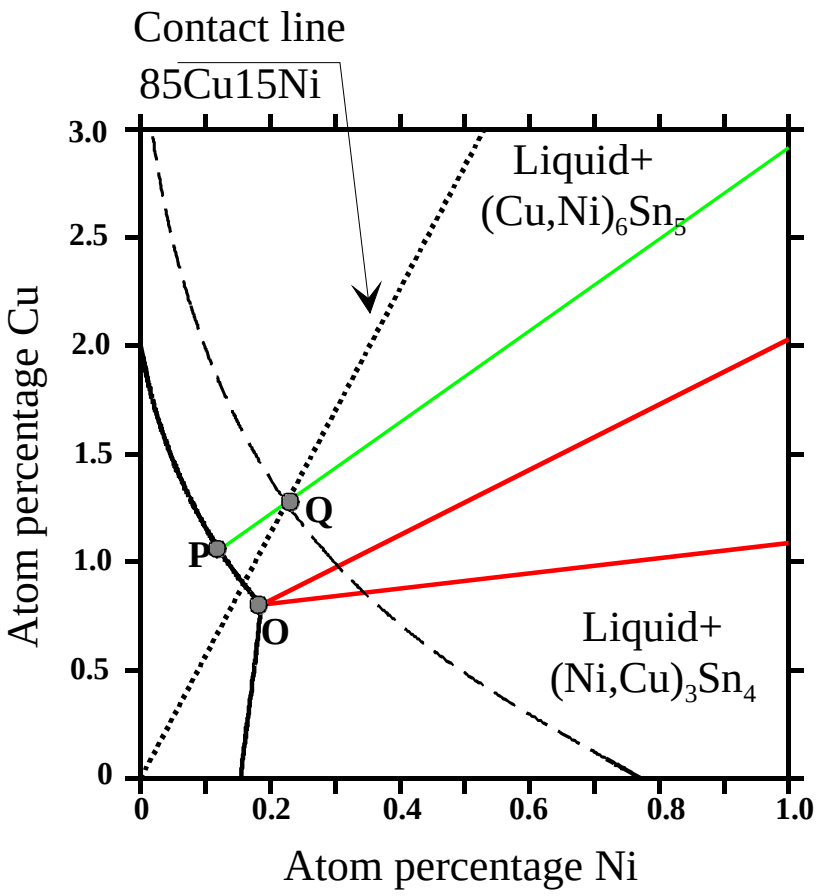

Figure 6.10: *Tin-rich corner of the optimised metastable phase diagram at 240℃[5].*

The one-phase liquid region (on the left) is bordered by the two-phase regions [$(Ni,Cu)_3Sn_4$ +Liq] and [$(Cu,Ni)_6Sn_5$ +Liq]. The two-phase boundaries intersect at the apex of the three-phase triangle denoted by the point O. The dashed curve cutting the contact line at the point Q indicates the metastable solubilities of CuNi alloys in liquid Sn. This metastable curve was calculated by suspending all the intermetallic phases. Hence, the composition of the liquid in local metastable equilibrium with solid Cu-Ni metallisation is determined by the metastable solubilities of the Cu and Ni atoms. These solubility values also determine the maximum driving forces for the formation of solid $(Cu,Ni)_6Sn_5$ or $(Ni,Cu)_3Sn_4$ intermetallics, as well as the mobilities of the Cu and Ni atoms in the liquid solder. Therefore, the thickness of the intermetallic compound(s) formed within the first few seconds is dependent on the metastable solubilities and the mobilities of the atoms. Since it is reasonable to assume that dissolved Cu and Ni atoms diffuse in the liquid at approximately the same rate, i.e. their diffusion coefficients in the

liquid are not markedly different (about 10^{-5} cm^2/s) [80, 142, 143], their concentration gradients are determined mainly by the metastable solubilities. When the local metastable solubility denoted by the intersection point Q (in Fig. 6.10, see Table VI.I) is reached at the interface, the solid $(Cu,Ni)_6Sn_5$ compound layer will nucleate on the Cu-Ni metallisation. The composition of the $(Cu,Ni)_6Sn_5$ reaction layer and that of the liquid (point P in Fig. 6.10, see Table IV.I) in local equilibrium with the reaction layer can be read from the ends of the tie-line passing the point Q. Since the diffusion of Cu and Ni atoms in the solid reaction layer, i.e. the uniphase layer, is very slow, the thickness of the initially formed $(Cu,Ni)_6Sn_5$ layer is controlled by the amounts of Cu and Ni atoms available on the liquid side of the interface.

Table VI.I *Calculated compositions of points O, P, and Q at 240℃*

Points (see Fig. 6.10)	Cu content (at-%)	Ni content (at-%)
Point O	0.80	0.19
Point P	1.05	0.12
Point Q	1.30	0.23

In order to explain the increase in the thickness of the intermetallic layer when Cu is alloyed with Ni, the effect on the dissolution rate and solubility must be considered. As can be seen from Figure 6.10, according to the thermodynamic assessment both the stable and metastable solubilities are reduced with the addition of Ni to Cu. In order to obtain data about the dissolution rate, a few experiments were performed which compared the amount (thickness) of dissolved metallisation between pure Cu and Cu12.5Ni as a function of time. The immersion times in liquid Sn (T=240°C) that were used were 1, 10, and 30 minutes. As can be seen from Fig. 6.11, the thickness of the Cu_6Sn_5 layer is almost the same in all samples with pure Cu (left) but changes markedly when Cu12.5Ni alloy is used (right). So even after 30 minutes the thickness of the pure Cu_6Sn_5 is only about 1µm, while that of the $(Cu,Ni)_6Sn_5$ is almost 10 µm. On the other hand, as much as about 200µm of Cu has dissolved from Cu to liquid Sn during the 30 minutes of immersion [see Fig. 6.12(a)]. It is to be noted that here a relatively large volume of liquid Sn (~200g) was used in order to prevent saturation. Figure 6.13 shows the measured [see Fig. 6.12(b)] average dissolution rates of pure Cu and Cu12.5Ni as a function of time.

Although the IMC thickness is much greater when using the Cu12.5Ni alloy, the dissolution rate is clearly lower than that of pure Cu. Therefore neither the effect of Ni on the magnitude of solubility nor the dissolution rate can explain the increased reaction rate observed in CuNi alloys. The effect of saturation can be seen from Figure 6.14 (Cu12.5Ni/Sn at 240°C for 30 minutes), where the reaction layer is considerably higher at the solder meniscus than further from the surface of the bath.

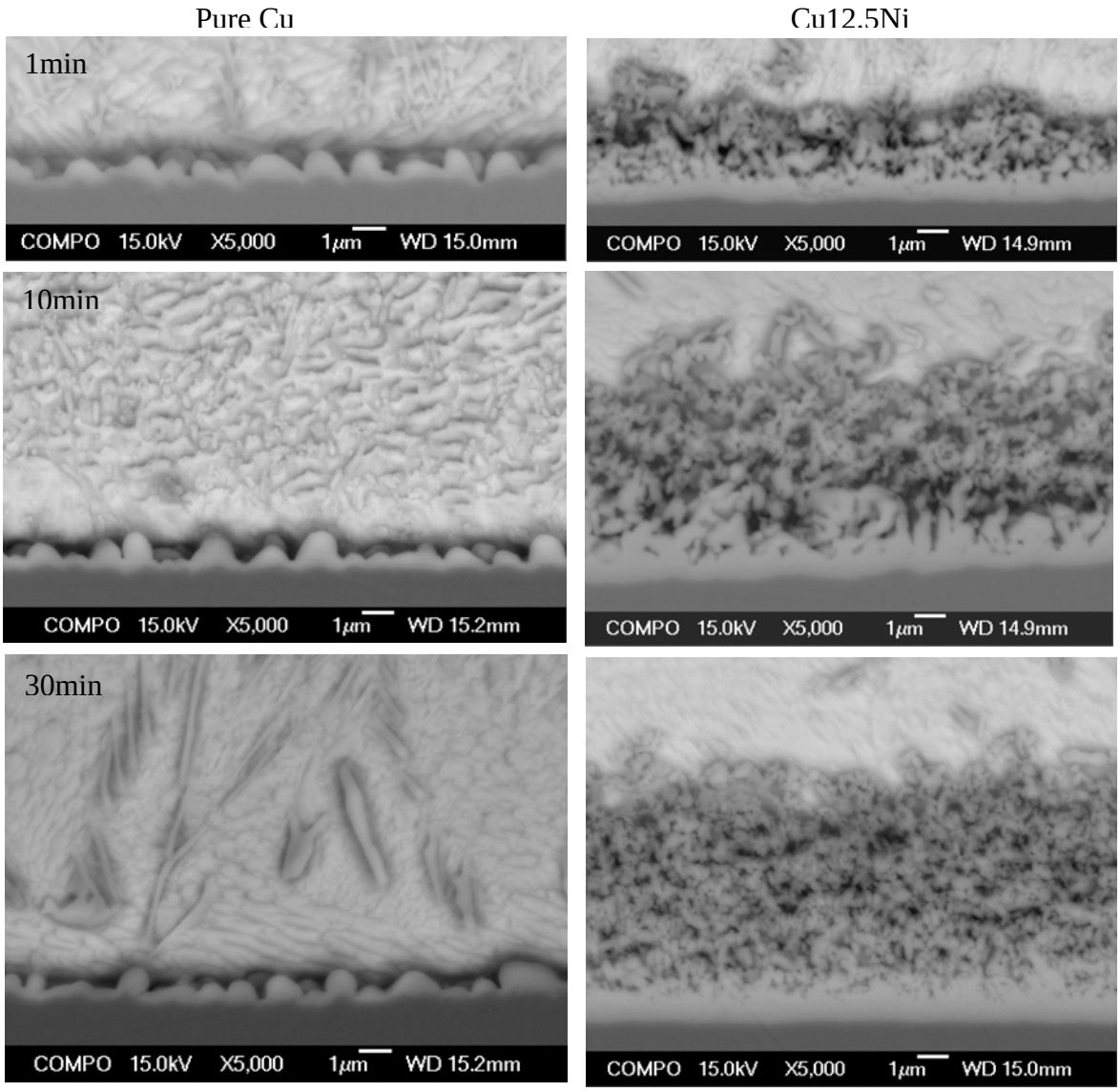

Figure 6.11: *Intermetallic layers in Pure/Sn (left) and 87.5Cu12.5Ni/Sn (right) diffusion couples annealed at 240℃ for 1 (top), 10 (middle), and 30 (bottom) minutes.*

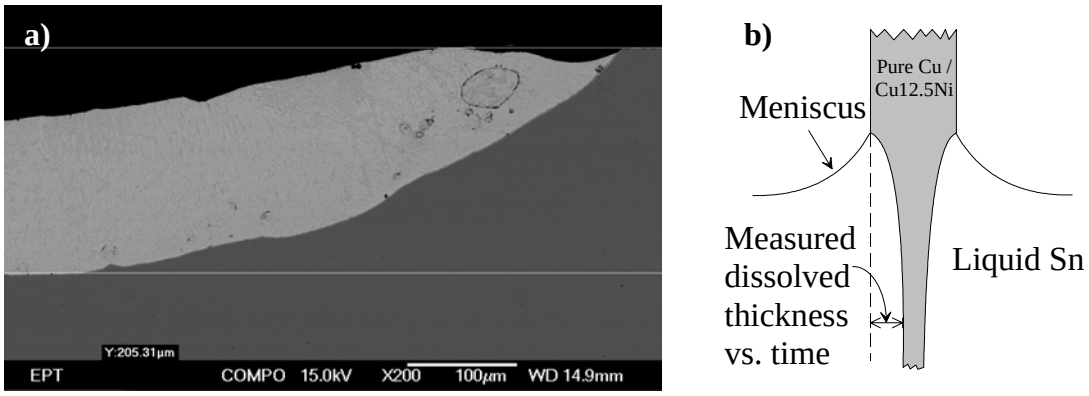

Figure 6.12: *(a) Amount of dissolved Cu after 30 min immersion in Sn at 240℃ (tilted 90° clockwise), and (b) schematic representation of the measurement setup.*

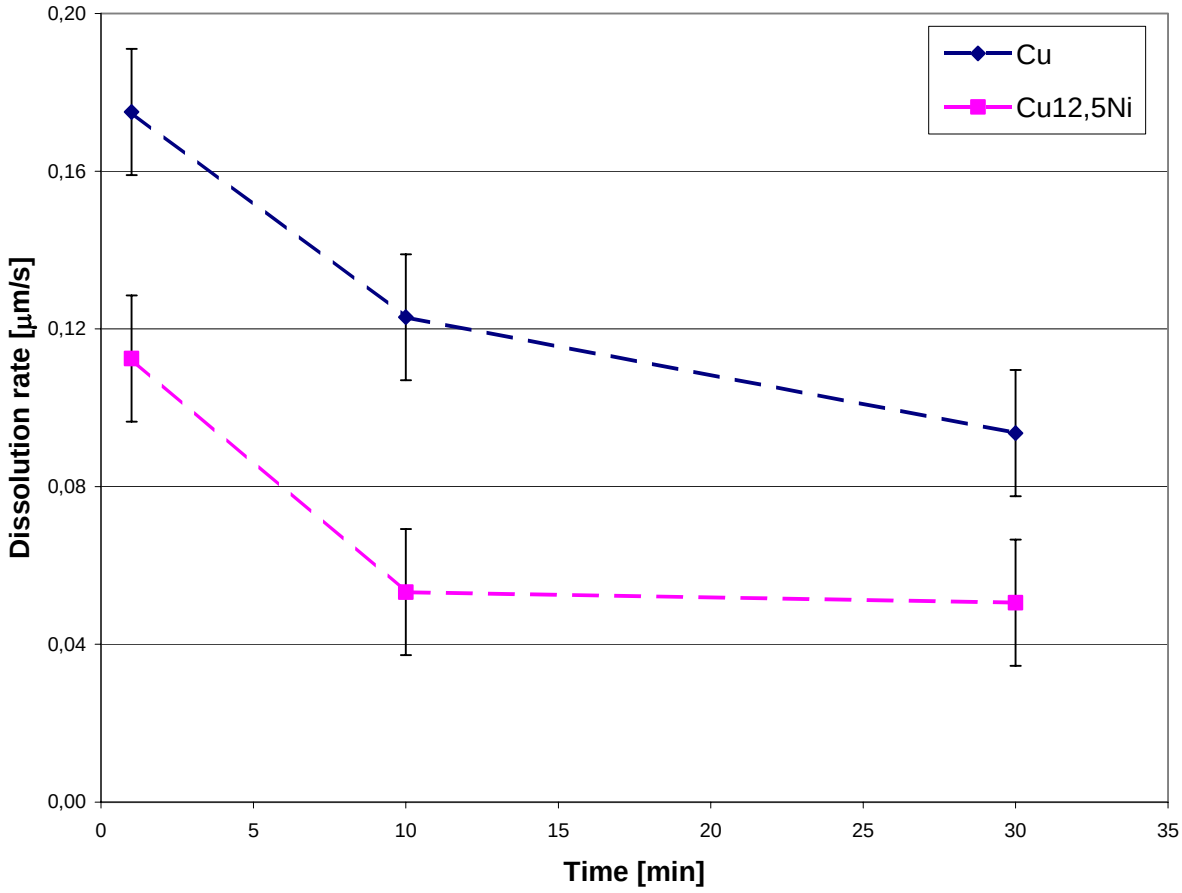

Figure 6.13: *Measured average dissolution rates of pure Cu and Cu12.5Ni in liquid Sn at 240℃ as a function of time.*

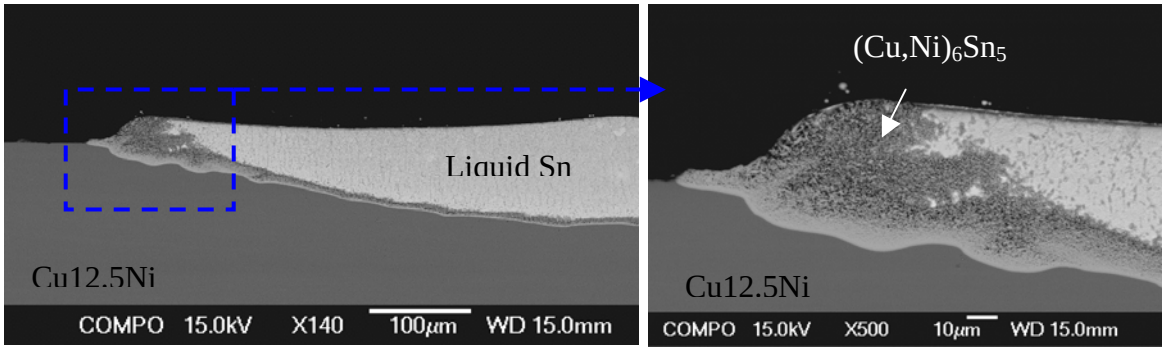

Figure 6.14: *Effect of saturation on the IMC thickness at the meniscus Cu12.5Ni/Sn at 240 ℃ for 30 minutes.*

During the cooling of the liquid the reactions depend primarily on the composition of the liquid next to the $(Cu,Ni)_6Sn_5$ uniphase layer. For example, in the diffusion couple between the liquid Sn and 85Cu15Ni metallisation the primary $(Cu,Ni)_6Sn_5$ crystals nucleate on and grow from the $(Cu,Ni)_6Sn_5$/liquid interface, generating long intermetallic needles or solder-filled tubes, which constitute, together with the tin matrix, the two-phase reaction layer as seen in Fig. 6.7. Using the optimised thermodynamic data, the evolution of different phases in the alloy system with the composition P (see Fig. 6.10) can be evaluated as a function of temperature. The results of the calculations presented in Fig. 6.15 (a-d) show that due to the low solubility of nickel in liquid tin the solidification starts with the formation of $(Cu,Ni)_6Sn_5$ at about 231°C and then continues by simultaneous formation of $(Cu,Ni)_6Sn_5$ and bct-Sn [Liq + $(Cu,Ni)_6Sn_5$ $\rightarrow$ bct-Sn + $(Cu,Ni)_6Sn_5$] between 229°C and the eutectic temperature of the binary Cu-Sn system, as can be seen form Fig. 6.15 (a). It is also to be noted that, as the solubility of Ni in solid Sn is very small and the Ni content of the liquid approaches zero during cooling, all the dissolved Ni atoms should be incorporated into $(Cu,Ni)_6Sn_5$. On the other hand, because of the small solubility, the Ni content beside the IMC can be higher than that indicated by point P and quasi-peritectic solidification ($L+Ni_3Sn_4 \rightarrow Cu_6Sn_5+Sn$) is possible.

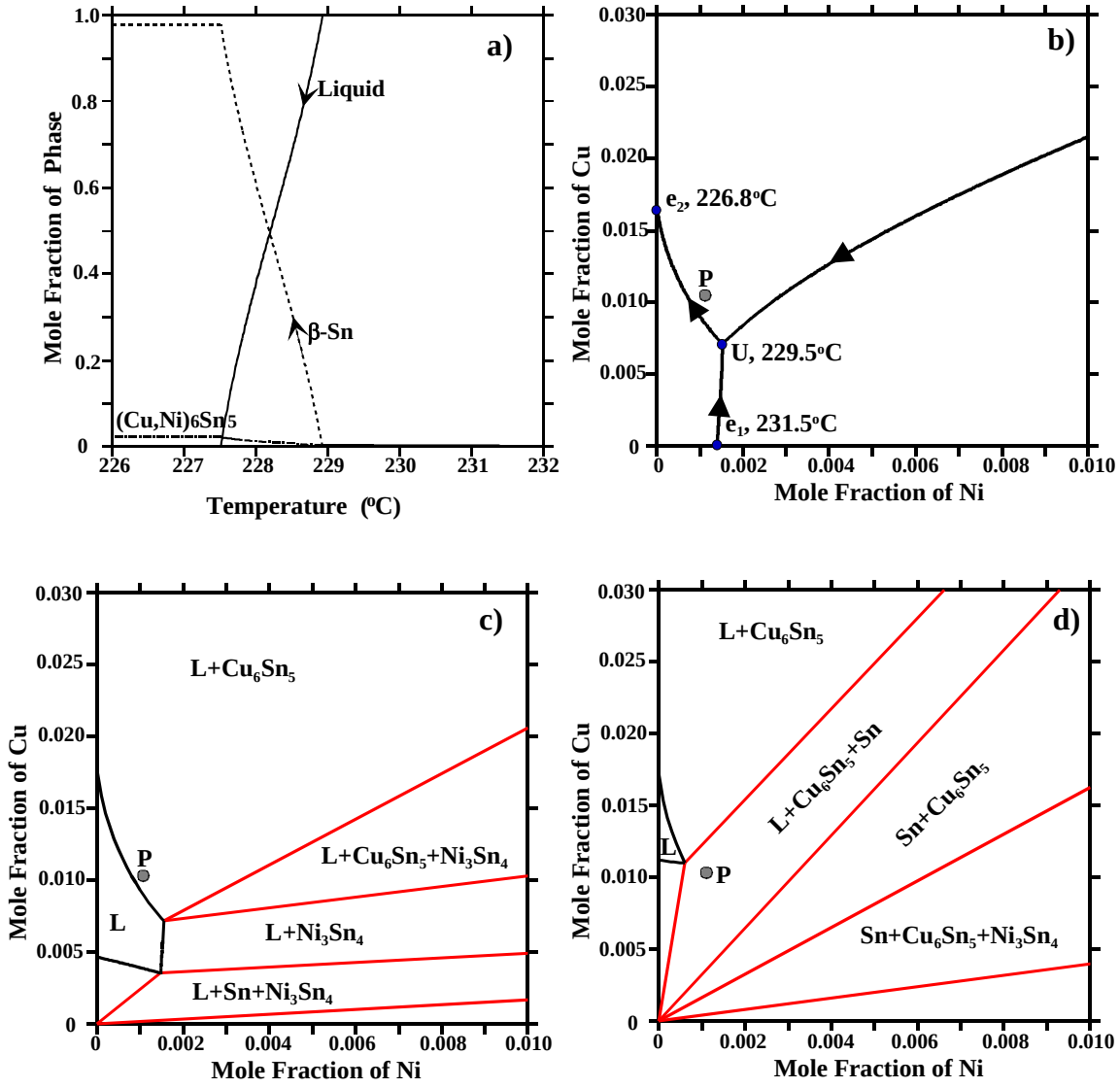

Figure 6.15: *(a) Relative amount of phases during cooling when the nominal composition is Sn1.05Cu0.12Ni (at-%), i.e. point P in Figure 6.10, (b) liquidus projection from the Sn-rich corner of the Sn-Cu-Ni system, and (c-d) isothermal sections from the Sn-rich corner of the Sn-Cu-Ni system one degree above (230.5 ℃) as well as below (228.5 ℃) the ternary invariant point U (L+Ni_3Sn_4→Cu_6Sn_5+Sn) respectively [5].*

It is obvious that the longer the CuNi metallisation is immersed in the liquid, the further the Cu and Ni atoms will have migrated. Therefore, the two-phase reaction layer is much thicker with longer immersion times. On the other hand, when the contact line (for example 25Cu75Ni) passes the point O from the right-hand side (Fig. 6.10), the Ni-to-Cu

ratio is high enough for the formation of a thin $(Ni,Cu)_3Sn_4$ layer, instead of $(Cu,Ni)_6Sn_5$. Another parameter that has a significant effect on both the morphology and the thickness of the intermetallic reaction layer is the cooling rate. The results presented above were obtained from samples where the cooling rate was high, i.e. the metal strips were removed from the solder bath and only a small amount of liquid Sn, containing some dissolved Cu and Ni, was left on the surface of the strips. Therefore another set of experiments was carried out in which the metal strip was allowed to cool down in the solidifying Sn bath. Two different relatively slow cooling rates (after 10 min immersion) from 240°C down to 225°C were used (4°C/min and 1.3°C/min). It is to be noted that because of the slow cooling rates the total times above liquidus were about 12 and 16 minutes, respectively, and therefore the thicknesses of the reaction layers are not comparable to the results presented above.

As can be seen from Fig. 6.16, the interfacial microstructure after slow cooling (1.3°C/min) is very uneven. On the Sn side, close to the reaction layer, the microstructure is composed of eutectic-type regions between Sn crystals. When comparing the microstructures between pure Cu and Cu12.5 Ni after 10 mins of immersion in liquid Sn at 240°C and cooling at the rate of 4°C/min (i.e. total liquid time about 12 minutes), it can clearly be seen [see Fig. 6.17(a-f)] that there are marked differences. First, the eutectic-type regions are observed further from the interface with pure Cu than Cu12.5Ni. Secondly, the amount of eutectic structure near the interface is higher with pure Cu than Cu12.5Ni [see Fig. 6.17 (c) and (d)]. These facts support the findings above, that the dissolution rate of pure Cu is higher than that of Cu12.5Ni. Finally, as expected, the total reaction layer thickness is considerably higher with Cu12.5Ni [see Fig. 6.17 (e) and (f)]. However, the uniphase layer has about the same thickness in both samples. On the basis of these results it can be concluded that a significant part of the two-phase layer is formed during cooling from the supersaturated liquid.

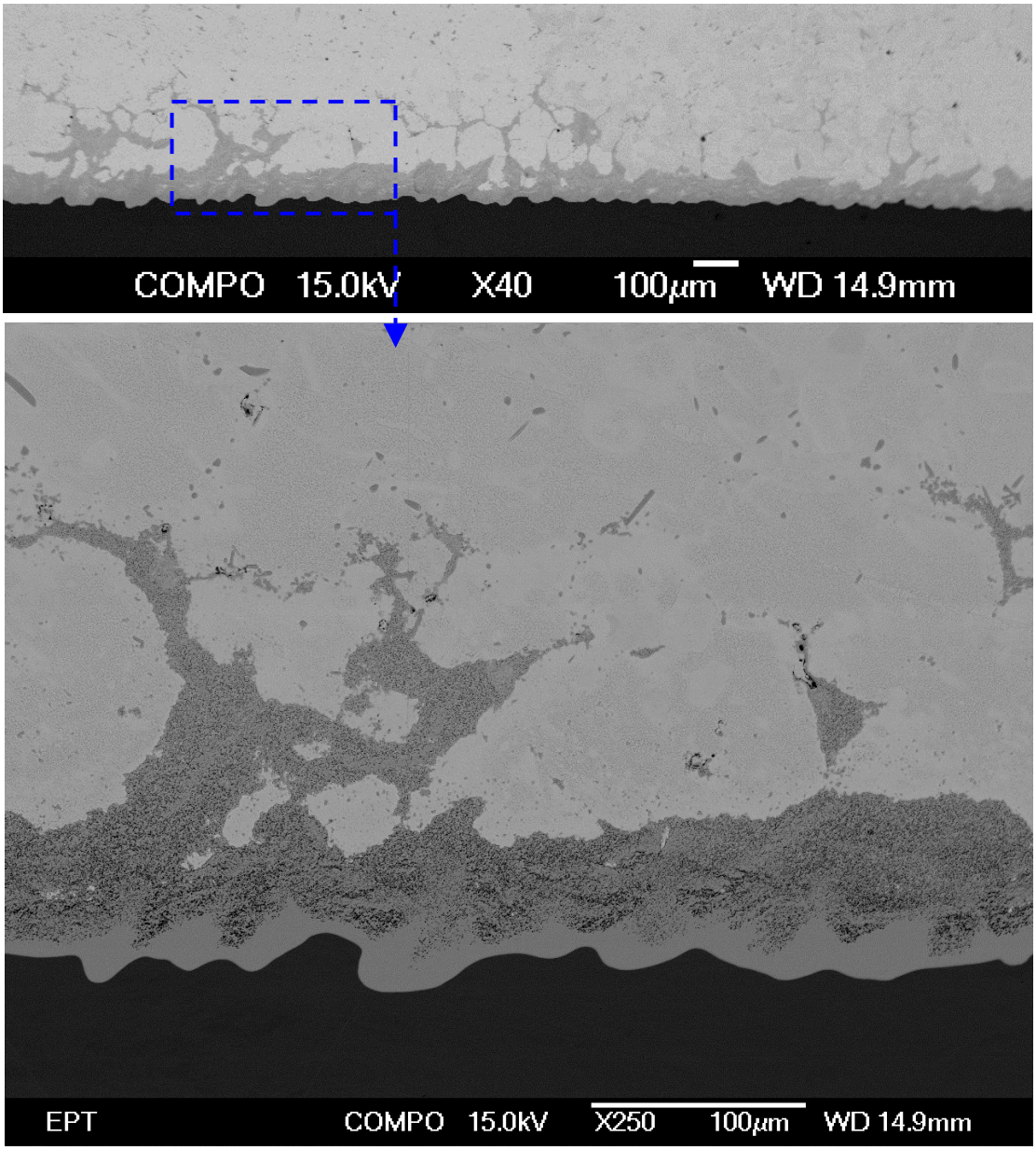

Figure 6.16: *Interfacial microstructures from Cu12.5Ni/Sn diffusion couple, slow* (1.3°C/min) *cooling.*

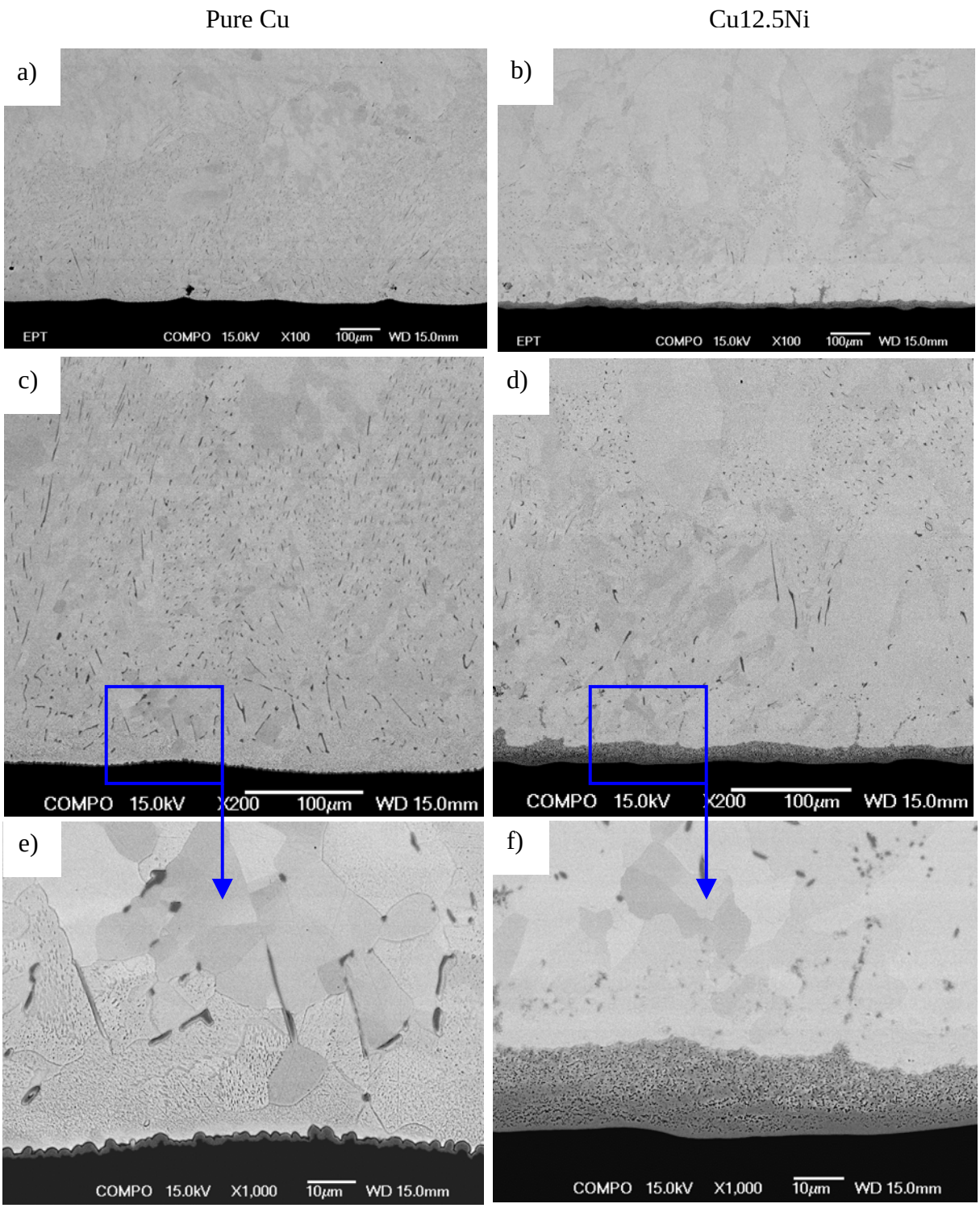

Figure 6.17: *Interfacial microstructure after 10 min at 240℃ and slow (2℃/min) cooling of pure Cu/Sn (left) and Cu12.5NI/Sn (right) diffusion couples.*

Reactions between SnAgCu|Ni and SnAgNi|Cu

The same approach can be used for predicting the intermetallic reactions in Cu-containing lead-free solders with Ni metallisations. Figure 6.18 shows the Sn-rich corner of the isothermal section of the Sn-Cu-Ni phase diagram at 250^0C. For the sake of simplicity it is presented here in weight percentages and the tie-lines are left out. If the Cu content of the solder is less than ~0.4 wt-% (indicated with a), the contact line intersects the metastable solubility curve in the Liq + $(Ni,Cu)_3Sn_4$ two-phase region (indicated with b) and therefore $(Ni,Cu)_3Sn_4$ nucleates at the Ni|solder interface. But, if the Cu concentration is larger than 0.6 wt-% (indicated with c), the intersection point d is in the Liq + $(Cu,Ni)_6Sn_5$ two-phase region and so $(Cu,Ni)_6Sn_5$ must be the first intermetallic phase to form.

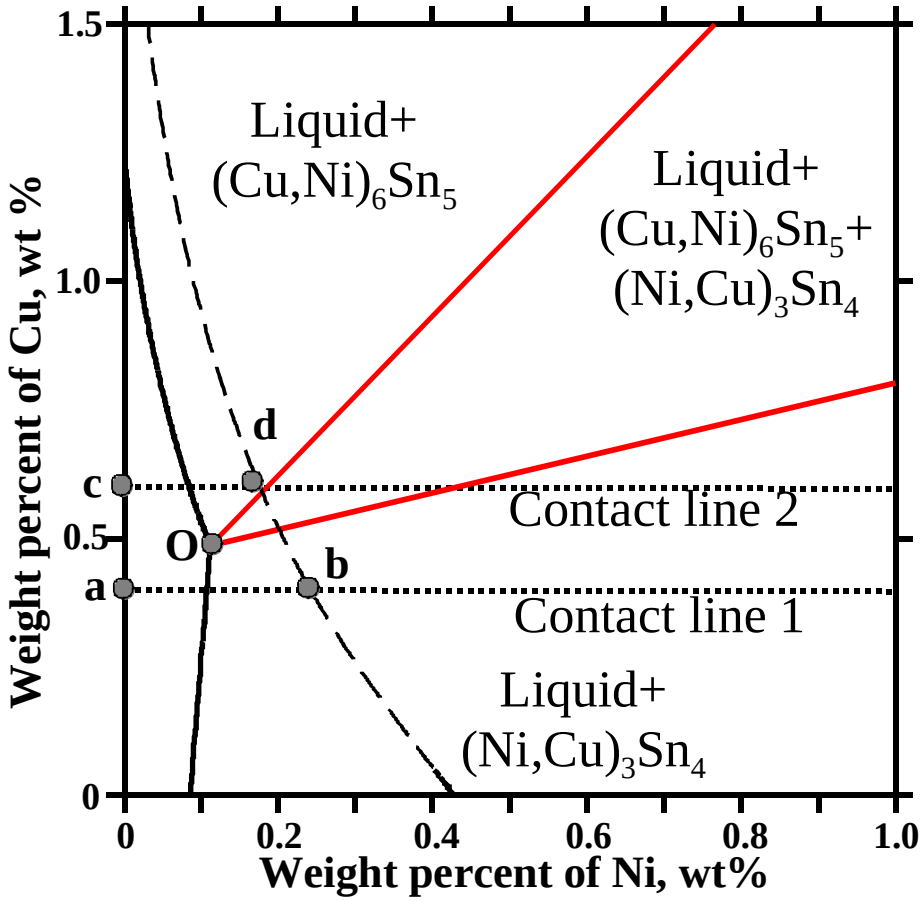

Figure 6.18: *Tin-rich corner of the optimised metastable phase diagram at 240℃ [5].*

When the Cu content in Sn-rich solder is near 0.5 wt-% as Ni atoms start to dissolve into solder containing Cu, the supersaturation causes the liquid to become local equilibrium with both $(Cu,Ni)_6Sn_5$ and $(Ni,Cu)_3Sn_4$ (i.e. metastable solubility line inside the three-phase triangle) and thermodynamically either of these can form at the interface. However, as the diffusion path cannot go through the three-phase triangle, later on the solder becomes in local equilibrium with $(Cu,Ni)_6Sn_5$. This most probably explains the experimental results presented by Chen et al. and Ho et al. [72, 73, 76, 77]. It must be emphasised, however, that when exploring the phase equilibria in great detail, as here, the values presented are temperature-dependent [see Fig 6.19, in which the apex of the three-phase triangle, i.e. the critical Cu content of the solder, is presented as a function of temperature] and the errors in the experimental results, as well as in the thermodynamic modelling, must be taken into account.

The dark grey and light grey areas in Figure 6.19 indicate the solid and solid+liquid areas respectively; above (to the left of) the dotted line the primary intermetallic is $(Cu,Ni)_6Sn_5$ and below (to the right of) it the primary intermetallic is $(Ni,Cu)_3Sn_4$. The circles [$(Cu,Ni)_6Sn_5$] and squares [$(Ni,Cu)_3Sn_4$] represent the experimental results performed to verify the movement of the apex of the three-phase triangle (point O, at Fig.6.18) as a function of temperature. It is obvious that the temperature dependency needs to be reoptimised. As can be seen from Figure 6.20, the primary intermetallic with constant Cu content is changed from $(Cu,Ni)_6Sn_5$ to $(Ni,Cu)_3Sn_4$ when the temperature is increased. It is interesting to note that the IMC thickness is clearly reduced when it is changed from $(Cu,Ni)_6Sn_5$ to $(Ni,Cu)_3Sn_4$, even if the temperature is increased. On the other hand, it seems that the interface between Ni and IMC is more uneven when the composition is near to the equilibrium curve. Therefore it can be concluded that the effect of temperature on the critical Cu composition is significant and thus it is now possible to explain the $(Cu,Ni)_6Sn_5$ “precipitates” on the top of the $(Ni,Cu)_3Sn_4$ observed by Ho et al. [73] when the Cu content of the SnAgCu solder was 0.4 wt-%.

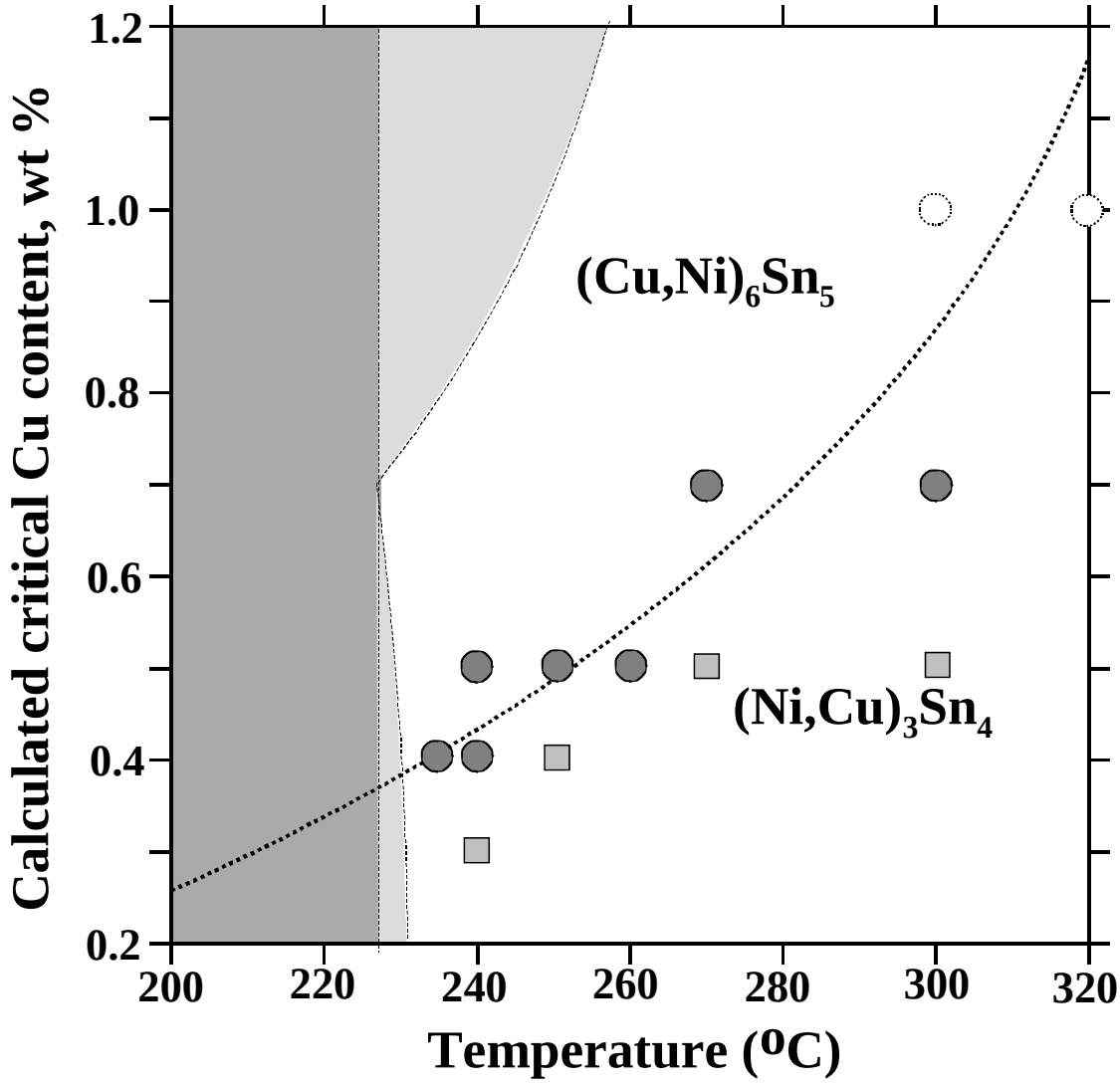

Figure 6.19: *Calculated critical Cu content in liquid Sn to change interfacial reaction product from $(Ni,Cu)_3Sn_4$ to $(Cu,Ni)_6Sn_5$, as a function of temperature together with the experimental points.*

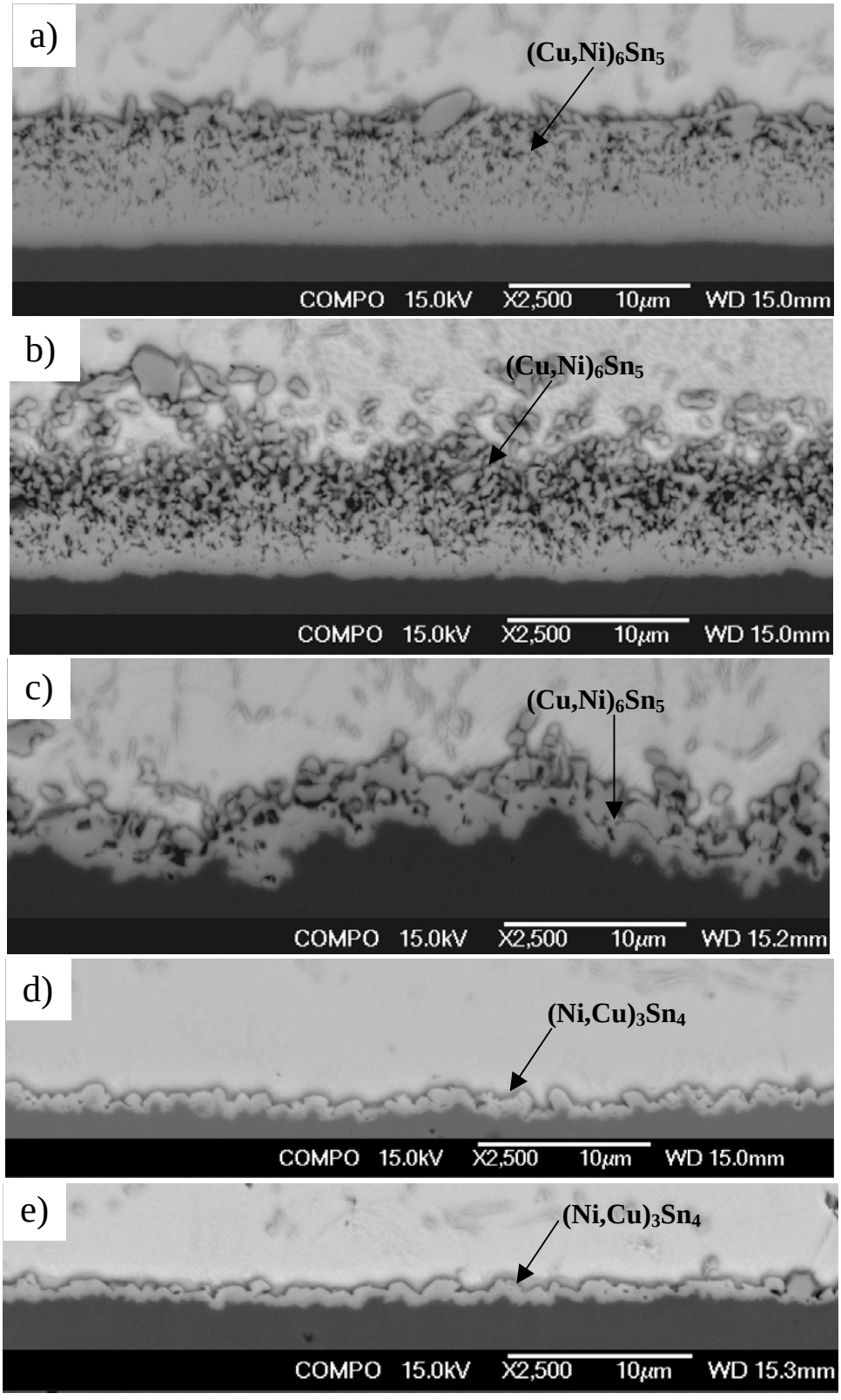

Figure 6.20: *Sn+0.5wt-%Cu /Ni diffusion couples annealed at (a) 240℃, (b) 250℃, (c) 260℃, (d) 270℃, and (e) 300℃ for 60 min.*

As can be seen from Fig 6.21, a similar trend can also be observed if the temperature is kept constant (T=240°C) and the Cu content is reduced.

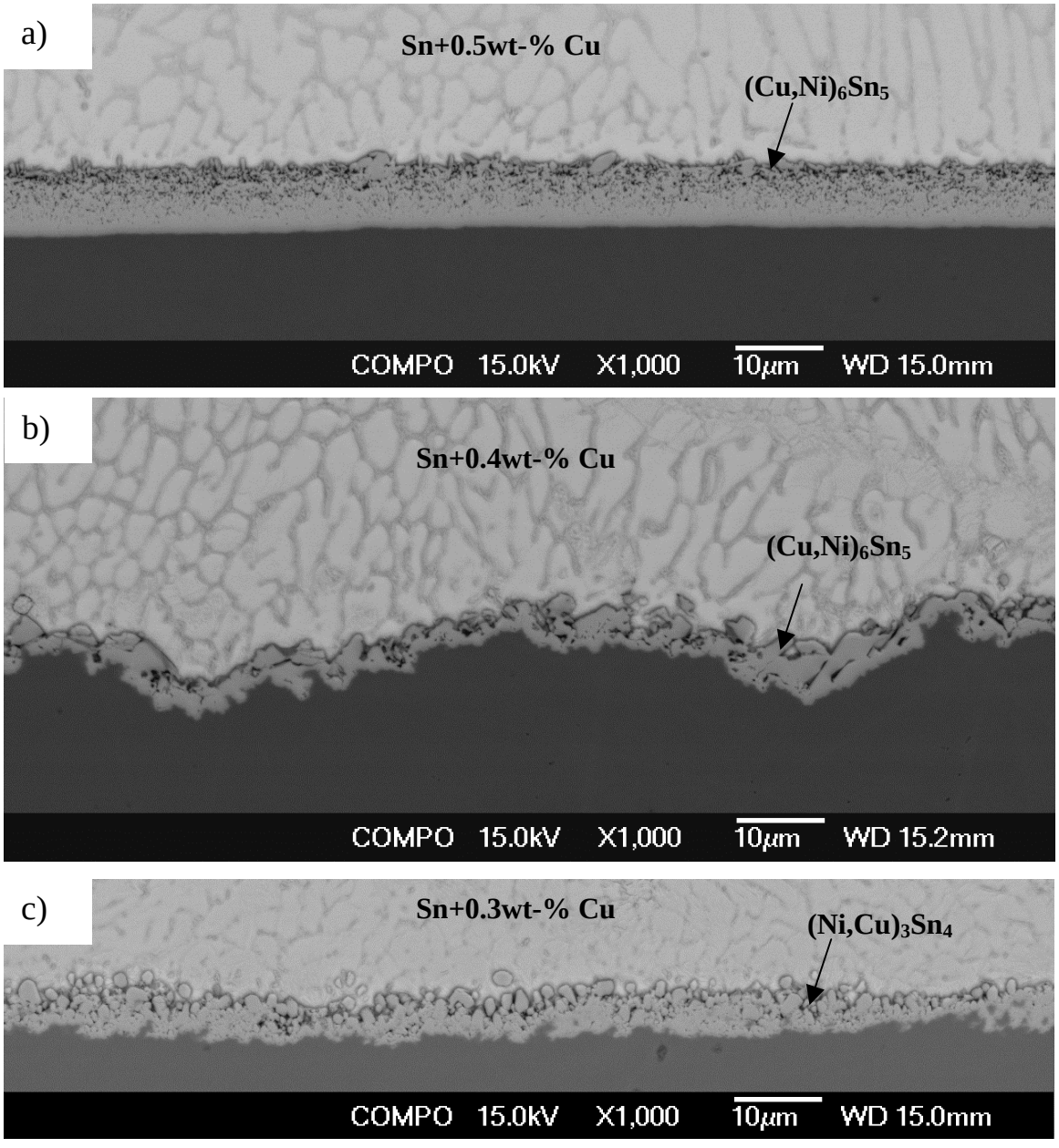

Figure 6.21: *Sn+ (a) 0.5wt-%Cu, (b) 0.4wt-%Cu, and (c) 0.3wt-%Cu/Ni diffusion couples annealed at 240℃ for 60 min.*

The analysis of the experimental results on the reactions between Ni-doped Sn3.5Ag (wt-%) solder and Cu presented by Tsai et al. [75] is similar to what is presented above. However, as the solubility of Ni in liquid Sn at this temperature is very low (less than 0.1 wt-%), the solders they used (except the binary Sn3.5Ag) were, in fact, two-phase alloys composed of almost pure liquid Sn and a small amount of solid Ni_3Sn_4. Hence, the diffusion couple approach they presented can be supplemented with the following prerequisites. First, as the phase equilibria do not change as a function of time, the local equilibria at the interfaces can be assumed. Second, the mass balance requirement must be obeyed, and therefore the diffusion path must intersect the contact line between the end members as least once and therefore the diffusion path can be directed from the original composition of the liquid towards $(Cu,Ni)_6Sn_5$, as well as $(Ni,Cu)_3Sn_4$. However, if $(Ni,Cu)_3Sn_4$ were the first phase to form in contact with the liquid, the diffusion path would have to intersect the contact line at $(Cu,Ni)_6Sn_5$ or $(Cu,Ni)_3Sn$, which requires the solid-state diffusion of Ni in either of these phases. Third, during the growth of intermetallic compounds the moving species cannot diffuse against their own activity gradients [144]. Because diffusion couple experiments utilising inert markers to locate the Kirkendall plane(s) (and thus the intrinsic diffusion fluxes) are practically impossible in solid|liquid reactions, detailed information about the mobilities of the species cannot be obtained.

The addition of other alloying elements may change the critical Cu content for $(Cu,Ni)_6Sn_5$ formation. Ho et al. [73] suggested that the existence of Ag in Sn-Ag-Cu solder does not have any effect, since it dissolves in neither $(Ni,Cu)_3Sn_4$ nor $(Cu,Ni)_6Sn_5$. Tsai et al. [75] used the same arguments in their analyses. This is only partly true, because the activities of the elements, not only in the compounds themselves but also in a liquid in (local) equilibrium with the compounds, determine the relative stabilities of $(Ni,Cu)_3Sn_4$ and $(Cu,Ni)_6Sn_5$. In order to demonstrate this, we collected the liquid parameters available in the literature for the Sn-Cu-Ni-Ag system and calculated the critical Cu content. As shown in Fig.6.22, the critical Cu content decreases from ~0.43 to ~0.36 wt-% Cu with the addition of Ag to the liquid solder. Bismuth is another much-used alloying element in lead-free solders. If we add, say, 3 wt% Bi to the liquid alloy the

critical composition of the liquid further decreases to ~0.32 wt-%Cu. It means that both Ag and Bi should reduce the critical Cu content and their combined effect could be up to 25% in the commercial lead-free alloys generally used in industry, even though they do not dissolve in either of the compounds. As for other alloying elements, their influences on the activities of components in both liquid and intermetallic compounds should be taken into account; this is an interesting subject for future studies.

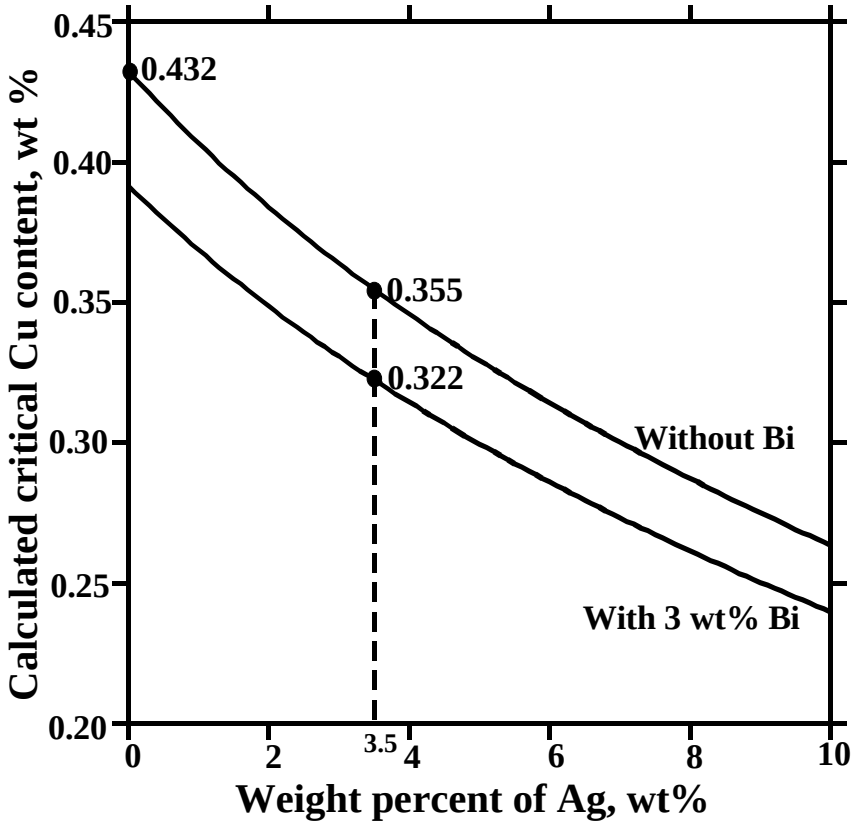

Figure 6.22: *Effect of alloying Ag and Bi to Sn on the critical Cu content at T=250℃*

In conclusion, the interfacial reactions between liquid tin (as well as Cu or Ni-alloyed SnAg solders) and Cu, Ni, or different CuNi alloy metallisations can be rationalised with the help of microstructural characterisation techniques and thermodynamic modelling of the interconnection system in order to have a better understanding of the formation of complex reaction zones in solder/conductor systems. It was discovered that the formation of the reaction layers during reflow annealing at 240^{o}C does not depend linearly on the Ni content of the alloy metallisation. Instead, when copper is alloyed with nickel, the rate

of increase of the thickness of the total reaction layer increases and reaches its maximum at the composition of about 10 at-% Ni. With higher Ni contents, the thickness of the reaction layer starts to decrease and attains a very low value with pure nickel. The reaction layer is composed of a relatively uniform $(Cu,Ni)_6Sn_5$ reaction layer (or uniphase layer) next to the Cu_xNi_{1-x} metallisations and a microstructurally more complex two- or three-phase layer between the uniphase layer and the tin matrix. With the help of the assessed data the critical Cu content of the liquid SnCu solder was evaluated. With a Cu content less than about 0.4 wt-% at 250°C, the $(Ni,Cu)_3Sn_4$ is thermodynamically more stable than $(Cu,Ni)_6Sn_5$. Even more important is the fact that the critical Cu content is temperature-dependent and it is also affected by alloying elements, such as Ag or Bi, that do not even dissolve in the intermetallic compounds.

6.1.3 Effect of additional elements on the Sn-Cu-Ni system

The effect of silver, which does not react with Cu or Ni, and the effect of bismuth on the Sn-Cu-Ni system were already discussed in previous chapter. Therefore this chapter concentrates on the effects caused by phosphorus, which is frequently present with Ni-based PWB coatings. The effect of vanadium is briefly introduced and gold is discussed in Chapter 6.2, as its major impacts appear during solid-state aging. The other quaternary alloying elements or impurities, such as chromium, which are used in component UMB metallisations are not considered here.

Effect of phosphorus

In investigating the interfacial reactions between Sn-Ag-Cu solder [Sn-4.1Ag-1.3Cu at-% (Sn-3.8Ag-0.7Cu wt-%)] and electroless Ni after one and five reflows (peak temperature 240°C and the duration of the spike zone was about 50 seconds) followed by solid-state annealing at 170°C for different periods of time (up to 640 hours) was used. The PCBs surface finish on Cu was composed of Ni(2µm)/Au(0.02µm) plating containing about 16 at-% (9 wt-%) P. Moreover, the same PCBs and solder pastes were used to solder commercial SnAgCu bumped WL-CSP components with different electroless Ni(P) UBM in order to investigate the effect of phosphorus content on the interfacial reactions.

The Ni(P) layer used contained about 30 at-% (~18 wt-%) P. Extended reflow times (up to 20 min) at 250°C were used to enhance the growth of the interfacial reaction products.

Fig. 6.23 shows the IMC layer between the NiP and near-eutectic solder from the sample that was reflowed four times after the assembly reflow. The point analysis taken from the interfacial IMC layer gives 40 at-% Cu, 15 at-% Ni, and 45-at% Sn, indicating that the IMC is $(Cu,Ni)_6Sn_5$, when Ni is dissolved into the Cu sublattice.

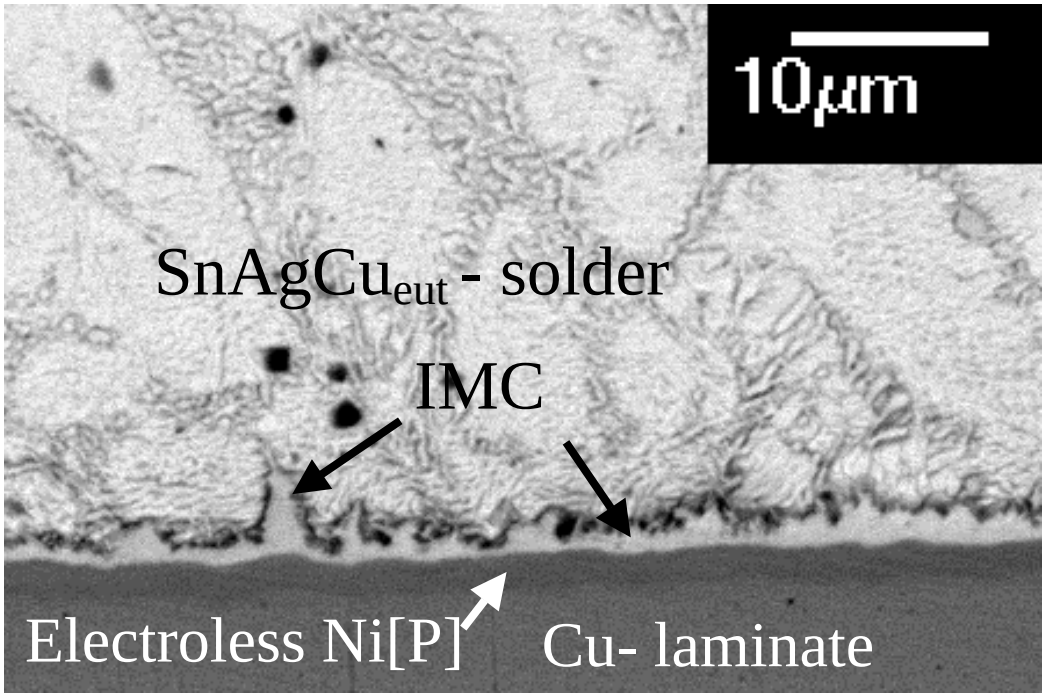

Figure 6.23: *Backscattered SEM image of a sample that was reflowed five times.*

Similar results have been reported in several papers dealing with the Sn-Cu-Ni system [73, 137, 138, 145]. However, Hwang et al. have suggested that this phase could be Ni_3Sn_2, where Cu is dissolved into the Ni sublattice [146]. As both phases have the same NiAs structure, with similar lattice parameters, the analysis is difficult to confirm, even with TEM. On the other hand, considering the relatively low solubility of Cu in $(Ni,Cu)_3Sn_2$ [47, 146], it is more likely that the intermetallic layer is $(Cu,Ni)_6Sn_5$. A TEM micrograph of the sample that was reflowed five times given in Fig. 6.24(a) shows that another phase has precipitated out from $(Cu,Ni)_6Sn_5$. The elemental maps [see Figs. 6.24(b)-(e)] reveal that the phase contains Ni and Sn and a small amount of Cu. The two

phases that can be in local equilibrium with $(Cu,Ni)_6Sn_5$ are $(Ni,Cu)_3Sn_4$ and $(Ni,Cu)_3Sn_2$ [70]. With the help of the selected area diffraction (SAD) pattern [see Fig. 6.24 (f)], it can be confirmed that this phase is $(Ni,Cu)_3Sn_4$ having the monoclinic structure.

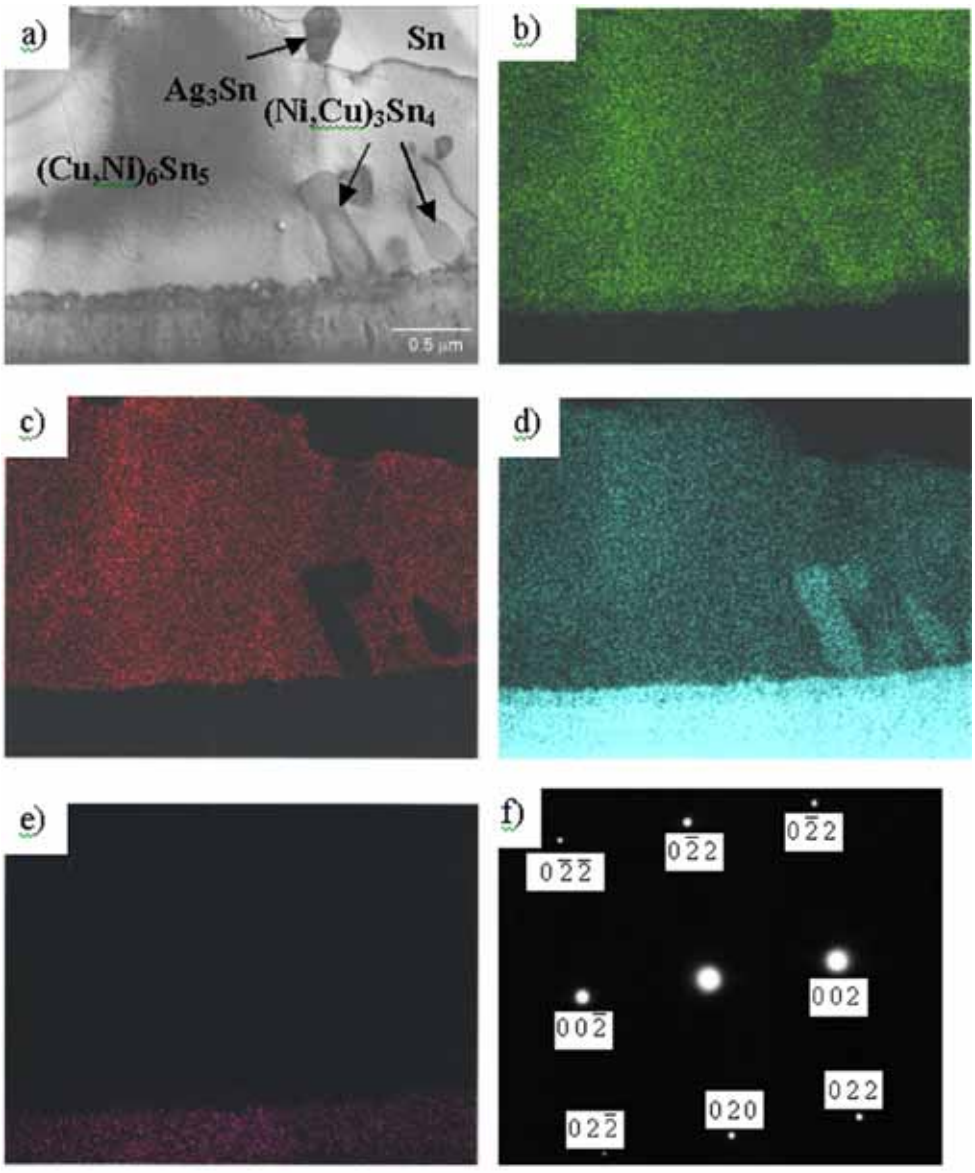

Figure 6.24: *a) Bright field TEM image of the interfacial region in the sample that was reflowed five times, b) Sn x-ray map, c) Cu x-ray map, d) Ni x-ray map, e) P x-ray map of the same area, and f) diffraction pattern taken from the $(Ni,Cu)_3Sn_4$ phase.*

Between the IMC and Ni[P] layers a thin (less than 0.5-µm) dark layer can also already be seen (Fig. 6.25) after the assembly reflow, meaning that the layers form fast. In fact, one can even distinguish two layers: the thicker one (dark) and on the top of that a very thin layer (light grey). The contrast difference in the back-scattered image indicates that the top layer contains heavier elements than the lower one. According to the point analysis, the lower dark layer seems to contain more P than the adjacent layers.

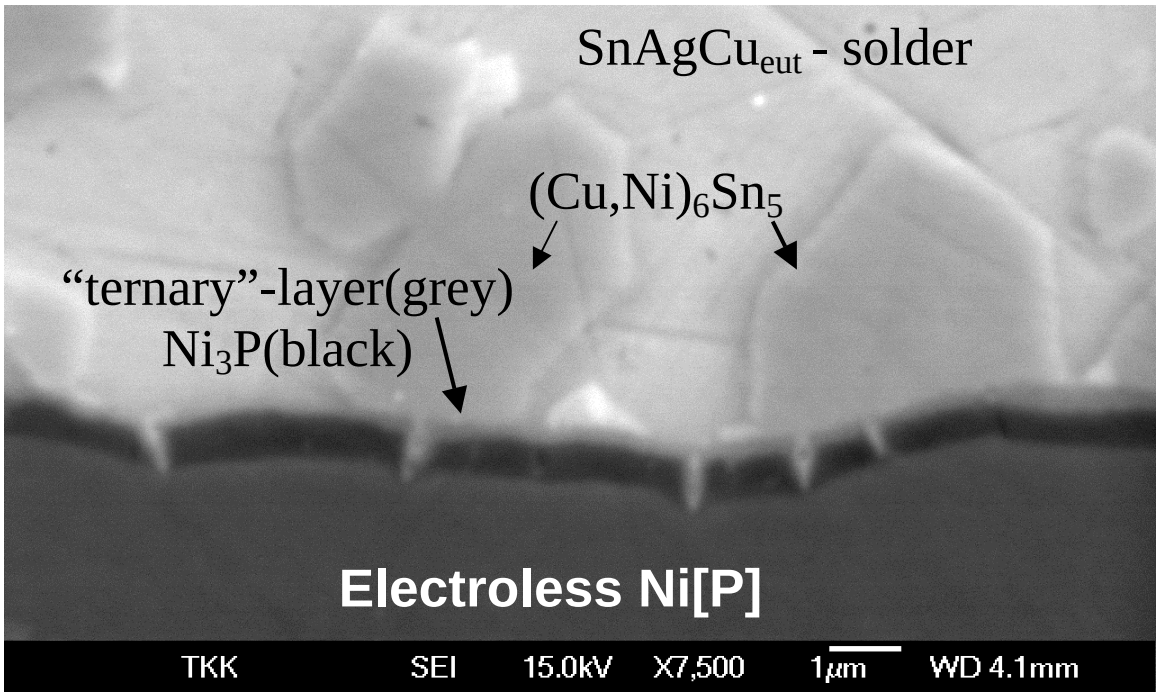

Figure 6.25: *Secondary SEM image revealing the presence of the dark P-rich layer after the first reflow.*

Figure 6.26(a), taken from the sample that was reflowed five times, shows a bright-field TEM image (tilted 90° clockwise) from the IMC and phosphorus-enriched areas, together with the line scan (Fig. 6.26(b). From the TEM micrograph it is confirmed that the P-rich phase between the electroless Ni[P] and the $(Cu,Ni)_6Sn_5$ is not a single reaction layer but is composed of two layers, as also indicated by the SEM micrograph (Fig. 6.25). The layer next to the electroless Ni[P] is a crystalline nickel phosphide containing more P than the initial electroless Ni[P]. Both the line scan and the electron diffraction pattern (see Fig. 6.27) show that this phase is Ni_3P. This phase was observed first by Jang et al. when studying a Si/SiO2/Al/Ni(P)/63Sn37Pb multilayer structure after reflow [113]. As

shown in Fig. 6.27, the crystalline Ni_3P next to the original Ni[P] coating has a columnar structure in which some organic impurities seem to be concentrated between the columns. In addition, some Sn can be observed between the Ni_3P columns, close to the ternary layer composed of Ni, Sn, and P.

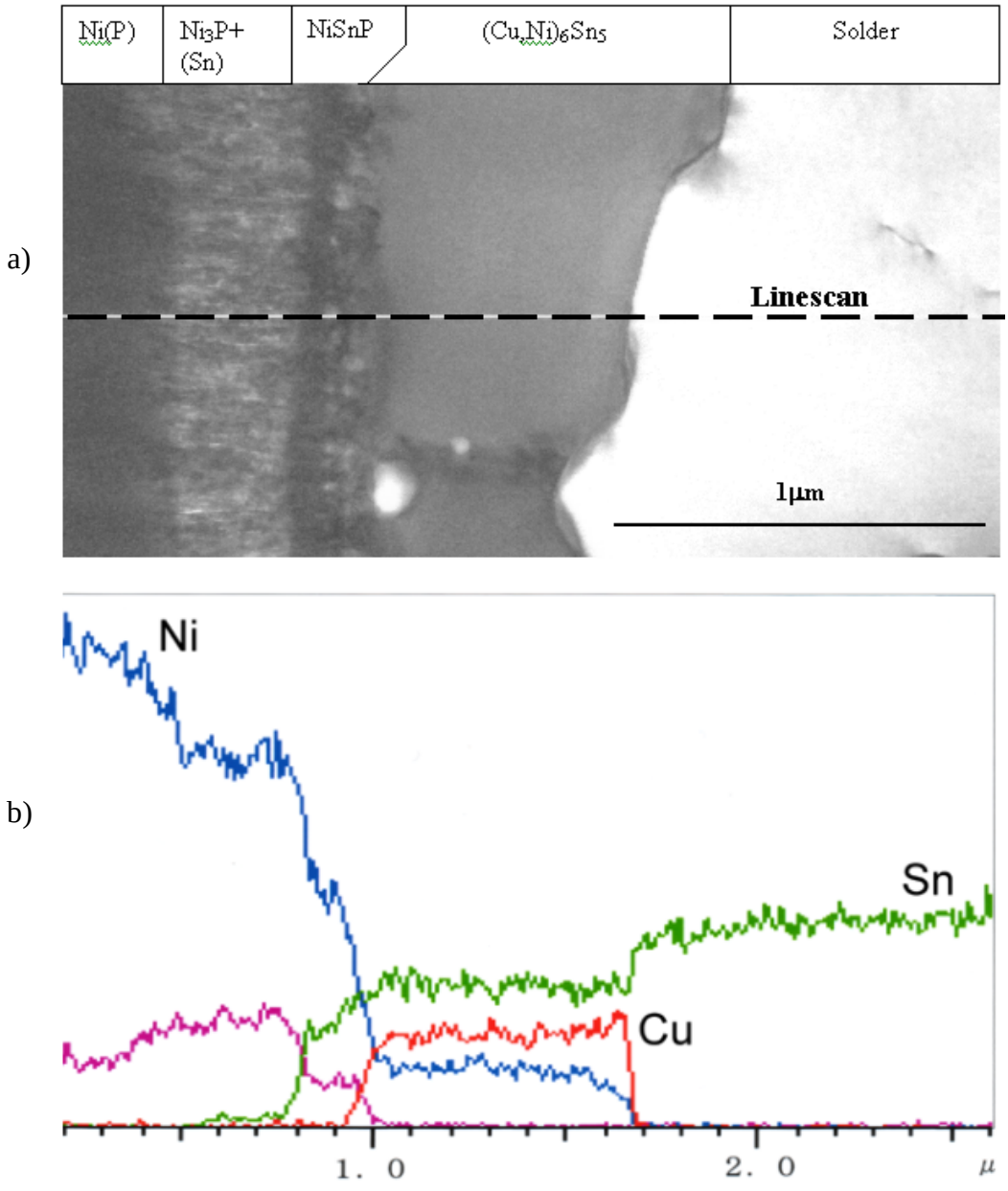

Figure 6.26: *a) Bright field image taken from the IMC and phosphorus-enriched regions in the sample that was reflowed five times. b) Linescan presenting the distribution of Ni, P, Sn, and Cu across the reaction zone [depicted with a dotted line in Fig 6.26(a)].*

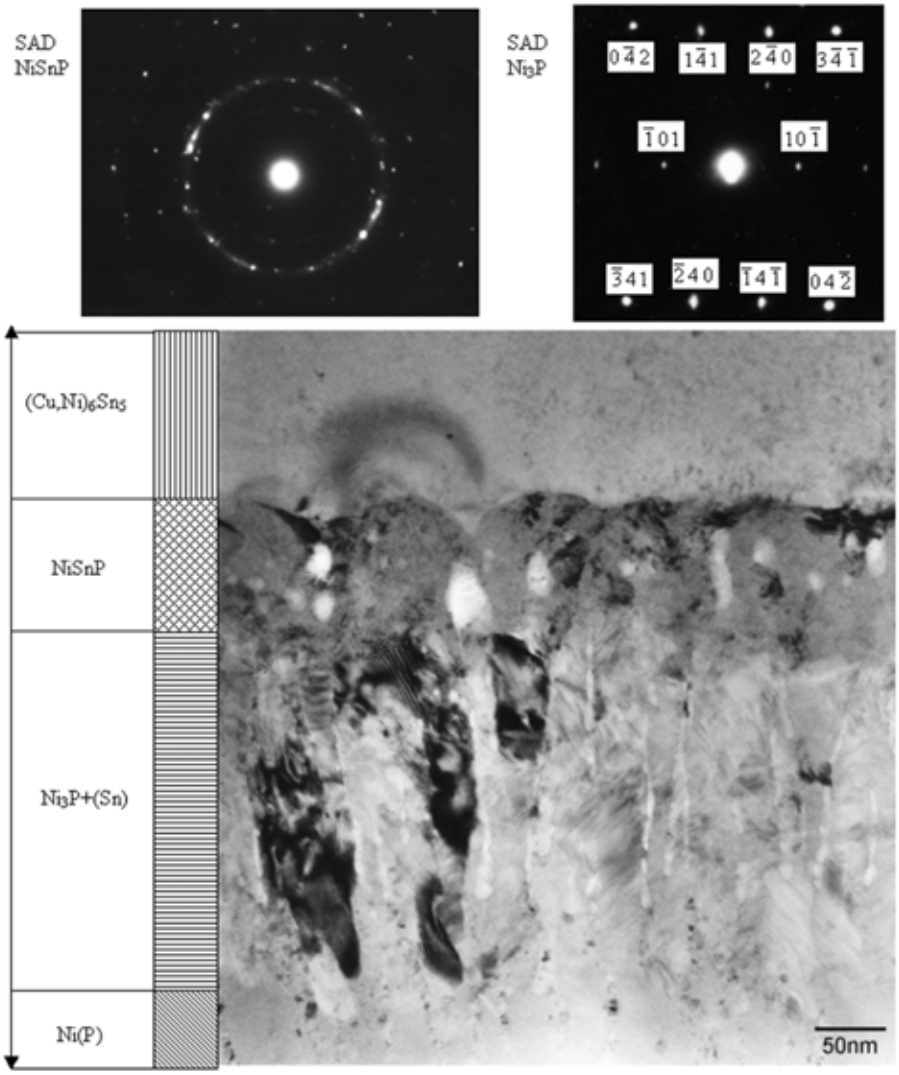

Figure 6.27: *Bright field image taken from the reaction zone together with the diffraction patterns taken from the NiSnP and Ni_3P layers.*

On the basis of the linescan [Fig 6.26 (b)], the composition of the NiSnP phase is estimated to be 55 at-% Ni, 35 at-% Sn, and 10 at-% P. As can be seen from the selected area diffraction pattern (Fig.6.27), this layer has a nanocrystalline structure. It is unlikely that this phase is the Ni_2SnP [147] or Ni_3SnP [11, 113] reported earlier. The unambiguous determination of the crystal structure of this phase is very difficult because of the fact that the diffraction pattern taken from such a thin phase (less than 100 nm) includes diffraction spots from the adjacent crystalline phases. The ternary NiSnP layer contains numerous small defects that have a pore-like appearance. It is likely that these structural

defects assist the propagation of cracks in the layer and thus cause interconnections to behave in a brittle manner. These “pores” are not artefacts generated during the thinning process, because they were readily observable before the thinning. The “pores” were also observed by Jeon et al. [148] in Ni[P]/(SnPb)eut reaction products and they claim that they are Kirkendall voids. It is difficult to accept that Kirkendall voids could form in the reaction layers in such a short time. Moreover, we did not observe any detectable change in the number or size of these “pores” in the ternary NiSnP layer when comparing the samples which were either reflow-soldered five times or annealed at 170°C for 64 hours after the assembly reflow (see Fig. 6.28). Therefore, it is unlikely that they are Kirkendall voids. In fact, the high resolution phase contrast images shown in Fig. 6.29 show that the pores contain organic material that most probably originates from the Ni(P) plating bath.

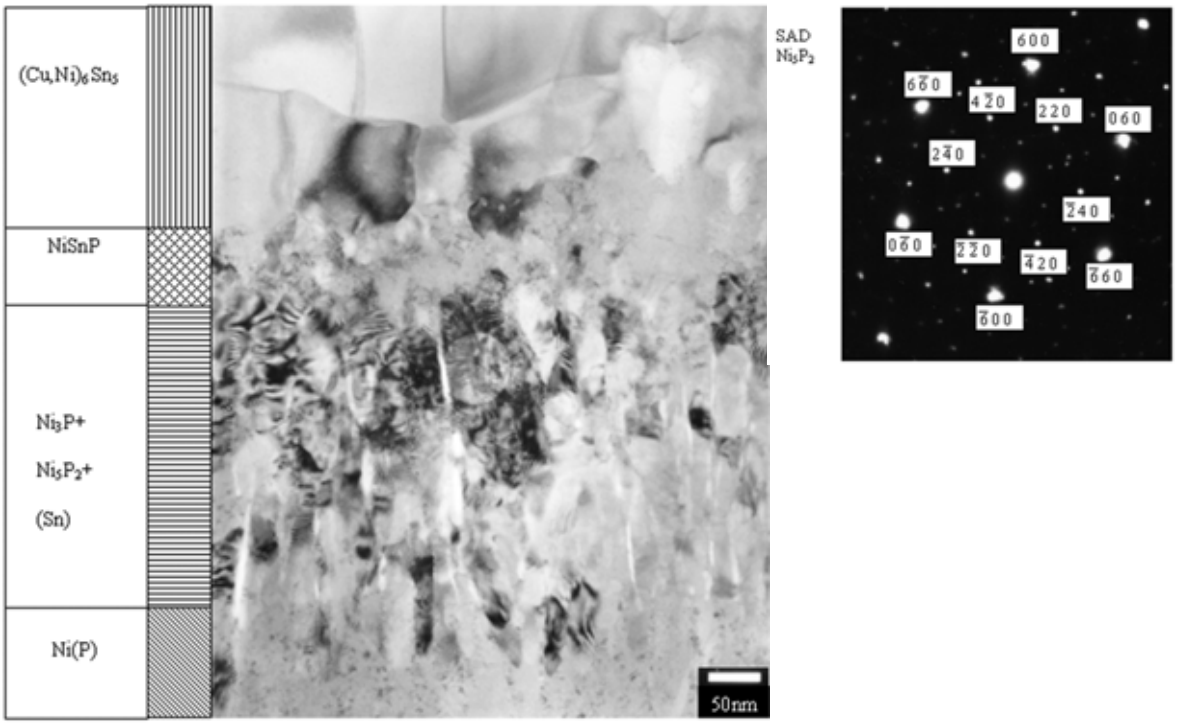

Figure 6.28: *Bright field image taken from the reaction zone in the sample that was annealed at 170°C for 64 hours after the assembly reflow, as well as the diffraction pattern taken from the Ni_5P_2 phase.*

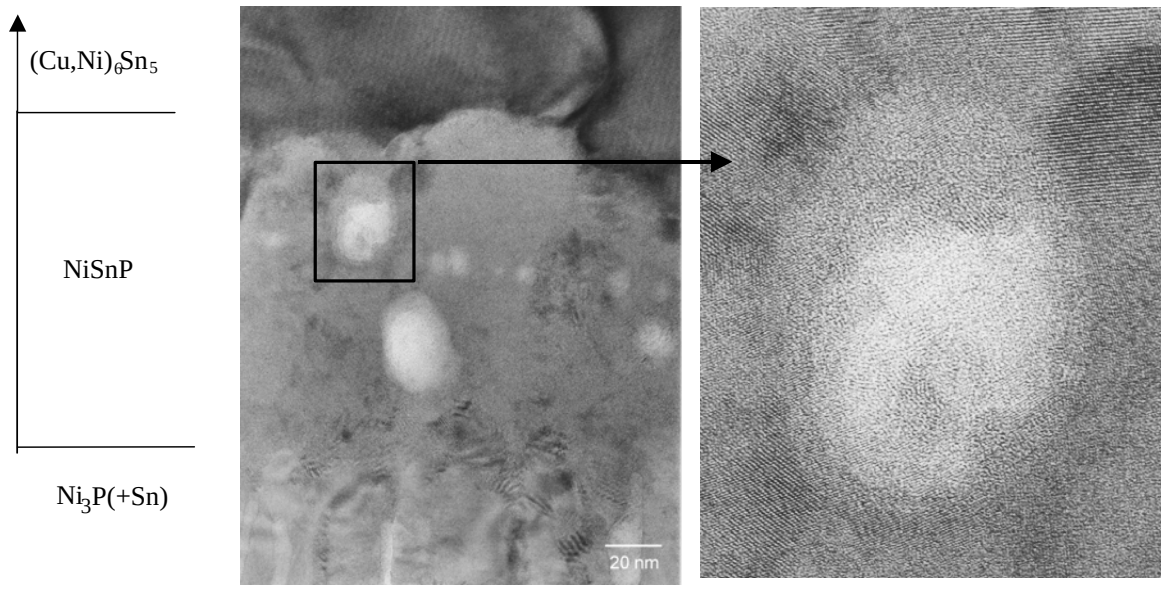

Figure 6.29: *High-resolution phase contrast image of the organic particles in the nanocrystalline Ni-Sn-P layer.*

When attempting to rationalise the formation of the observed reaction structures - also reported in other recent publications [146-148] - with the help of the solder-assisted crystallisation approach, we encountered several problems which most probably stem from the fact the system studied by Jang et al. [113] is metallurgically different from ours. In particular, the presence of a nanocrystalline NiSnP layer between the Ni_3P and IMC complicates the situation. Firstly, to obtain such a high Ni content as was found in the NiSnP layer requires substantial Ni dissolution. However, as both the stable and metastable solubilities of Ni in liquid Sn or eutectic SnAgCu alloy - and therefore also the dissolution rates - are very small, it is hard to accept that such high amounts of Ni could be incorporated in the ternary layer. Second, what is even more problematic is that in the solder-assisted crystallisation approach only Ni dissolves from the amorphous Ni[P] coating, leaving a phosphorus-rich layer behind. This, in turn, requires the solid-state diffusion of Ni inside the Ni[P] coating, so that Ni atoms can reach the Ni[P]/solder interface. This can hardly take place in such a short period of time. Therefore, in our opinion the solder-assisted crystallisation approach cannot be applied to our system.

In order to explain the formation of the above-mentioned reaction products more quantitatively, the thermodynamic description of the quaternary Sn-Ni-P-Cu system is needed. Unfortunately, there are not enough reliable data on the quaternary system as would be required for its critical thermodynamic assessment. However, it is still plausible to analyse the reactions by making use of the available experimental phase diagram information on the lower-order systems. To explain the microstructures generated in the reactions between the amorphous Ni(P) coating and liquid near-eutectic Sn-Ag-Cu solder, we utilise primarily the binary phase diagrams Sn-P and Ni-P [8], as well as thermodynamic evaluations concerning the stability of ternary Sn-P-Ni liquids [5].

The successive reactions between Ni(P) and liquid SnAgCu solder alloy start with the instant dissolution of a thin (flash) Au layer, which is followed by the dissolution of Ni and P. Because of the supersaturation of phosphorus in the Sn-rich liquid, a thin layer of new liquid (L2) is formed between the solid Ni(P) and the bulk liquid solder (L1). This argument is supported by the presence of the liquid miscibility gap in the binary Sn-P system, which extends to lower temperatures as a metastable miscibility gap [5]. On the basis of thermodynamics, it is evident that the binary miscibility gap extends to the ternary Sn-P-Ni system. In fact, according to our calculations the metastable miscibility gap seems to be heavily stabilised by dissolved Ni. Because the two liquids are in local equilibrium with each other and the L2 with the Ni(P) substrate, Ni, P, and Sn will distribute between the liquids in such a manner that the liquid L2 contains large amounts of Ni and P and a small amount of Sn, while the Sn-rich liquid L1 has some Ni and a small amount of P. On the basis of the mass balance calculations, the average composition of the L2 was estimated to be about 70 at-% Ni, 10 at-% Sn, and 20 at-% P. Because of the high Ni content, the liquid L2 must be unstable at these low temperatures and therefore it rapidly turns into the ternary NiSnP layer providing a solid substrate for the $(Cu,Ni)_6Sn_5$ to nucleate and grow. After this the reactions take place essentially in the solid state

During cooling from the upper reflow temperature or during successive reflows, the NiSnP layer transforms partially into the more stable crystalline compound Ni_3P, with a

columnar structure. During the transformation the extra atoms not used in the formation of Ni_3P are rejected to the ternary NiSnP layer. In addition to P and Sn, organic additives that are always present in electroless Ni(P) coatings also precipitate out at the interfaces between the columnar Ni_3P crystals, as well as in the NiSnP phase, where they are revealed as numerous small "pores", as shown in Fig. 6.29. The fact that they are organic impurity particles has been confirmed with the high-resolution transmission electron microscopy (Fig. 6.29). Therefore, the Kirkendall voids reported earlier [146, 147] may, in fact, be organic impurity particles. Additionally, the white stripes between the columnar Ni_3P crystals in Fig. 6.27, also observed by Matsuki et al. [147], seem to be organic material, because their bright field contrast does not change if the specimen is tilted. When the specimens were annealed in solid state at 170°C, the Ni_3P phase transformed into Ni_5P_2, implying that some more Ni has diffused towards the solder and the P concentration of this layer has increased accordingly.

It is interesting to note that when the P content of the electroless Ni(P) coating is high enough, the formation of Ni_3P seems to be suppressed. This is shown in Fig. 6.30(a), where Ni(P) with 30 at-% P has reacted with the near-eutectic Sn-Ag-Cu solder at 250 C° for 5 minutes. Only the ternary NiSnP layer is visible between the electroless Ni(P) coating and the solder. Furthermore, as the time above the liquidus is now longer (5 min), more Ni (and P) is dissolved into the solder and the $(Cu,Ni)_6Sn_5$ has transformed into $(Ni,Cu)_3Sn_4$ as a result of the limited supply of Cu. Fig. 6.30(b) shows clearly the dark Ni_3P layer in the reaction zone on the PWB side, where the P concentration of the electroless Ni(P) is about 16 at-%. The suppression of the formation of Ni_3P when using electroless Ni with a high P concentration is, in our opinion, due to the increase in the P concentration in the NiSnP layer, which is related to the shape of liquid miscibility gap. According to our extrapolated metastable ternary Sn-Ni-P phase diagram, the miscibility gap extends to the ternary system in such a manner that the P concentration of liquid L1 always remains low, while the P content in liquid L2 may vary significantly. Calculations suggest that most of the dissolved P atoms stay in the liquid L2 and that a higher P content in the original Ni(P) results in a higher P content in the NiSnP layer.

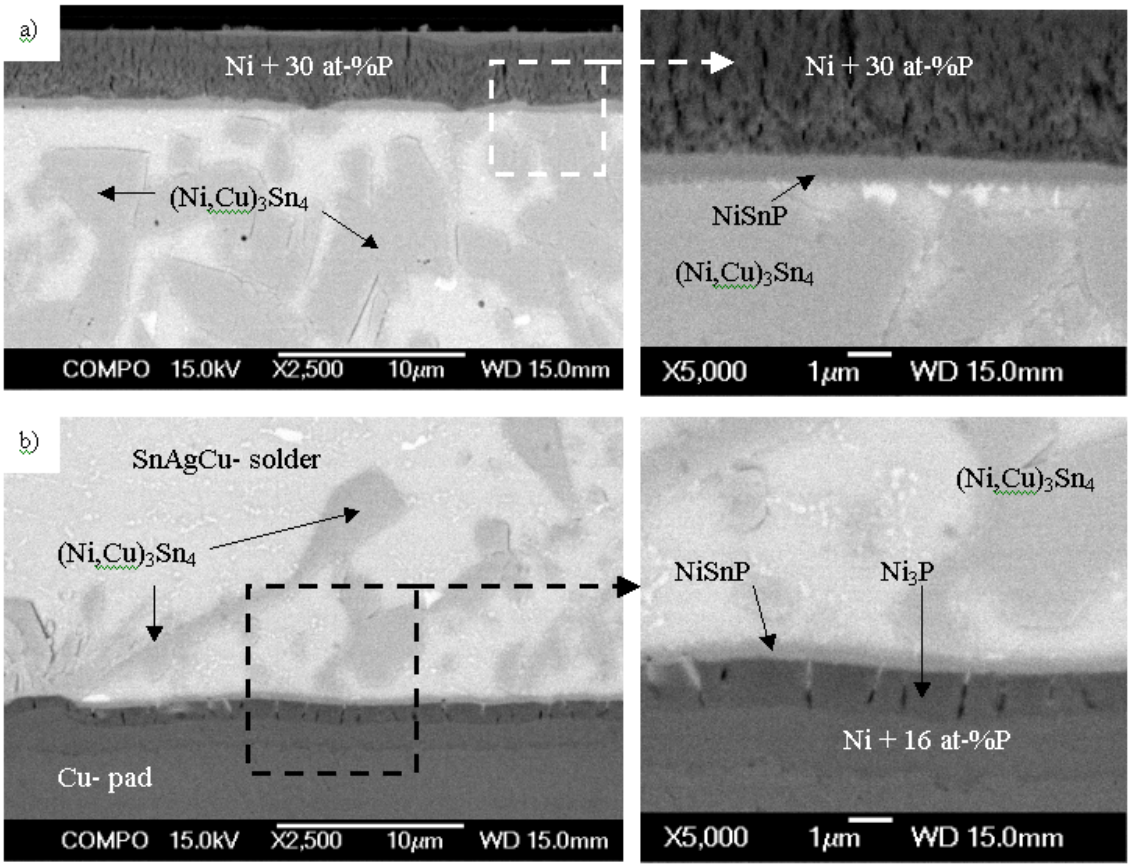

Figure 6.30: *Backscattered SEM images taken from the samples that were annealed for 5 min at 250°C: a) the component side, where the P concentration in Ni(P) is about 30 at-% and, b) the PWB side, where the P concentration in Ni(P) is about 16 at-%.*

What has been stated above leads to the situation where the P content of L2 can be quite high when the Ni(P) substrate has a high P concentration. Therefore, the P content of the resulting NiSnP phase should also be higher than, for example, in the previous case discussed above. We expect that the higher phosphorus content will further stabilise the NiSnP phase at the expense of the crystalline Ni_3P, mainly for the following reason. It is known that the temperature of crystallisation - and also the glass transition temperature - of an amorphous phase is usually lower close to the eutectic point (19 at-% P in the Ni-P system) than near intermediate compounds or end elements [149]. Therefore, we can expect that an increase in the P content of the NiSnP layer will also increase its crystallisation temperature, as the composition is shifted further away from the eutectic

point. Further support for the effect of P on the stability of amorphous structures can be found in the literature, where it has been widely documented that when diffusion barriers for thin film applications are processed, amorphous structures are frequently realised by alloying elements such as B, C, N, Si, and P with transition metals [150].

On the basis of the above-mentioned results, it can be concluded that the interfacial reactions between the Sn-Ag-Cu solder and Ni(P)/Au coatings on printed wiring boards start immediately after the solder has melted. Then Au, Ni, and P start dissolving rapidly into the liquid solder, which, because of the existence of a metastable liquid miscibility gap in the Sn-P-Ni system, is divided into Sn-rich liquid (L1) and (Ni,P)-rich liquid (L2). Because of the high Ni content the L2 is unstable and it transforms into the nanocrystalline NiSnP, which provides the substrate for the formation of the $(Cu,Ni)_6Sn_5$. Subsequently, the metastable NiSnP layer starts to transform into columnar Ni_3P. In this transformation Sn atoms and impurities which do not dissolve into the Ni_3P diffuse towards the remaining NiSnP layer. The impurities in this ternary layer are revealed as numerous small “pores” detected with high-resolution transmission electron microscopy. What is of special interest is that when the P content of the Ni(P) layer is increased, only the NiSnP layer is formed in the assembly reflow within the resolution limits of SEM. The total thickness of the reaction layers does not change greatly during additional reflows. On the other hand, when the specimens were annealed in solid state at 170°C, the Ni_3P phase transformed into Ni_5P_2, implying that some more Ni had diffused towards the solder.

Effect of vanadium

When drop test reliability was studied with NiV/Cu and NiP/Au UBMs (in WL-CSP components) by Alajoki et al. it was found out that both the reliability performance and the failure mechanisms differ significantly [151]. They found out that the components with the Ni(V)/Cu metallisation were more reliable than those with the electroless Ni(P)/Au metallisation, irrespective of the bump, solder paste, surface finish materials, or the pad structure of the boards. As can be seen from Fig 6.31, the primary failure mode

(red arrows) was the cracking of interconnections along a brittle NiSnP layer (blue arrow) between the electroless Ni(P) with a high P content and the solder alloy, while components with Ni(V)/Cu UBM fail as a result of cracking along the $(Cu,Ni)_6Sn_5$ intermetallic layer (green arrow). It is interesting to note that the transformation from $(Cu,Ni)_6Sn_5$ to $(Ni,Cu)_3Sn_4$ has advanced only partially.

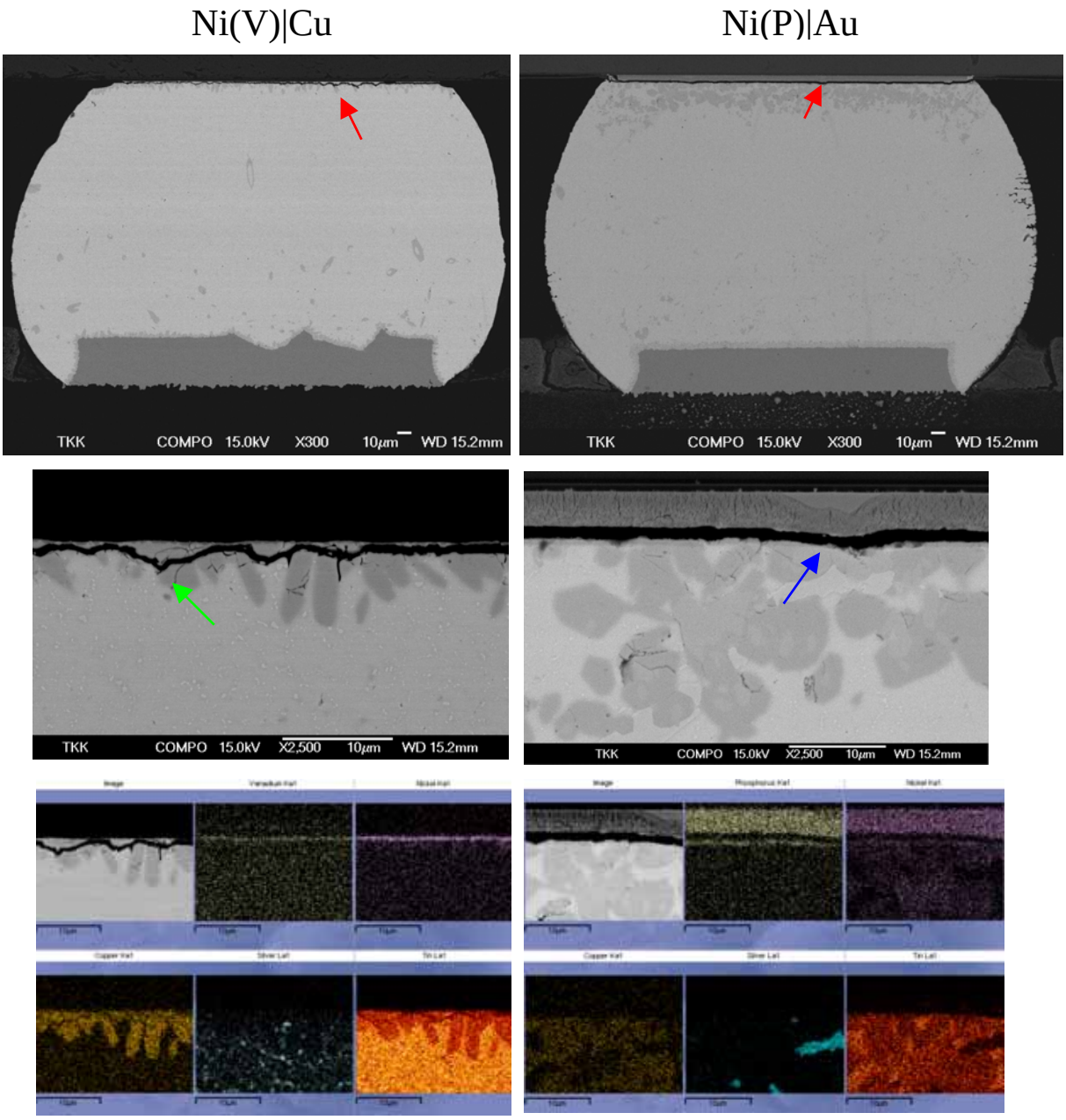

Figure 6.31: *The failure mechanisms in Ni(V)/Cu (left) and Ni(P)/Au UBMs in drop testing.*

6.2 Evolution of interfacial intermetallic structures in solid state

As has already been mentioned, there are a few special features that are typical of solid-state reactions in solder interconnections. First, the bulk solder material has a solidification structure and the solder-metallisation interface has been subjected to at least one solid|liquid reaction cycle, which means that usually there is quite a thick intermetallic layer (or layers) present at the interface. Second, the temperature during tests or use is high if compared with the melting temperature of the typical solder materials on an absolute scale i.e. the homologous temperature $T_{\mathrm{hom}}\left(=\frac{T_{Test\ \mathrm{or}\ Use}}{T_{mp}}\right)$>0.5, which indicates that the microstructural changes can be relatively rapid. Finally, the temperature which the solder joint is subjected to is hardly ever constant and therefore the stresses (and strains) caused by thermal cycles can accelerate the evolution of microstructures even more. It should be noted that the local equilibrium conditions in the solder interconnections will change locally because of the consumption of one or more of the components [14]. On the other hand, the reliability of electronic products as regards the mechanical properties of both bulk solder material and, especially, the intermetallic reaction layers is more important now than ever before. Therefore the fundamental information about the factors controlling the solder joint microstructure is essential, in particular from the reliability point of view.

6.2.1 Effect of additional elements on Sn-Cu reactions

The effect of additional elements on the reactions between Sn (or Sn-based solder) and Cu metallisation is studied in this chapter. The source of the impurities can be either the solder material (paste) or the Cu metallisation. Recently some investigators have observed the formation of pores (claimed to be Kirkendall voids) in Cu_3Sn or at the Cu/Cu_3Sn interface with both SnPb and SnAgCu solder interconnections with electrochemically deposited Cu [30, 152]. The formation of these pores must be significantly influenced by the additional elements (impurities) present in the solder interconnection, as with high-purity Cu-Sn reactions these voids are practically not observed at all. Figure 6.32 shows the interfaces between Sn and three different coppers:

(a) commercial electrolytic Cu; (b) EPT electrolytic Cu, and (c) EPT electrolytic Cu with brightener addition after 500 hours' annealing at 125°C.

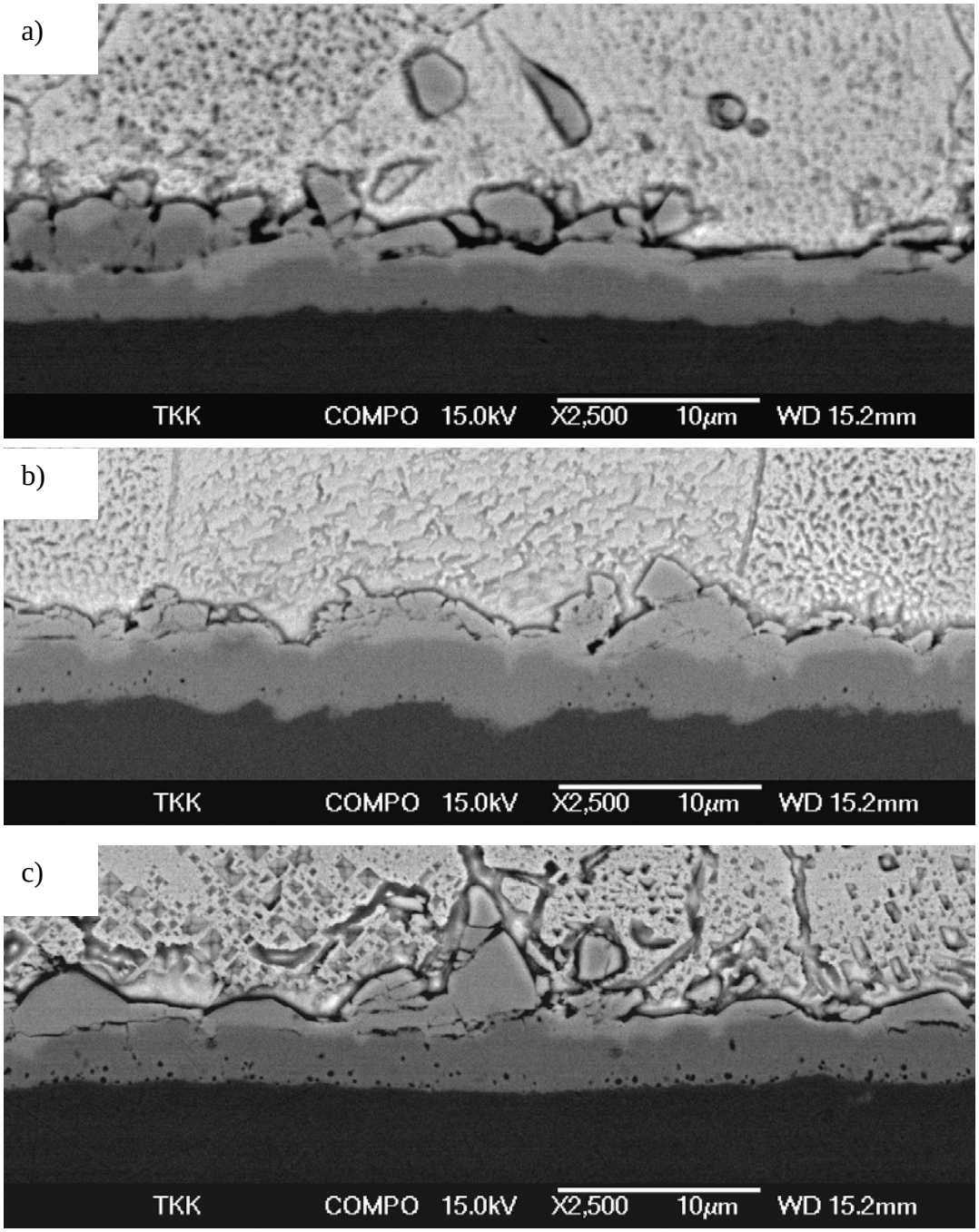

Figure 6.32: *Interfaces between Sn and three different coppers: a) commercial electrolytic Cu; b) EPT electrolytic Cu, and c) EPT electrolytic Cu with brightener addition after 500 hours' annealing at 125℃.*

Typical elements from commercial solder materials (Au, Ag, Fe, Ni)

In order to study the effect of typical impurities on the growth kinetics of Cu_6Sn_5 and Cu_3Sn, as well as on the formation of voids, commercially pure Sn was alloyed with Ni (2 at-%), Ag (12 at--%), Au (1 at--%), and Fe (1 at--%). These alloys were then used for soldering high-purity OFHC Cu substrates. After the standard reflow the samples were annealed at 150°C for up to 2560 hours. Figure 6.33 shows the interfaces after 2560 hours' annealing at 150°C. Practically no voids can be observed at the solder|Cu interface, but the growth kinetics of the IMCs vary with respect to the additional element. It is to be noted that the alloying elements can be divided into two groups, according to their solubility in Cu_6Sn_5: i) elements such as iron or silver, which do not dissolve to any significant extent in Cu_6Sn_5, and ii) elements such as Ni (~20 at-%) and Au (~15 at-%), which have high solubility in the intermetallic compound.

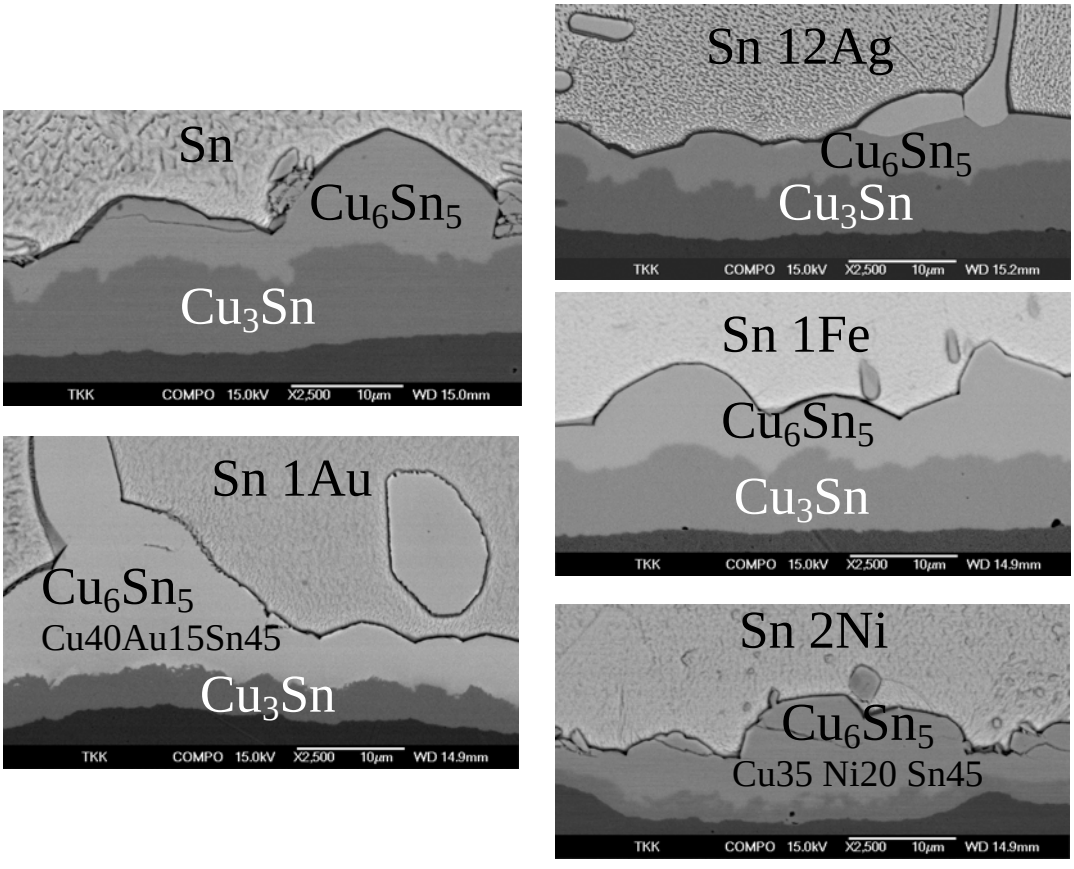

Figure 6.33: *Alloyed solder|Cu interfaces after 2560 hours' annealing at 150℃*

Effect of Titanium

Titanium is also considered a potential alloying element to Sn when the objective is to control the growth kinetics of Sn-Cu intermetallics, because it is generally known to be highly reactive. Ghosh has observed an Au-Sn-Ti intermetallic compound in a thin film metallisation|solder reaction [153]. Titanium also has a similar M_6Sn_5 compound with Sn to Cu, as can be seen from the phase diagram in Figure 5.3 [8]. High-temperature-phase βTi_6Sn_5 has a hexagonal crystal structure (hP22). Therefore, one could expect significant solubility of Ti in Cu_6Sn_5.

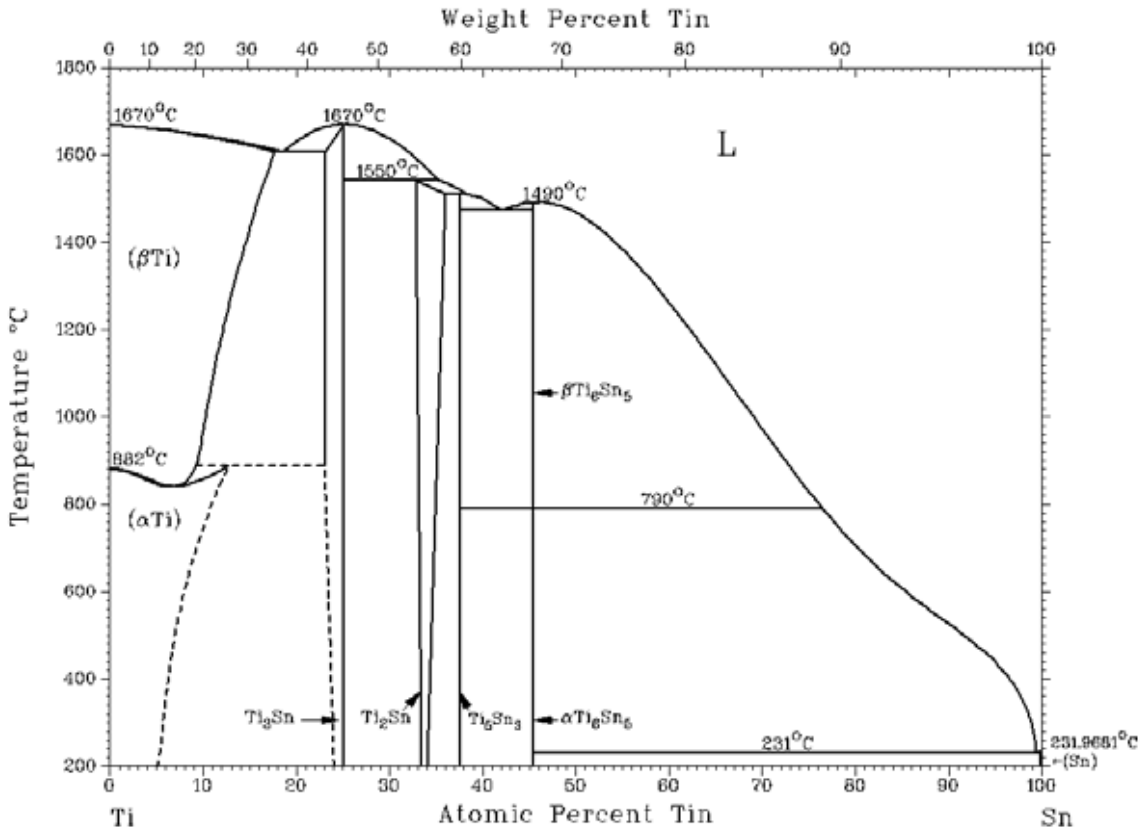

Figure 6.34: *Binary Sn-Ti phase diagram [8].*

Figure 6.35 (a) shows the interfacial microstructure after the $SnAg_{eut}$+2.5at-%Ti/Cu diffusion couple had been annealed at 125°C for 2700 hours. On the basis of the EDS element maps [Figure 6.35 (b) to (d)] and point analyses, it is obvious that, unexpectedly, Ti does not dissolve in Cu_6Sn_5, and neither does Cu dissolve in Ti_6Sn_5. On the other

hand, it seems that the addition of Ti has retarded the growth of both Sn-Cu intermetallic compounds at the interface quite significantly. However, as there is not currently any knowledge about the effect of Ti on the mechanical properties of SnAg solder, more experimental research is needed to verify its potential as an alloying element. Ti also oxidises easily, and this might cause wetting problems.

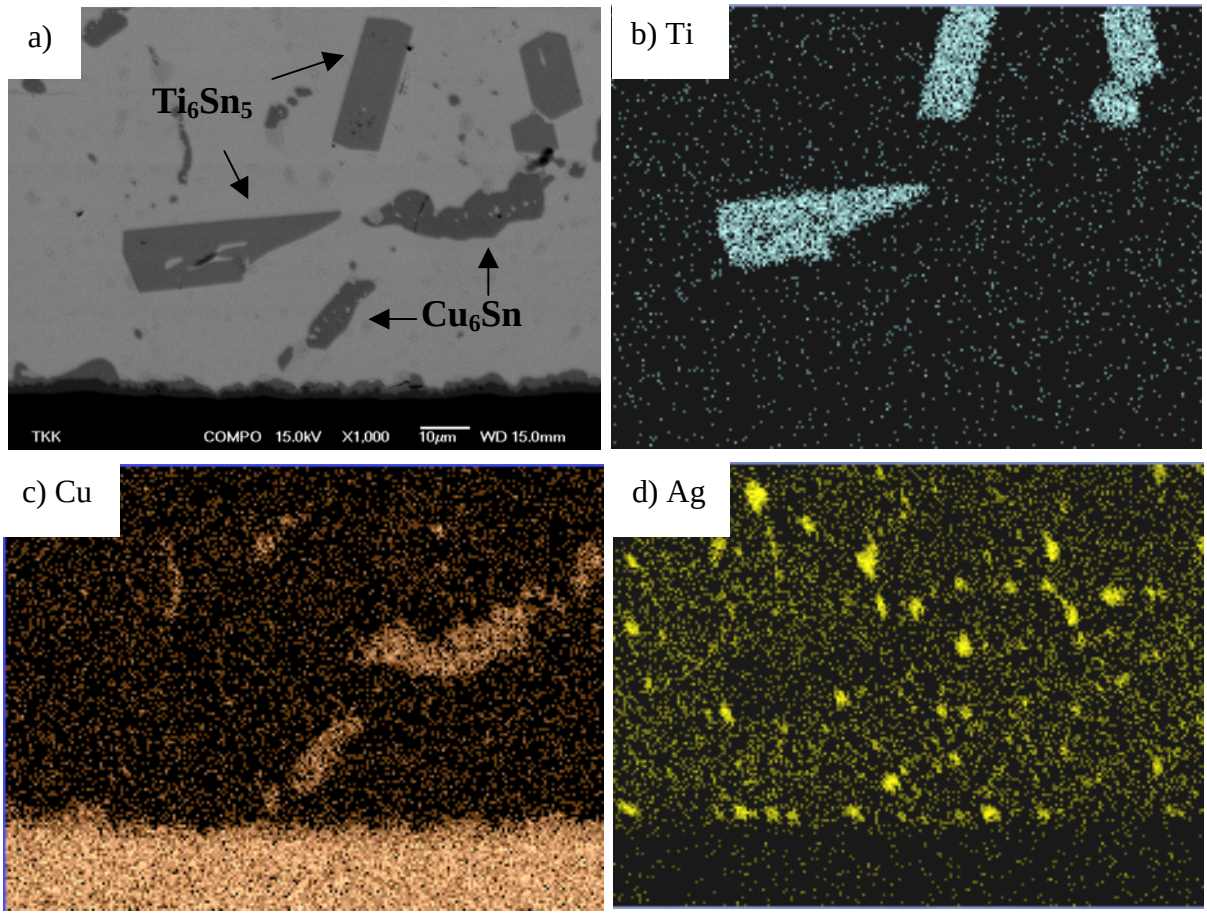

Figure 6.35: *(a) interfacial microstructure after annealing the $SnAg_{eut}$+2.5at-%Ti/Cu diffusion couple at 125℃ for 2700 hours and corresponding element maps: (b) Ti, (c) Cu, and (d) Ag.*

Effect of the addition of Ni to Cu

In this chapter experimental results (at 125°C for up to 3500 hours) concerning the influence of various amounts (1 to 10 at-%) of Ni in Cu on the growth of $(Cu,Ni)_6Sn_5$ are

presented. The possible absence of Cu_3Sn and the formation of pores inside the reaction zone in solid state are also discussed.

When pure Cu is soldered with pure Sn and the diffusion couple is subsequently annealed at 125°C for 3500 hours, the resulting reaction layers are as shown in Fig. 6.37 (a). Both Cu_6Sn_5 and Cu_3Sn are clearly visible. If one compares the thickness ratio of Cu_6Sn_5 to Cu_3Sn to that typically observed after reflow (see Fig. 6.37 (b)), it is evident that the relative thickness of the Cu_3Sn layer has increased markedly during the solid-state aging.

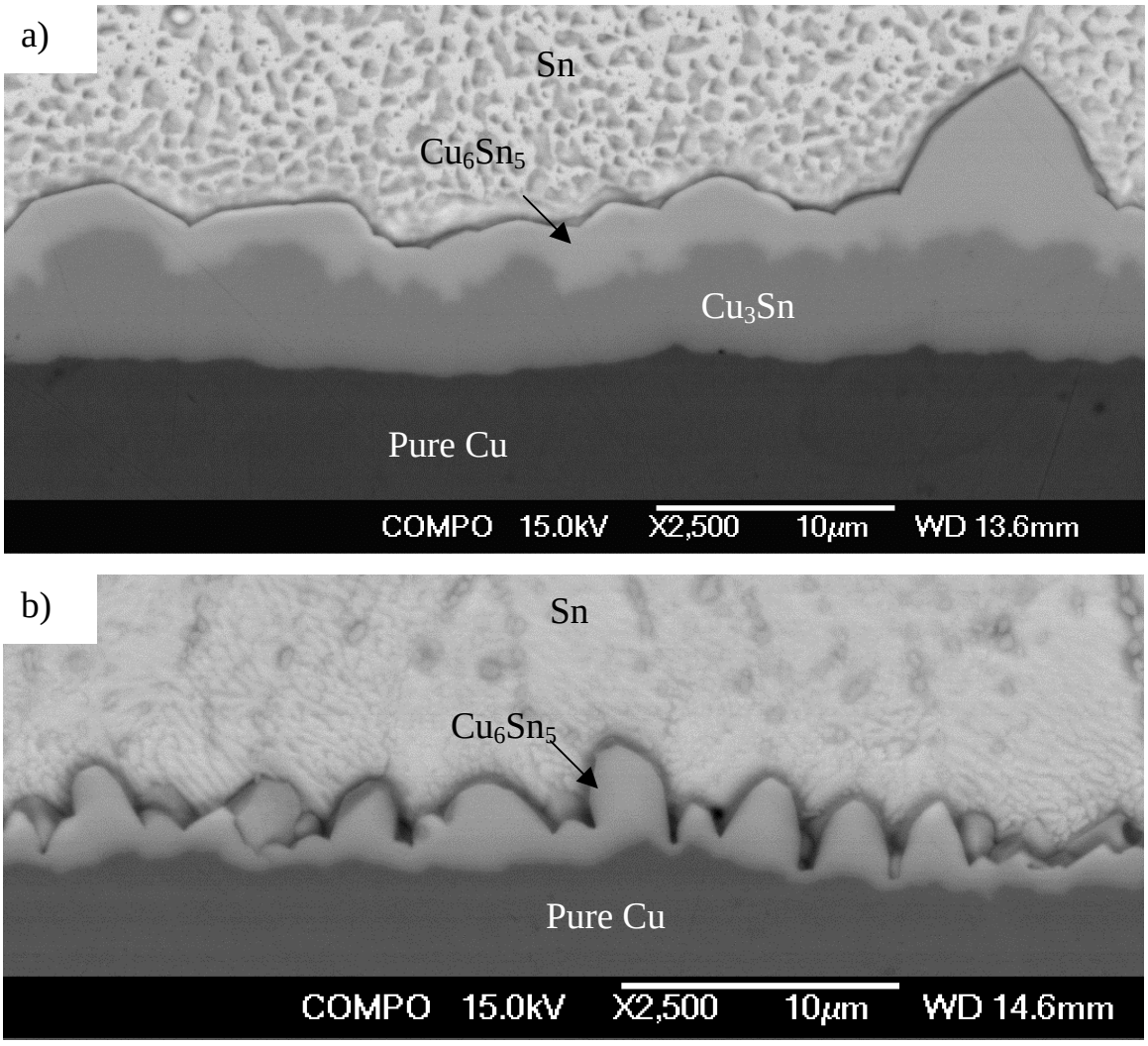

Figure 6.37: *Backscattered SEM images from the sample where pure Cu is soldered with pure Sn. (a) After reflow the diffusion couple is subsequently annealed at 125℃ for 3500 hours and (b) interfacial reaction zone after reflow.*

When only 0.1 at-% of Ni is added to Cu and the alloy is subsequently soldered with Sn and the diffusion couple is then annealed at 125°C for 3500 hours, the resulting interfacial reaction layers are as shown in Fig. 6.38. Both Cu-Sn intermetallic compounds (Cu_6Sn_5 and Cu_3Sn) are present. What is different, when compared to the pure Cu case, is that the fraction of Cu_3Sn out of the total IMC thickness is much smaller than in the Cu/Sn couple. Thus it seems evident that the addition of 0.1 at-% of Ni has a marked effect on the growth kinetics. If one compares the total thickness of the reaction layers to the previous pure Cu/Sn couple, it can be seen that the total IMC thickness has also decreased because of the reduction in the thickness of Cu_3Sn. The average thickness of Cu_6Sn_5 is, however, about the same as in the Cu/Sn couple and the main effect of Ni addition has been on the growth of Cu_3Sn.

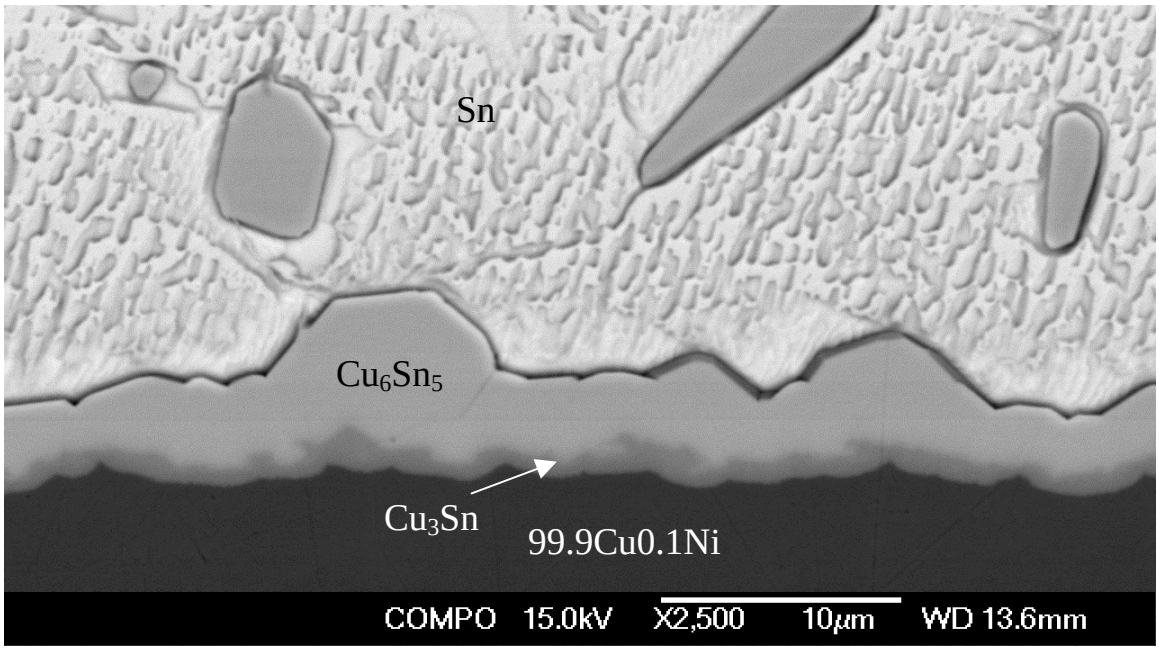

Figure 6.38: *Backscattered SEM images taken from the 99.9Cu0.1Ni/Sn sample annealed at 125℃ for 3500 hours.*

By increasing the Ni content in Cu up to 1 at-%, the interfacial microstructure after solid-state annealing continues to change (see Fig. 6.39). In addition to the reduction in the thickness of Cu_3Sn, there is a marked density of pores in this case, mostly situated at the Cu/Cu_3Sn interface or inside the Cu_3Sn layer. Some authors have claimed these to be

Kirkendall pores, but the situation is not necessarily so simple. Whatever their formation mechanism is, these pores will contribute to the markedly small thickness of the Cu_3Sn layer.

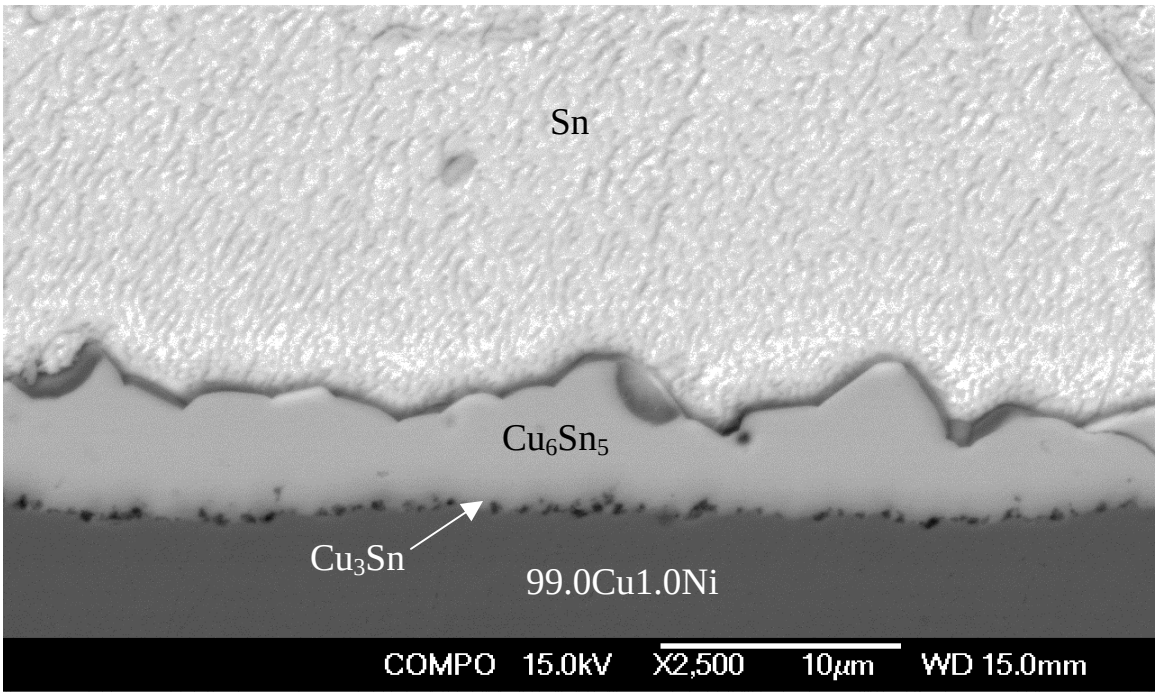

Figure 6.39: *Backscattered SEM image taken from the 99.0Cu1.0Ni/Sn sample annealed at 125℃ for 3500 hours showing the formation of pores at the Cu/Cu_3Sn interface.*

The addition of 2.5 at-% of Ni to Cu does not provide any major microstructural changes in comparison to the Cu1Ni case, as can be seen from Fig. 6.40. Both phases are still present, but Cu_3Sn is hardly detectable and the porosity is even higher. The Cu_6Sn_5 has a wide variation in thickness, but the average thickness is somewhat greater than in the Cu1Ni case. However, when the Ni concentration in the Cu(Ni) alloy is further increased to 5 at-% (annealed at 125°C for 3500 hours), Cu_3Sn can only barely be observed at the interface. Practically only $(Cu,Ni)_6Sn_5$ (containing about 6-8 at-%Ni, as measured from non-etched samples) is present and its thickness is much greater than in the previous cases (Fig. 6.41). The amount of pores has also decreased significantly.

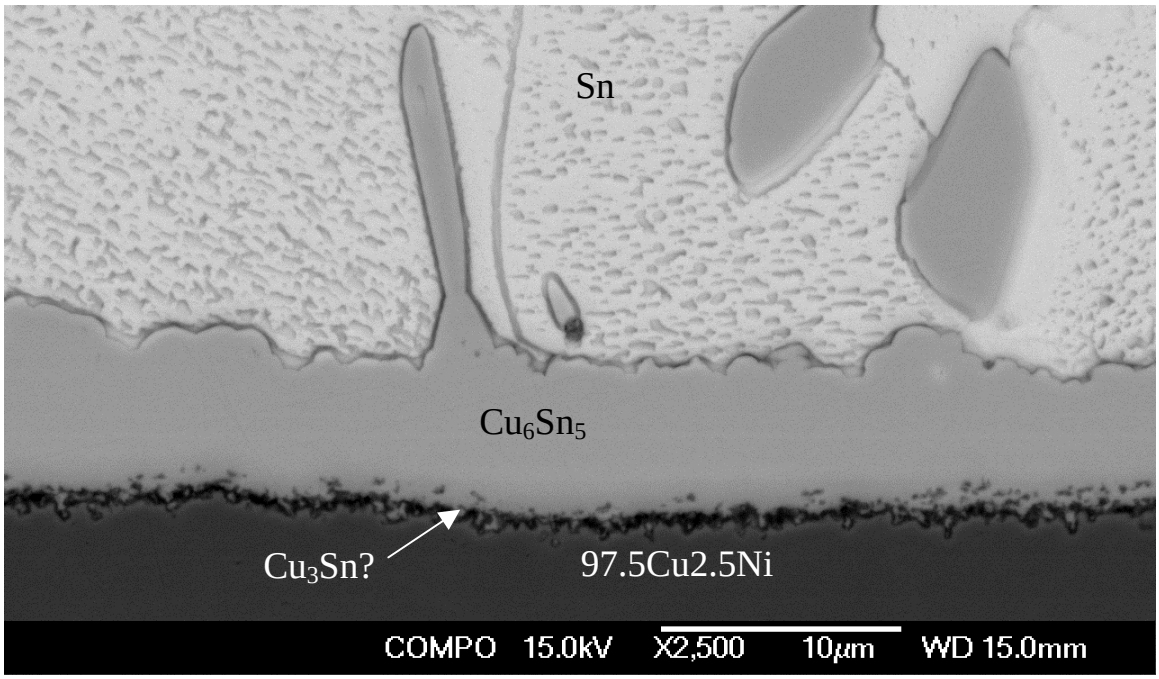

Figure 6.40: *Backscattered SEM image taken from the 97.5Cu2.5Ni/Sn sample annealed at 125℃ for 3500 hours.*

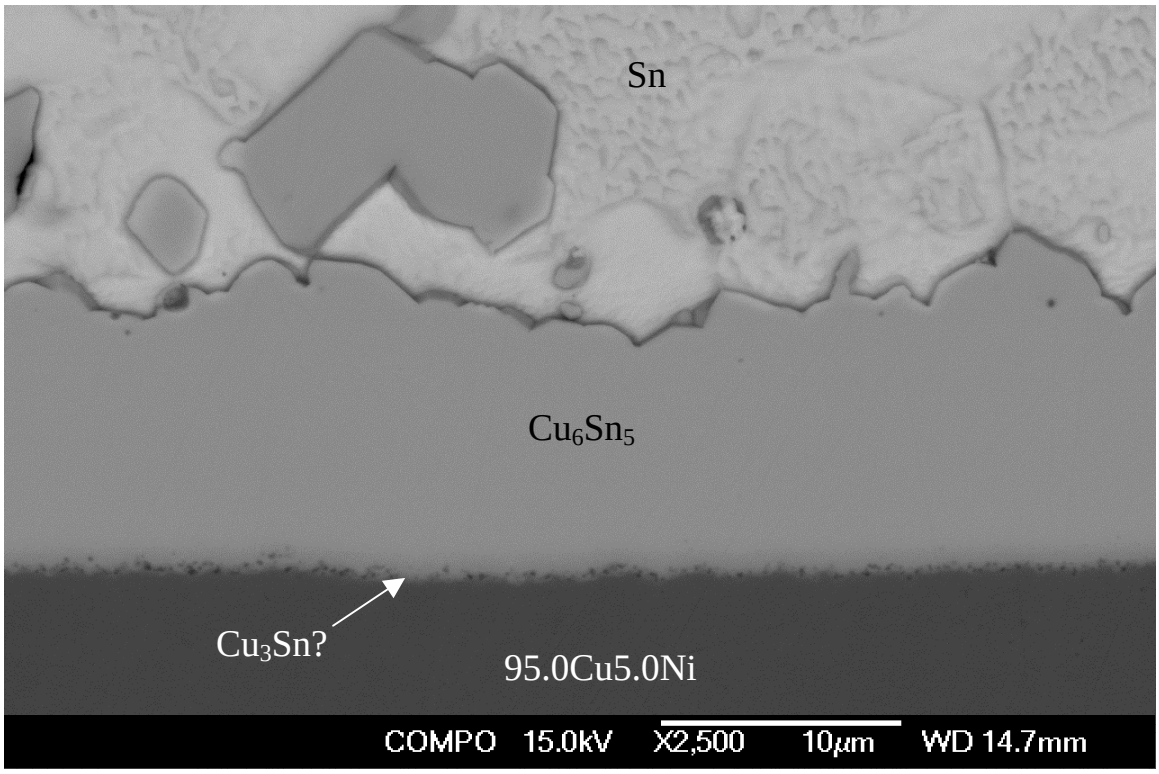

Figure 6.41: *Backscattered SEM image taken from the 95.0Cu5.0Ni/Sn sample annealed at 125°C for 3500 hours.*

Increasing the Ni content to 10 at-% does not change the situation significantly. $(Cu,Ni)_6Sn_5$ is still the only phase visible and the number of pores is extremely low (Fig. 6.42). The thickness of the $(Cu,Ni)_6Sn_5$ has not increased. In fact, it has decreased in comparison to the Cu5Ni case.

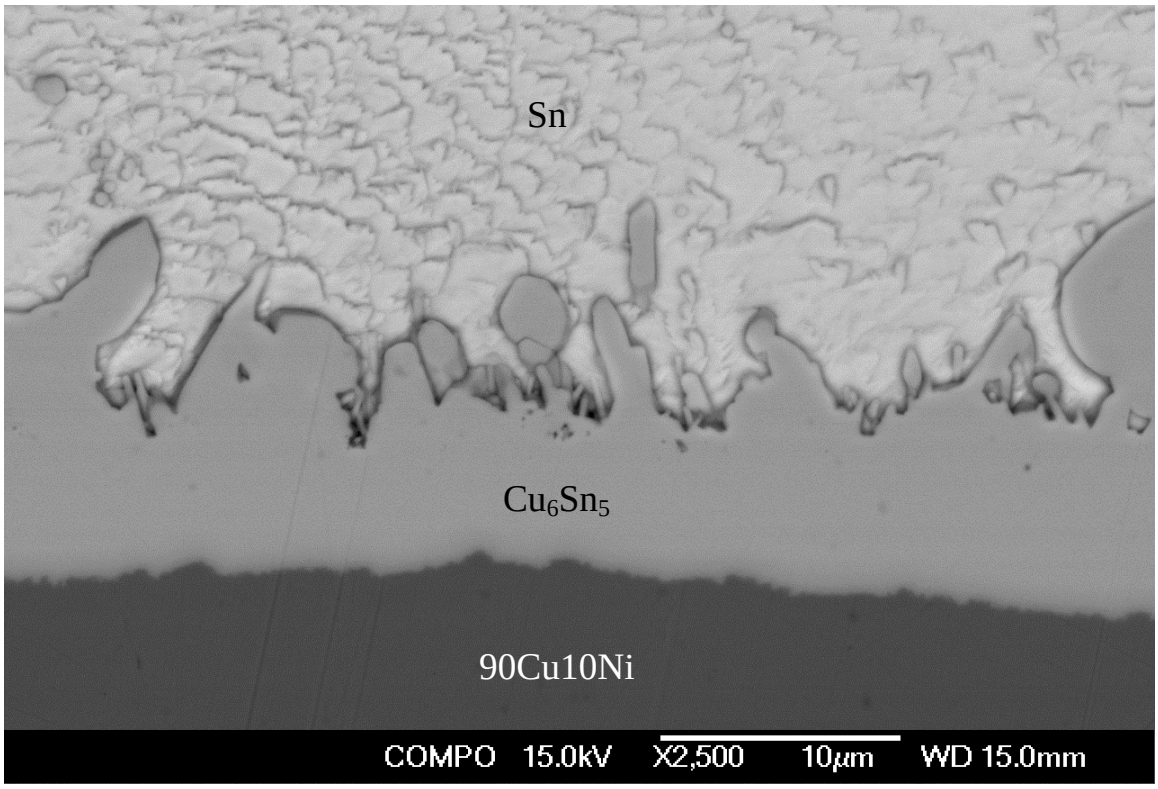

Figure 6.42: *Backscattered SEM image taken from the 90Cu10Ni/Sn sample annealed at 125°C for 3500 hours.*

Essentially similar results (see Figs 6.43-44) are also observed when using eutectic SnAgCu solder instead of commercially pure Sn. Hence, as can be seen from Figures 6.45 (a) and (b), when Ni is added to Cu the following phenomena take place in the Cu(Ni)/Sn diffusion couple: (i) the addition of 0.1 at-% of Ni to Cu reduces the total thickness of the IMC layer to about half that in the Cu/Sn diffusion couple and markedly reduces the ratio of Cu_3Sn to Cu_6Sn_5; (ii) the addition of 1 to 2.5 at-% of Ni to Cu continues the latter trend, produces a significant amount of pores at the Cu/Cu_3Sn interface, and increases the thickness of Cu_6Sn_5 in comparison to that in the pure Cu/Sn couple; (iii) the further addition of 5 at-% Ni to Cu increases the total thickness of the

IMC layer to about twice that in the Cu/Sn diffusion couple and causes Cu_3Sn to almost completely disappear (within the resolution limits of SEM), and (iv) the addition of 10 at-% of Ni to Cu causes pores to disappear and reduces the total IMC thickness again to close to that of the Cu/Sn diffusion couple.

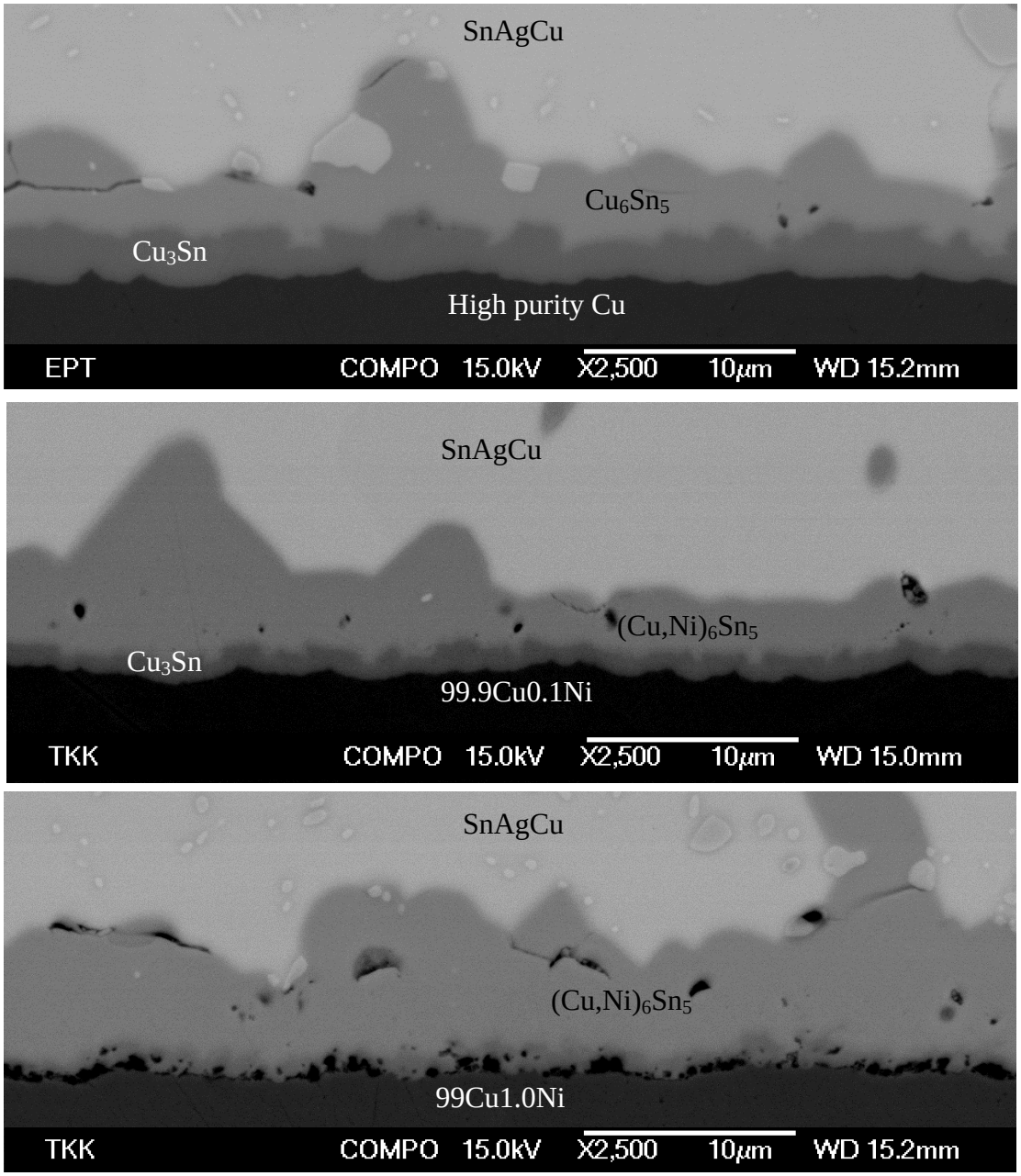

Figure 6.43: *Backscattered SEM images taken from the high-purity Cu/SnAgCu (top), 99.9Cu0.1Ni/SnAgCu (middle) and 99Cu1.0Ni/SnAgCu (bottom) samples annealed at 125℃ for 3500 hours.*

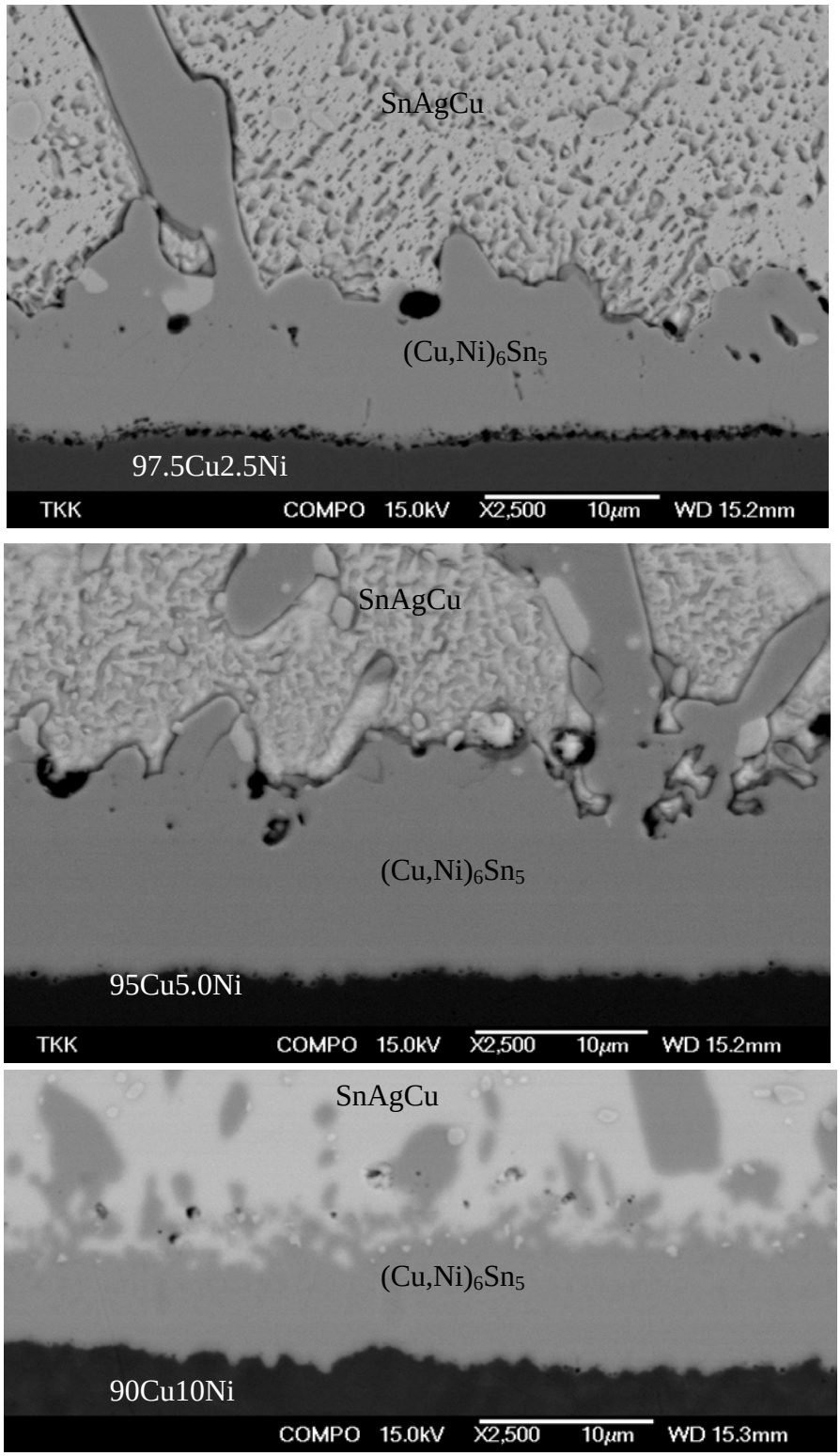

Figure 6.44: *Backscattered SEM images taken from the 97.5Cu2.5Ni/SnAgCu (top), 95Cu5.0Ni/SnAgCu (middle) and 90Cu10Ni/SnAgCu (bottom) samples annealed at 125°C for 3500 hours.*

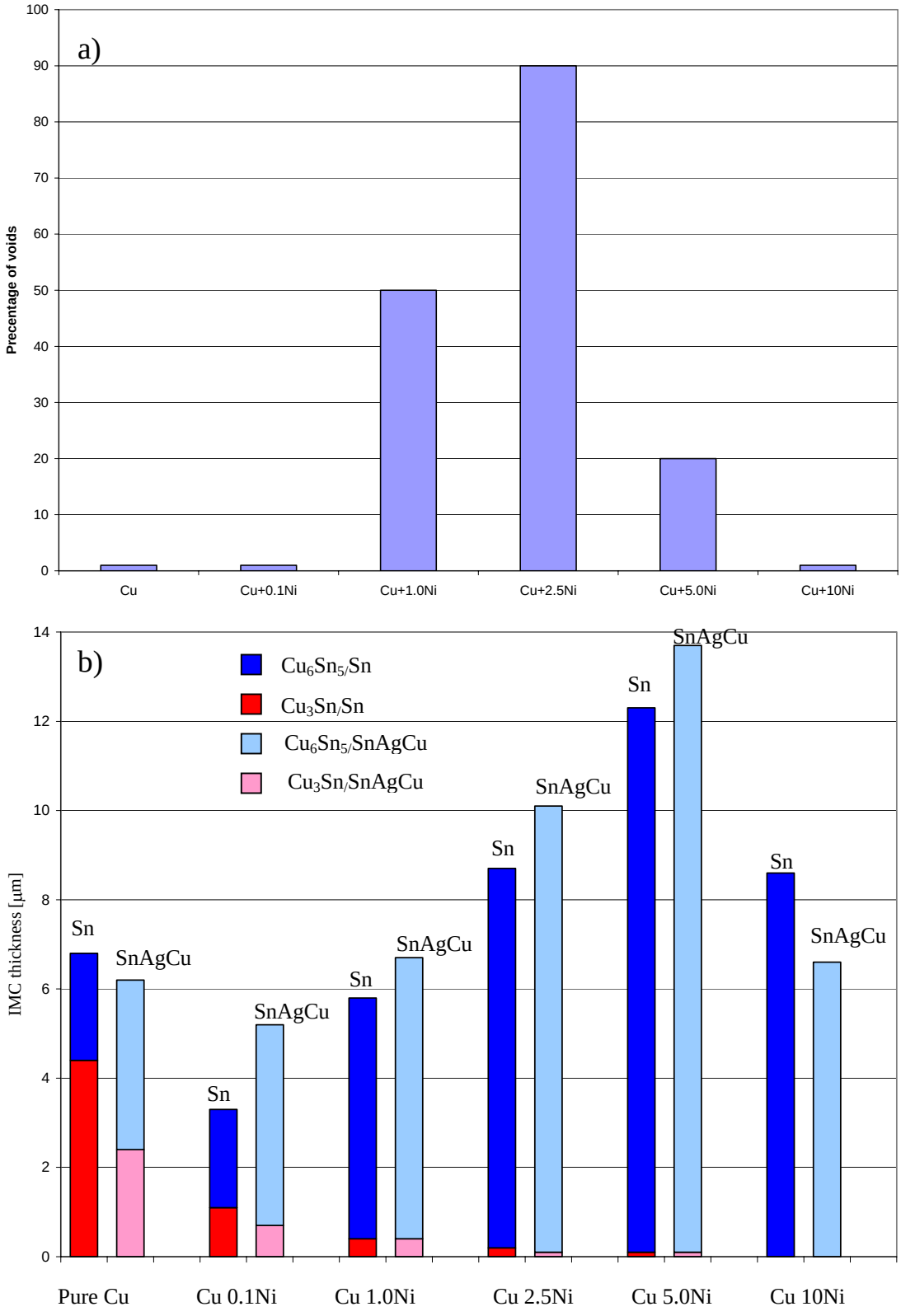

Figure 6.45: *(a) The percentage of voids at the Cu/Cu3Sn interface and (b) IMC thickness versus the Ni content of the Cu(Ni) alloy substrate after annealing for 3500 h at 125°C with Sn and SnAgCu.*

In order to rationalise the possible thermodynamic phenomena behind the above-mentioned results, the ternary Sn-Cu-Ni phase diagram is required. The metastable isothermal section at 125°C is shown in Fig. 6.46.

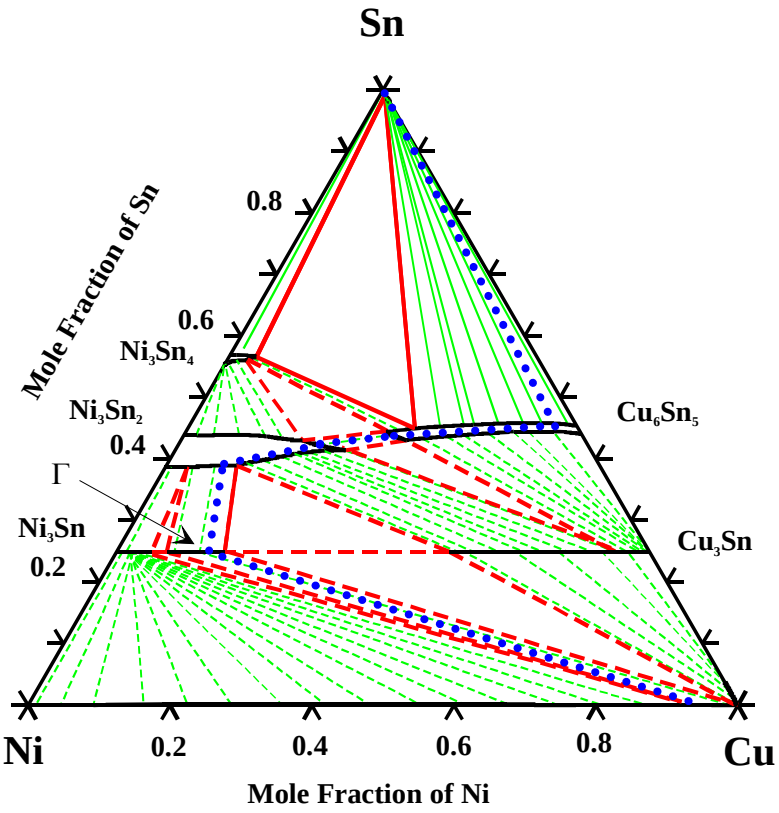

Fig. 6.46: *Isothermal section at 125℃ of the assessed Sn-Cu-Ni ternary phase diagram with superimposed diffusion path. [5]*

This metastable diagram includes neither the solid miscibility gap in the Cu-Ni system nor the ternary phase 44Sn27Cu29Ni (τ) observed in [47]. This is because the formation of τ requires very long annealing times (up to 10,000 hours) and, furthermore, this compound has not been reported elsewhere. Another ternary compound, $CuNi_5Sn_2$ (Γ_1), has also been reported [154]. This compound has been taken into account in the optimisation of the diagram for reasons that are discussed later on. It should be noted that up to 50% metastable solubility of Ni in the Cu sublattice of Cu_6Sn_5 has been reported at 220°C [29]. However, at the moment many aspects of the phase equilibria in

the ternary Sn-Cu-Ni phase diagram have not been unambiguously determined, especially in the low Sn region, and thus the phase equilibria are presented with dashed lines. On the basis of the diagram shown in Fig. 6.46, the addition of more than 5 at-% of Ni to Cu would lead to local equilibrium between Cu(Ni) and $(Ni,Cu)_3Sn$ or ternary compound $CuNi_5Sn_2$ (Γ_1), contrary to the diagram by Lin et al [70]. The diffusion path (presented with the dotted line in Fig. 6.46) could then go through $(Ni,Cu)_3Sn_2$ and then to $(Cu,Ni)_6Sn_5$. Thus, in this reaction sequence the Cu_3Sn would not be stable and could not form. In addition, as Ni compounds are known to be very slow to grow they could be present as such thin layers that they cannot be detected within the resolution limits of the FEG-SEM. On the other hand, according to the diagram determined experimentally by P. Oberndorff [47], the maximum stable solubility of Ni in $(Cu,Ni)_3Sn$ is about 3 at-%. Thus the addition of Ni to Cu could lead to the diffusion path Cu(Ni) | 44Sn27Cu29Ni | $(Cu,Ni)_6Sn_5$| Sn, which bypasses Cu_3Sn. Unfortunately, the formation of ternary 44Sn27Cu29Ni (τ) is not easy to verify as it has the same Sn content as Cu_6Sn_5 and can thus be $(Cu,Ni)_6Sn_5$. In fact, as no structural information about the 44Sn27Cu29Ni (τ) phase was presented in [47], it can also be binary Cu_6Sn_5 with extensive ternary solubility of Ni.

Hence, as the thermodynamic information alone cannot explain the effect of Ni, kinetic considerations also have to be utilised to rationalise the absence of Cu_3Sn from the Cu(Ni)/Sn diffusion couples with more than 5 at-% of Ni, the accelerated growth of $(Cu,Ni)_6Sn_5$, and the formation of pores at the Cu/Cu_3Sn interface. As the chemical potential difference provides the driving force for diffusion, the thermodynamic assessment of the Sn-Cu-Ni system, even though it is not complete, will provide relevant information about the effect of Ni for use in the kinetic considerations. As demonstrated by Yu et al., the driving force for the diffusion of Sn through Cu_6Sn_5 is increased when the Ni content of this phase is increased [36]. Sn is generally assumed to be the main diffusing species in Cu_6Sn_5, whereas Cu is the main diffusing species in Cu_3Sn [29, 90]. However, opposite claims also exist [24]. Therefore, we will concentrate on the magnitudes of the driving forces for the diffusion of Sn and Cu through Cu_6Sn_5 and Cu_3Sn, respectively. When Ni dissolves in $(Cu,Ni)_6Sn_5$, its stability will increase rapidly.

On the other hand, the Ni content of $(Cu,Ni)_3Sn$ in local equilibrium with $(Cu,Ni)_6Sn_5$ remains low and therefore its stability increases much more slowly. This will have an effect on the chemical potentials (and therefore the activities) at the Sn/$(Cu,Ni)_6Sn_5$ and Cu_3Sn/Cu interfaces in such a way that the driving force for the diffusion of Sn through $(Cu,Ni)_6Sn_5$ increases, whereas the driving force for the diffusion of Cu through Cu_3Sn decreases. Figure 6.47 shows the Gibbs free energy diagram of the binary Sn-Cu system at 125°C, together with the effect of dissolved Ni. It is to be noted that in ternary systems the tie-lines are in the plane of the vertical section only in special cases (such as from a pure component to an ideally stoichiometric intermetallic compound) and therefore the free energy values must be obtained along the diffusion path (tie-lines) and not along the contact line. As can be seen from Fig. 6.47, the driving force for the diffusion of Sn atoms through Cu_6Sn_5 (from Interface I to II) is about 3100 J/mol (ΔG_{Sn}) and that of Cu atoms through Cu_3Sn (from Interface III to II) is about 10000 J/mol (ΔG_{Cu}) in the binary Sn/Cu diffusion couple. When Ni is incorporated into IMCs, the situation is changed in the following way. The EDS measurements indicate that the Ni content of the $(Cu,Ni)_6Sn_5$ that is formed is close to that of the original Cu(Ni) alloy. Therefore, when 1 at-% of Ni is added to Cu, the Ni content of $(Cu,Ni)_6Sn_5$ is about 1 at-% and its stability is increased to g^{η^*}. The Cu_3Sn in equilibrium with it is practically free of Ni, as can be seen from the direction of the tie-lines in Fig. 6.46, and therefore its stability will remain practically the same as that of pure Cu_3Sn (g^{ε^*}). As a result, the driving forces for diffusion over the intermetallic compounds have changed and are $\Delta G_{Sn}^{\ *}$ (about twice ΔG_{Sn}) for Sn and $\Delta G_{Cu}^{\ *}$ (about 9/10 ΔG_{Cu}) for Cu atoms. If the Ni content of $(Cu,Ni)_6Sn_5$ increases to 5 at-%, the stability is increased even more ($g^{\eta^{**}}$) and the $(Cu,Ni)_3Sn$ in equilibrium with it has also stabilised slightly (g^{ε^*}). Thus the driving force for the diffusion of Sn atoms though $(Cu,Ni)_6Sn_5$ has increased up to 4-5 times and the driving force for the diffusion of Cu atoms though $(Cu,Ni)_3Sn$ has decreased to about 2/3 that of the pure Sn-Cu system. Further, if Cu_3Sn does not form at all, as the experimental evidence indicates, the driving force for the diffusion of Sn through $(Cu,Ni)_6Sn_5$ will increase even further (dashed tangent line in Fig. 6.47 for g^{η^*} and g^{α^*}, which is the Gibbs free energy curve for Fcc(α)-phase containing 5 at-%Ni).

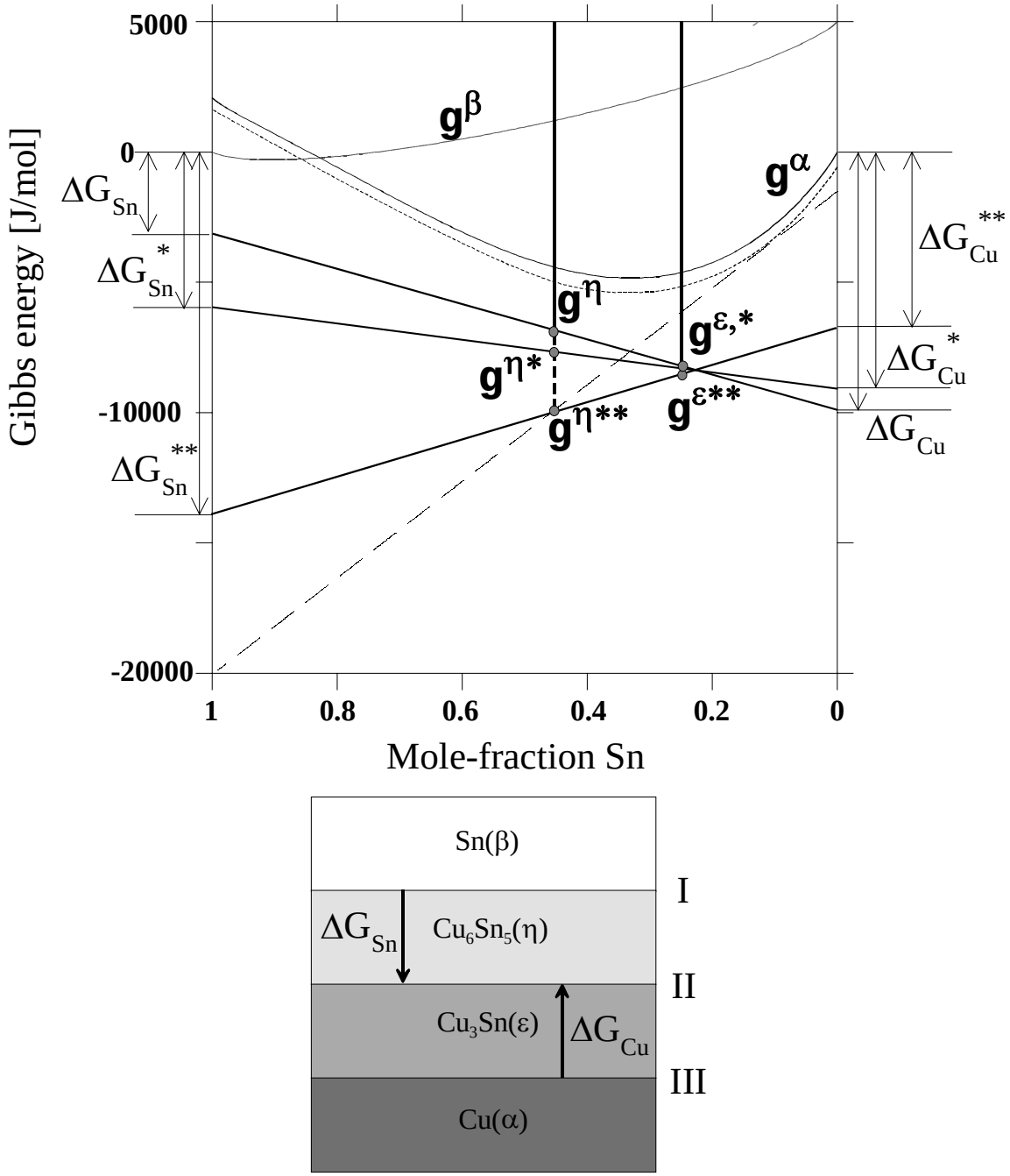

Figure 6.47: *Gibbs free energy diagram [5] at 125 °C showing the driving forces for diffusion over the schematically represented interfacial reaction zone.*

As the diffusion flux is directly proportional to the driving force, according to the well-known Nernst-Einstein relation, the material flux can be expected to grow over Cu_6Sn_5 and to decrease over Cu_3Sn when Ni is brought into the Sn-Cu system. By extrapolating

the data reported by Oh [29] (at temperatures between 180°C to 220°C) down to 125, the following ratios for the intrinsic diffusion coefficients are obtained: $\frac{D_{Cu}^{Cu_3Sn}}{D_{Sn}^{Cu_3Sn}} \approx 3$ and $\frac{D_{Sn}^{Cu_6Sn_5}}{D_{Sn}^{Cu_3Sn}} \approx 3.5$. Paul [90] determined the ratio of diffusion fluxes at 220°C as $\frac{\left|J_{Sn}^{Cu_5Sn_5}\right|}{\left|J_{Cu}^{Cu_5Sn_5}\right|}\left(=\frac{D_{sn}V_{Cu}}{D_{Cu}V_{sn}}\right)=1.6$ and $\frac{\left|J_{Sn}^{Cu_3Sn}\right|}{\left|J_{Cu}^{Cu_3Sn}\right|}=0.9$. On the basis of these, the following estimation is made for the relative diffusion fluxes in the pure Sn-Cu system at 125°C: $J_{Sn}^{Cu_6Sn_5}=1(=\text{reference value})$, $J_{Cu}^{Cu_6Sn_5}=0.6$, $J_{Sn}^{Cu_3Sn}=0.3$ and $J_{Cu}^{Cu_3Sn}=0.9$. By assuming that when Ni is dissolved in Cu_6Sn_5 the changes in driving forces (presented above) are directly proportional to the changes in the fluxes of the faster-moving species (i.e. Sn in Cu_6Sn_5 and Cu in Cu_3Sn) and that the magnitudes of $J_{Cu}^{Cu_6Sn_5}$ and $J_{Sn}^{Cu_3Sn}$ remain unchanged, the following flux values are obtained:

i) when the Ni content of $(Cu,Ni)_6Sn_5$ is 1 at-%

$J_{Sn}^{Cu_6Sn_5}=2$, $J_{Cu}^{Cu_6Sn_5}=0.6$, $J_{Sn}^{Cu_3Sn}=0.3$ and $J_{Cu}^{Cu_3Sn}=0.8$

ii) when the Ni content of $(Cu,Ni)_6Sn_5$ is 5 at-%

$J_{Sn}^{Cu_6Sn_5}=4.5$, $J_{Cu}^{Cu_6Sn_5}=0.6$, $J_{Sn}^{Cu_3Sn}=0.3$ and $J_{Cu}^{Cu_3Sn}=0.6$

As can be seen from Fig. 6.48, the vacancy flux balance $\left(J_v^{Cu_6Sn_5}\text{ and }J_v^{Cu_3Sn}\right)$ is therefore also drastically changed (note that the thickness of the IMC layers are not to scale, but the flux vectors are). This issue and possible deviations from the equilibrium vacancy concentration in Cu_3Sn are addressed in more detail later on.

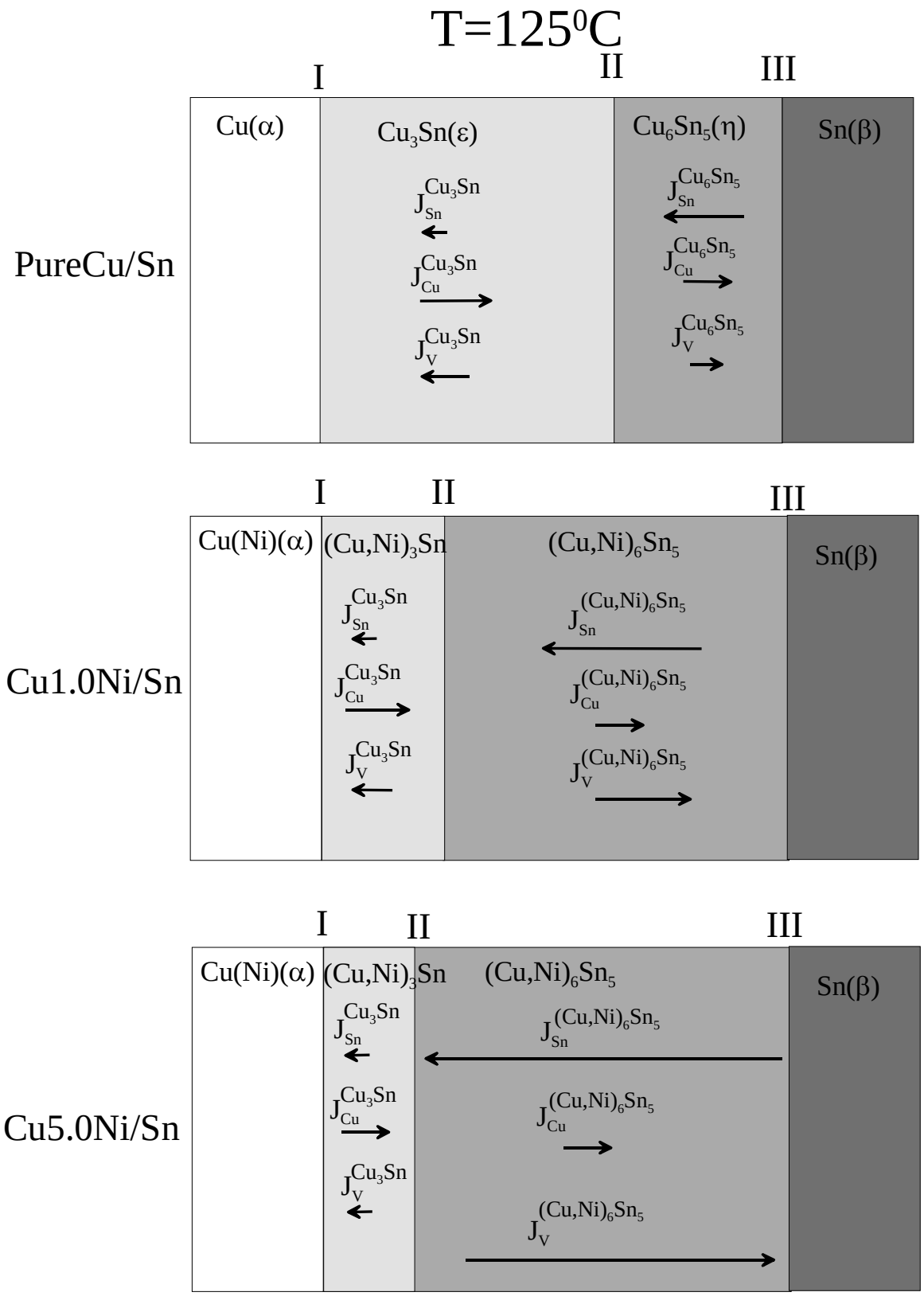

Figure 6.48: *The effect of Ni on the intrinsic fluxes through the IMCs*

Explaining the effect of dissolved Ni on the diffusion kinetics in Cu_3Sn (and Cu_6Sn_5), Garner et al. [155] used another approach based on phase diagram information on the Sn-Cu-Ni ternary system. Their approach was based on a "rule of thumb" (or helpful generalisation) originally presented by Birchenall [156]. According to this rule, the interdiffusion coefficient $\tilde{D}$ in a solution phase is decreased if the addition of component i will raise its melting point (i.e. liquidus temperature), and vice versa. On the basis of their interpretation of the Cu_3Sn-Ni_3Sn isopleth [157], Garner et al. concluded that the addition of Ni slows down the Cu_3Sn growth kinetics. This conclusion is not easy to accept. First, the rule is based on the experimental results obtained with binary solution phases and not with ternary ordered compounds (i.e. Cu_3Sn). Second, in the case of the Cu_3Sn-Ni_3Sn isopleth [157], Ni does not increase the melting point of Cu_3Sn, as the authors claim [155], but another high temperature phase (Cu_4Sn or γ-phase).

Recently Paul [90] has presented interesting results from his investigations of Cu(Ni)/Sn reaction couples. On the basis of marker experiments at 215°C, he was able to show that Sn is a remarkably faster-diffusing species than Cu in the $(Cu,Ni)_6Sn_5$ compound. This, together with the previous discussion about the driving force for Sn diffusion, indicates that the mobility of Sn in the $(Cu,Ni)_6Sn_5$ layer can be significantly accelerated if Ni is added to the compound. It is known that the growth of phases with high diffusion fluxes is favoured over phases with small fluxes and that they can limit the growth of other phases or even consume previously formed phases [158]. Thus the increased material flux inside $(Cu,Ni)_6Sn_5$ could explain why Cu_3Sn is not formed or does not grow to an observable thickness. Extrapolation of these results [90] to lower temperatures in our case can of course be criticised on the basis of possible changes in diffusion mechanism, structural transition of Cu_6Sn_5, etc. Nevertheless, we think that the same tendency as observed at 215°C can also be expected at 125°C, since the experimental results are so consistent. However, two questions still remain: (i) in addition to the larger ΔG_{Sn}, what makes the Sn flux so large in $(Cu,Ni)_6Sn_5$, and (ii) how is the formation of pores related to all of this?

In relation to the first question, Paul [90] made quite an interesting observation regarding the grain size of $(Cu,Ni)_6Sn_5$. He observed that when Cu was alloyed with 5-15 at-% of Ni, the grain size of the $(Cu,Ni)_6Sn_5$ was more than one order of magnitude smaller than in the case of pure Cu [90]. We have also observed that Ni has an effect on the grain size of $(Cu,Ni)_6Sn_5$. Enhanced grain boundary diffusion, combined with the increased driving force for Sn diffusion, could, of course, contribute to the observed increase in thickness. But can this alone explain the observed growth effects? Why would Sn preferentially diffuse via grain boundaries? Ohriner proposed that the addition of nickel to the η-phase might have important effects on the concentration of structural vacancies present in the intermetallic compound [89]. Unfortunately, Ohriner's XRD results could not verify this hypothesis unambiguously. Since the random motion of vacancies is not possible in highly ordered alloys or compounds, as it would disrupt the equilibrium-ordered arrangement of atoms on lattice sites, all changes in the atomic environment are expected to influence the diffusion of elements in the intermediate compound in question. Belova and Murch [159, 160] have developed several theoretical models for diffusion in stoichiometric and non-stoichiometric intermetallic compounds that predict the heavy dependence of composition on diffusion. On the basis of these models, the addition of Ni to $(Cu,Ni)_6Sn_5$ could induce structural vacancies to form in the Sn sublattice and this could have some effect on the growth behaviour of $(Cu,Ni)_6Sn_5$. However, as $(Cu,Ni)_6Sn_5$ has relatively high electrical conductivity, the possible formation of structural vacancies is not expected to have a significant effect.

At the moment it is not unambiguously clear what microstructural effects Ni induces in the $(Cu,Ni)_6Sn_5$ compound layer. However, what is evident is that the presence of Ni will accelerate the diffusion of Sn through this layer. An appropriate question is, then, whether the formation of the pores is also related to the changes in the diffusion fluxes inside the Cu_6Sn_5 and Cu_3Sn layers. Van Loo et al [161] have analysed the effect of intrinsic diffusion coefficients and initial and interfacial concentrations of each phase on the creation and annihilation of vacancies. Any interphase boundary must be able to serve as either a source or sink for vacancies to accommodate the differences in vacancy fluxes. In our case, the Cu_6Sn_5/Cu_3Sn interface must be a source of vacancies for both

intermetallic compound layers. This is because Sn is the main diffusing species in Cu_6Sn_5 and Cu is the main diffusing species in Cu_3Sn. In order to maintain the vacancy flux balance, these vacancies, which are created at the Cu_6Sn_5/Cu_3Sn interface, must be annihilated at other interfaces or in the bulk phases. Since it is evident that Sn flux through Cu_6Sn_5 is very large, it is likely that the vacancies are not accumulated on that side, even though their creation will be accelerated at the Cu_6Sn_5/Cu_3Sn interface as a result of the increased Sn flux (see Fig. 6.48). However, because the Cu_6Sn_5/Cu_3Sn interface supplies vacancies to both phases, the accelerated diffusion of Sn in the Cu_6Sn_5 layer could also cause extra vacancies to be injected into the Cu_3Sn layer. This can lead to the accumulation of vacancies at the Cu_3Sn/Cu interface and eventually to the formation of macroscopic voids. Especially if we assume that the ratio of mobilities of Cu and Sn in $(Cu,Ni)_3Sn$ does not markedly change as a result of the addition of Ni, the Kirkendall effect should be enhanced, as material flux through $(Cu,Ni)_3Sn$ is reduced. When more Ni is added to Cu, the fluxes in $(Cu,Ni)_3Sn$ will be reduced further and further, finally resulting in the (almost) total disappearance of $(Cu,Ni)_3Sn$, as well as the pores. Thus, the changes in the diffusion fluxes resulting from the addition of Ni can result in both the observed alterations in thickness of the IMC layers and the formation and disappearance of pores.

Other possible impurities from Cu platings

Iron and zinc were considered as other possible impurity elements in electroless Cu deposits. Therefore, high-purity Cu was alloyed with Fe (1 at-%) and Zn (1 at-%) and the results were compared with those of Cu+1Ni (at-%) presented above. Commercially pure Sn and SnAgCu were used to solder the substrate materials. After standard reflow the samples were annealed at 125°C for up to 2500 hours. The results (See Fig 6.49 and 6.50) show that the Fe and Zn alloying does not have a significant effect on the void formation. However, it seem that zinc and, especially, iron slow down the growth of Cu_3Sn.

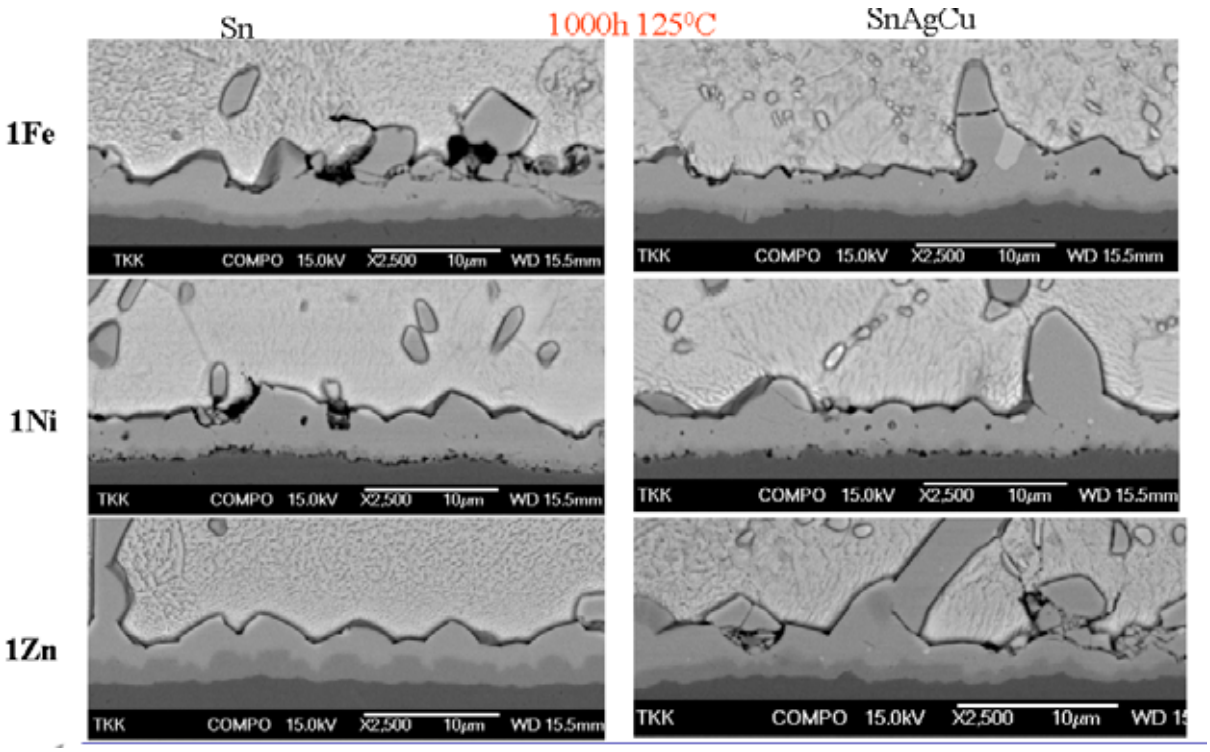

Figure 6.49: *Sn and SnAgCu solder|Fe, Ni, Zn (1at-%) alloyed Cu interfaces after 1000 hours' annealing at 125 ℃.*

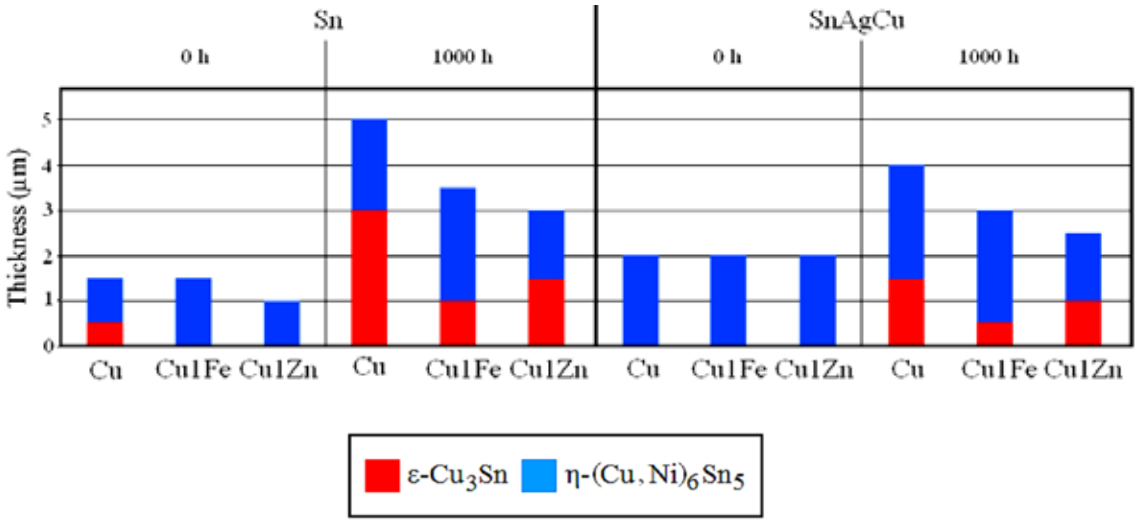

Figure 6.50: *Thickness of the intermetallic compounds after reflow (0h) and after 1000 hours' annealing at 125 ℃ Sn (left) and SnAgCu solder (right) |Cu, Fe, Zn (1at-%) alloyed Cu diffusion couples.*

6.2.2 Effect of Au on Sn-Ni reactions

The formation of the brittle intermetallic compound $(Au,Ni)Sn_4$ (Au redeposition) is a characteristic feature of many Sn-based alloys, as was briefly introduced in Chapter 4. A more detailed analysis has been given by Laurila et al. [21, 114]. The boundary between Ni_3Sn_4 and $(Au,Ni)Sn_4$ is weak and hence provides a low-energy path for crack propagation and the opportunity for ductile-to-brittle fracture transition to occur. Subsequent aging indicates cracks in the $(Au,Ni)Sn_4$ layer [162]. Therefore, in this chapter, the redeposition of $AuSn_4$ intermetallic compound on the top of Ni/Au metallisation after extensive solid-state annealing will be studied with three different solders, i.e. SnPbAg, SnAg, and SnAgCu. The purpose is to provide a theoretical background for the observed redeposition of $AuSn_4$ and to explain why the phenomenon does or does not take place in a given system. The solder pastes were dispensed on the soldering pads of a printed wiring board (PWB), which had been coated with electrochemical Ni (~ 4 μm), on top of which there was an Au layer approximately 5 μm thick. The reason for using such a thick Au layer was to enhance the formation of interfacial reactions and thereby make experimental investigations more straightforward. The solder paste compositions (wt-%) were Sn3.5Ag, Sn3.8Ag0.7Cu, and Sn36.0Pb2.0Ag. The melting of all the solder pastes on the Ni/Au pads was carried out with the same reflow profile, which had a peak reflow temperature of 240°C, reflow time of about 50 s, and cooling rate of 1.8°C/s. After that the samples were annealed at 150°C for up to 3000 hours.

After annealing for 250 h at 150°C, the $(Au,Ni)Sn_4$ redeposition is clearly seen in the (SnPbAg)/Ni/Au system (Fig. 6.51). The thickness of the $(Au,Ni)Sn_4$ was remarkable and the numerous cracks visible in the layer also indicated that it is most probably brittle. Likewise, the interface between Ni_3Sn_4 and $(Au,Ni)Sn_4$ showed some cracking (Fig. 6.51). It should be emphasised that the excessive thickness of the $(Au,Ni)Sn_4$ was related to the thick Au coating used in this study. Thus, the results of this study should not be compared directly to the earlier investigations, where much thinner Au layers were used [100, 118-120]. Nevertheless, it is equally important to realise that the reaction

mechanisms themselves are most probably identical. The formation of a Pb-rich layer in front of the redeposited $(Au,Ni)Sn_4$ intermetallic compound is also evident.

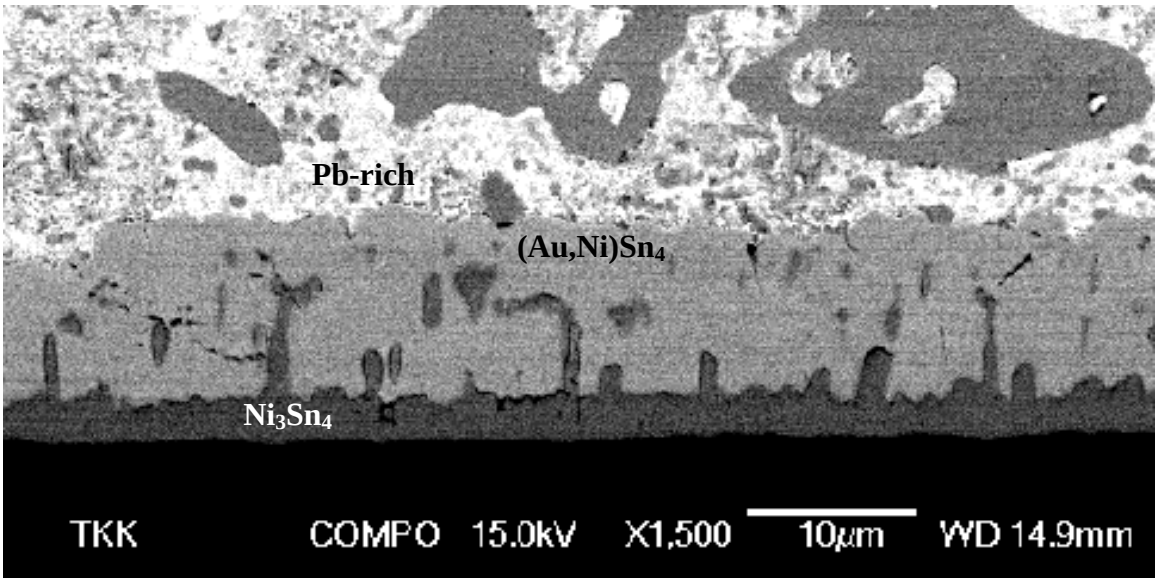

Figure 6.51: *SEM micrograph taken from the (SnPbAg)/Ni/Au system after annealing for 250 hours at 150℃.*

The Ni content of the $(Au,Ni)Sn_4$ was about 10 at-% [i.e. 50 % of the Au atoms in the Au sublattice have been replaced by Ni atoms]. In contrast, no Au could be detected inside the Ni_3Sn_4 within the resolution limits of EDS. Likewise, no Ag was found in any of the above-mentioned IMC layers. It was detected only in the form of an Ag_3Sn compound throughout the solder matrix. Despite the fact that Ag_3Sn can exist in local equilibrium with $AuSn_4$ (Fig. 6.52) at 150°C, it was not found at the interface. However, inside the bulk solder matrix Ag_3Sn and $AuSn_4$, precipitates were commonly found to be in contact.

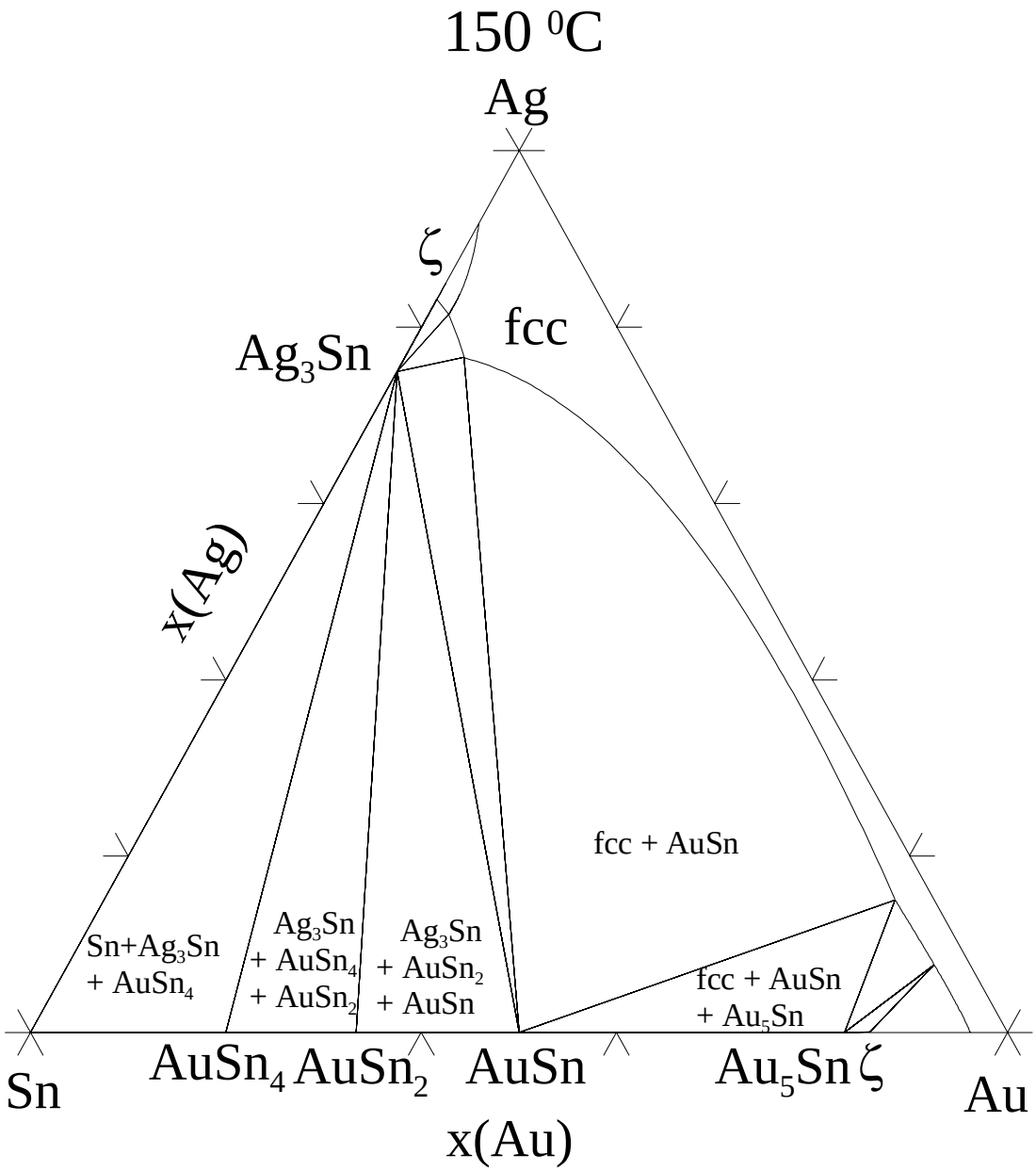

Fig. 6.52: *Isothermal section at 150°C of the evaluated Ag-Au-Sn ternary phase diagram. Phase equilibria of interest have been marked on the isotherm.*

The (SnAg)/Ni/Au system shows behaviour similar to the (SnPbAg)/Ni/Au system. The interfacial structure after annealing at 150°C for 250 hours is shown in Figure 6.53. The thickness of the (Au,Ni)Sn_4 is less than half that in the (SnPbAg)/Ni/Au system.

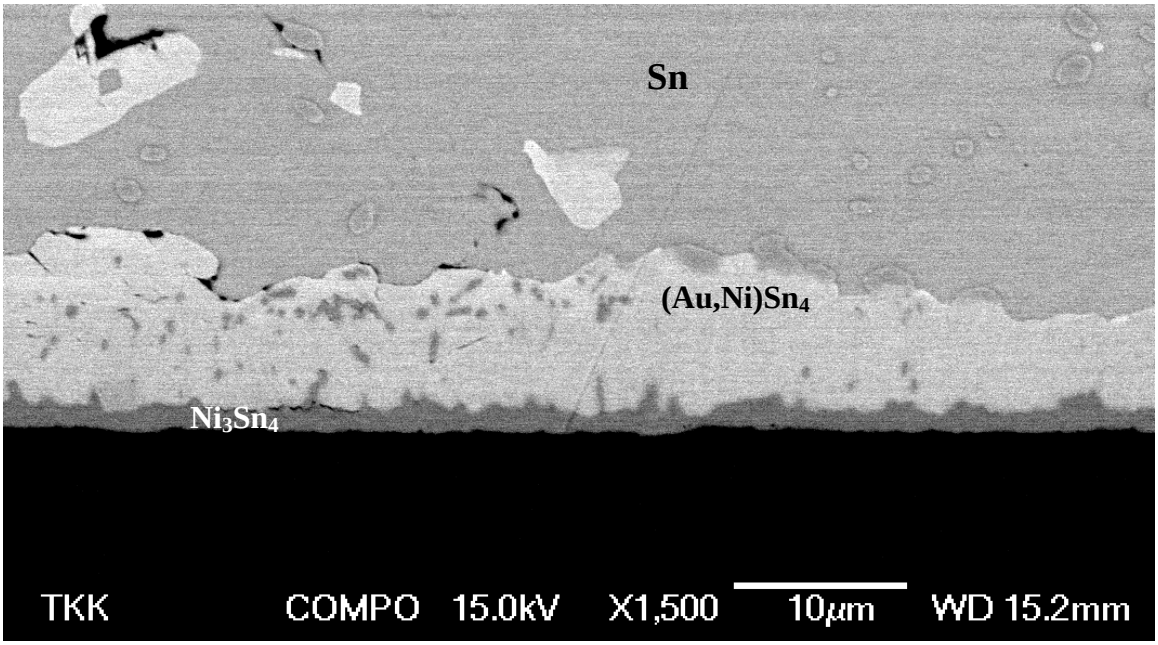

Fig. 6.53: SEM micrograph taken from the (SnAg)/Ni/Au system after annealing for 250 hours at 150°C.

In comparison to the (SnPbAg)/Ni/Au and (SnAg)/Ni/Au systems, the (SnAgCu)/Ni/Au system behaves quite differently. From Figure 6.54 it can be seen that no redeposition of $AuSn_4$ intermetallic compound takes place during annealing at 150°C for 250 hours (or even up to 3000 hours).

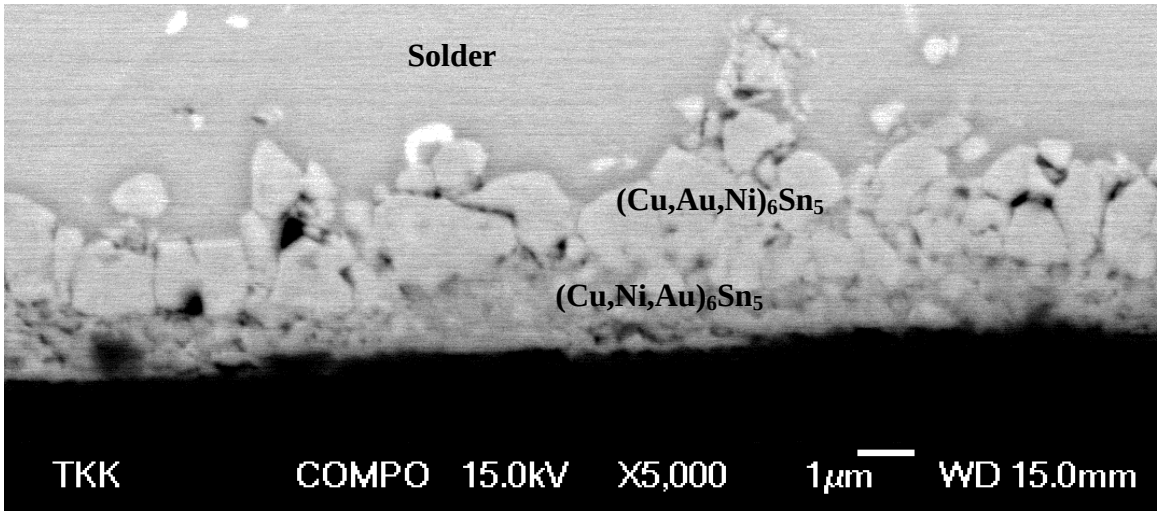

Fig. 6.54: *SEM micrograph taken from the (SnAgCu)/Ni/Au system after annealing for 250 hours at 150°C.*

The morphology of the structure shown in the micrograph (Fig. 6.54) and the compositional analyses indicated that there are two reaction product layers with different Au-to-Ni ratios. The top layer is $(Cu,Au,Ni)_6Sn_5$, where the Au content is about 12 at-%, and the Ni content is about 2 to 3 at-%. The lower $(Cu,Ni,Au)_6Sn_5$ layer contains only about 5 at-% Au and about 17 at-% Ni. Some of the Ni signal may arrive from the underlying Ni substrate as a result of the low thickness of the lower reaction layer.

The first and foremost difference between the three systems investigated is that in both the (SnAgPb)/Ni/Au and the (SnAg)/Ni/Au systems, the first phase to form is Ni_3Sn_4, whereas in the (SnAgCu)/Ni/Au system, the first phase is $(Cu,Ni,Au)_6Sn_5$. Since this is strongly related to the differences observed in the redeposition behaviour of $AuSn_4$ as $(Au,Ni)Sn_4$, it is important to understand why the formation of $(Cu,Ni,Au)_6Sn_5$ takes place instead of that of Ni_3Sn_4 in the (SnAgCu)/Ni/Au system. A detailed explanation of this has already been given and is not repeated here. The observation of $(Cu,Au,Ni)_6Sn_5$ is most probably related to the excessive thickness of the Au layer used. Normally, the Au layer is very thin and so the overall concentration of Au remains very low and, even though some Au is dissolved in $(Cu,Au)_6Sn_5$, the amount is so low that it cannot be detected. However, in this case, the concentration of Au remains reasonably high and the Au concentration in the $(Cu,Au,Ni)_6Sn_5$ phase is high enough to be easily detected. This result is quite important, as it shows that significant amounts of Au can be incorporated into $(Cu,Au)_6Sn_5$.

In order to analyse the reasons for the redeposition of the $AuSn_4$, all the appropriate interfaces formed in the reaction couples, i.e. $Ni_3Sn_4/(Au,Ni)Sn_4$, $Cu_6Sn_5/AuSn_4$, and $(Au,Ni)Sn_4$/solder, must be investigated to check that they fulfil the requirement of local equilibrium with each other. The $(Au,Ni)Sn_4$/solder interface will be investigated first. The solder side is, in all cases, either SnPb (Fig. 6.51) or practically pure tin (Fig. 6.53). In the case of almost pure tin, the local equilibrium is fulfilled, as the $(Au,Ni)Sn_4$ can exist in local equilibrium with tin. The more interesting case is the SnPb (or in our case

the SnPbAg) solder, as it can be seen that the Pb-rich layer is preferentially located next to the (Au,Ni)Sn_4 layer (Fig. 6.51).

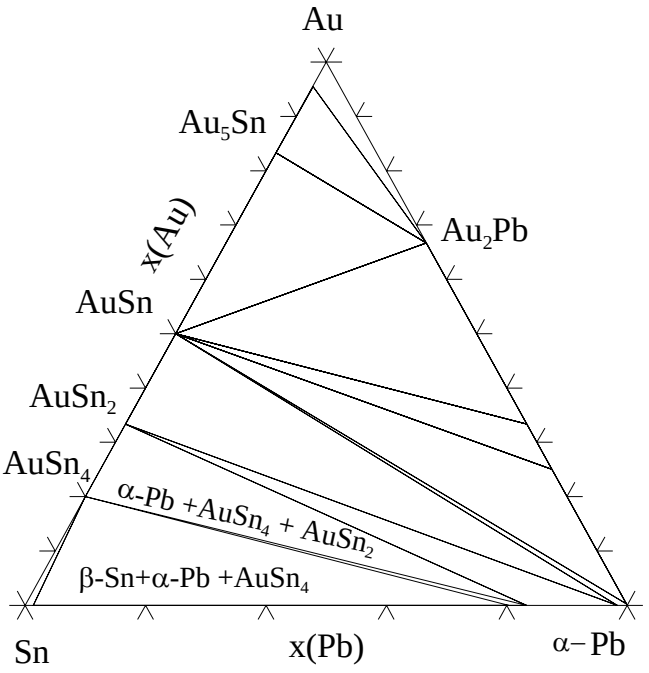

Fig. 6.55: *Isothermal section at 150℃ of the evaluated Au-Pb-Sn ternary phase diagram. Phase equilibria of interest have been marked on the isotherm.*

From Figure 6.55, one can see that lead, with about 20 at-% tin dissolved in it (marked as α-phase), can exist in local equilibrium with $AuSn_4$. Therefore, the (Au,Ni)Sn_4 can also most probably exist in local equilibrium with the Sn-saturated Pb[Sn] solid solution, thus explaining why the Pb-rich layer can be located beside the (Au,Ni)Sn_4 layer. The preferential location of the α-phase in contact with the (Au,Ni)Sn_4 has sometimes been explained with the help of interfacial energies [82], as it is known that Pb can form low-energy interfaces [163]. Nevertheless, as no reliable experimental values for the surface energies of solids exist, the explanation is highly qualitative. The more probable reason is that tin has been consumed during the reactions with Au and Ni, and a Pb-rich layer has been left behind. It should be noticed that the layer cannot be pure lead but instead is saturated with Sn, as only an Sn-saturated Pb[Sn] solid solution can exist in local equilibrium with $AuSn_4$ (and also probably with the (Au,Ni)Sn_4). As lead and gold form

intermetallics with each other, an appropriate question is why they are not formed. From the Au-Pb-Sn isothermal section at 150°C it can be seen that AuPb intermetallics can exist in local equilibrium only with almost pure lead, not a lead-rich solid solution. But if the Pb-rich layer becomes almost pure lead (as more and more tin is consumed) during the evolution of the microstructure, AuPb intermetallic compounds can start to form. Before this can take place, one should see the formation of two other AuSn intermetallic compounds, namely $AuSn_2$ and AuSn, between the $(Au,Ni)Sn_4$ and the Sn-saturated Pb[Sn] solid solution as the tin content of the Pb-rich region decreases.

When considering the interface between Ni_3Sn_4 and $(Au,Ni)Sn_4$ (Figs. 6.51 and 6.53), the situation is quite similar to that above. On the basis of the ternary Au-Ni-Sn phase diagram determined experimentally at room temperature [164], it is obvious that both phases involved in the reaction discussed above (Ni_3Sn_4 and $AuSn_4$) can exist in local equilibrium and, further, that they exhibit extended solid solubilities (Fig. 6.56).

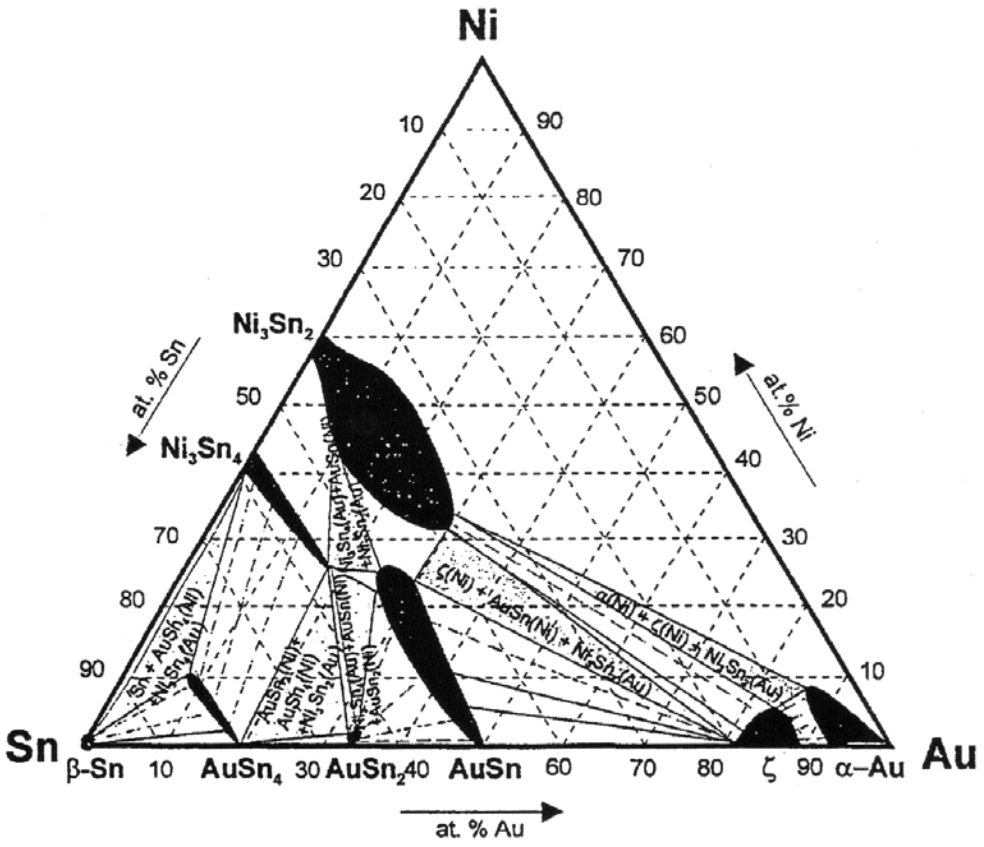

Fig. 6.56: *Isothermal section of the Au-Ni-Sn system at room temperature [164].*

According to the literature, approximately 40% of Ni atoms in the Ni sublattice of the Ni_3Sn_4 phase can be substituted by Au at room temperature [164], thus giving an overall solubility of 17 at-% of Au in Ni_3Sn_4. In the $AuSn_4$ phase, approximately 50% of the Au atoms in the Au sublattice can be substituted by Ni atoms [164], corresponding to the overall solubility of 10 at-% of Ni in $AuSn_4$. This is also the solubility detected in this study. Consequently, it seems that the maximum solubility of Ni in $AuSn_4$ has been achieved after 250 hours of annealing in the (SnPbAg)/Ni/Au and the (SnAg)/Ni/Au reaction couples. In their investigation of the crystal structure of $(Au_{1-x}Ni_x)Sn_4$, Zavalij et al. [165] discovered that in that compound Ni atoms substitute for Au atoms in the $AuSn_4$ structure, resulting in a compound with a general composition of $(Au_{1-x}Ni_x)Sn_4$ (and $x \leq 0.5$). The structure of the compound is isotypical with the $AuSn_4$ phase (i.e. orthorhombic). They also observed distinct changes in the unit cell dimension of the initial substitution of Au atoms by Ni atoms. After an initial substitution of 9 at-% of Ni, they observed that the length of the *a*-axis increased substantially [165]. After that, as the Ni content increased, a linear decrease in all cell dimensions was observed. This may partly explain the cracks that are visible in the $(Au,Ni)Sn_4$ layer.

On the basis of what has been stated above, it is not surprising that the $(Au,Ni)Sn_4$ redeposits on top of the Ni_3Sn_4. This is for the following reasons. First, the $(Au,Ni)Sn_4$ can exist in local equilibrium with the Ni_3Sn_4. From Figure 6.56 it can be seen that the condition for the local equilibrium at the [Ni_3Sn_4/$(Au,Ni)Sn_4$ and $(Au,Ni)Sn_4$/Sn (Fig. 6.53)] interfaces is fulfilled simultaneously only if the $(Au,Ni)Sn_4$ contains the maximum amount of Ni in the Au sublattice. Under the same equilibrium conditions, the Au content of the Ni_3Sn_4 is restricted to almost zero. Second, on the basis of the thermodynamic calculations, we know that the dissolved Ni stabilises the $(Au,Ni)Sn_4$ effectively. The calculations point out that with 10 at-% of Ni dissolved in the $(Au,Ni)Sn_4$ compound, its Gibbs free energy reaches its minimum value (-10.5 kJ/mol) at 150°C, which is about 40% lower than that of the pure $AuSn_4$ [5]. This provides the driving force for the reaction, since the redeposition process could reduce the total Gibbs free energy of the system. As the Ni_3Sn_4 has already formed during the melting of the solders, the formation of the layered structure most probably occurs as follows: during the solid-state annealing

Au diffuses through the tin-rich matrix/tin- and Sn-saturated Pb[Sn] solid solutions (depending on the solder) towards the Ni_3Sn_4, because of the stabilising effect of Ni. Au reacts with the Ni_3Sn_4 at the Ni_3Sn4/solder interface to release Ni, which is subsequently incorporated into the growing $(Au,Ni)Sn_4$. Since the $(Au,Ni)Sn_4$ must exist in equilibrium simultaneously with both Ni_3Sn_4 and Sn (Fig. 6.56), it will dissolve the maximum amount of Ni in the Au sublattice. Further, by dissolving the maximum amount of Ni, $(Au,Ni)Sn_4$ can attain its minimum Gibbs free energy, as shown by the thermodynamic calculations.

As has been described, solders containing Cu do not exhibit the redeposition of $(Au,Ni)Sn_4$ at the interface. In fact, some of the available Au is incorporated into the $(Cu,Au,Ni)_6Sn_5$ compound. Further, no Ni_3Sn_4 is formed, for the reasons discussed above. It is not immediately clear why the redeposition of $AuSn_4$ does not occur when Cu is present in the solder, since from the experimentally determined partial isothermal section of the Au-Cu-Sn systems at 170°C (Fig. 6.57) by Roeder [166], it can be seen that Cu_6Sn_5 and $AuSn_4$ can exist in local equilibrium. However, what is different when compared to the local equilibrium established between Ni_3Sn_4 and $AuSn_4$ is that $AuSn_4$ does not dissolve Cu as it does Ni. Even though we cannot calculate – because of the lack of thermodynamic data - the stabilising effect of Cu, the low solubility of Cu in the $AuSn_4$ indicates that Cu does not stabilise $AuSn_4$ as much as Ni does. Furthermore, the phase diagram points out that Cu_6Sn_5 can dissolve large amounts of Au and that the local equilibrium between the $AuSn_4$ and the $(Cu,Au)_6Sn_5$ (as well as with Sn) is possible only if the amount of Au in $(Cu,Au)_6Sn_5$ is close to 20 at-% (Fig. 6.57). Thus, with the thinness of the Au layer used in practice, the redeposition of $AuSn_4$ should not occur, since it is highly unlikely that such high Au concentrations inside $(Cu,Au)_6Sn_5$ could be realised. Nevertheless, in these investigations, there should be enough Au available and the equilibrium described above should be attainable. The appropriate question is, then, why $AuSn_4$ does not redeposit on top of the $(Cu,Ni,Au)_6Sn_5$. We propose that this is for the following reasons. The limited solubility of Cu in $AuSn_4$ indicates that Cu does not markedly increase the stability of $AuSn_4$. Further, the stabilising effect of Ni on the $(Cu,Ni)_6Sn_5$ ensures that the Ni is strongly bonded in the Cu-Sn-IMC and is not available for the $AuSn_4$.

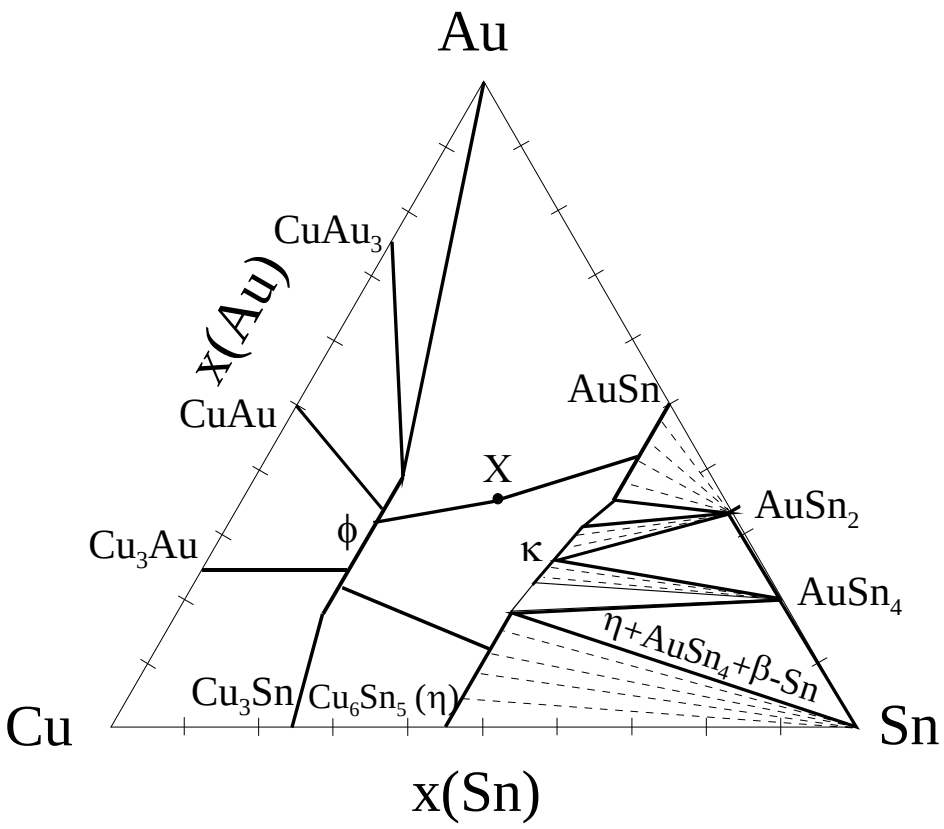

Fig. 6.57: *Experimentally determined partial isothermal section through the Au-Sn-Cu system at 170°C. Redrawn from [166]. $(Cu,Au)_6Sn_5$ + $AuSn_4$ + β - Sn three-phase equilibrium has been marked on the isotherm.*

The dissolution of Ni (and also probably that of Au) makes the $(Cu,Ni,Au)_6Sn_5$ stable enough that the $AuSn_4$ cannot decompose it and form $(Au,Ni)Sn_4$. Hence, since there is not enough Ni available at the IMC/solder interface the $AuSn_4$ remains dispersed inside the bulk solder. The maximum amount of Au that we could find from the $(Cu,Au,Ni)_6Sn_5$ in any of the samples was about 12 at-%. The isothermal section in Fig. 6.57 was determined at 170°C, whereas our annealing was carried out at 150°C. Therefore, the maximum solubility at the annealing temperature should be somewhat less than that in Fig. 6.57. Further, since there is also Ni in the $(Cu,Au,Ni)_6Sn_5$, we are actually dealing with quaternary solubility. Thus, the maximum solubility under these conditions may well be closer to the measured 12 at-%. The behaviour of Cu_6Sn_5 is very interesting, since it seems to be able to accommodate various species into its structure. This is

expected to be related to the fact that Cu_6Sn_5 has a NiAs-based structure that is known to be flexible with respect to its solubility and, therefore, to be able to incorporate both small and large atoms [54].

7. SUMMARY OF THE THESIS

In this thesis the interfacial reactions between Sn-based solders and the most commonly used metallisations in electronics have been studied by employing thermodynamic-kinetic approach together with detailed microstructural observations from solid-liquid and solid-solid reaction couples.

The fundamentals of the thermodynamic-kinetic method are presented in a very concise form in Chapter 2. The emphasis was placed on the thermodynamics, as it provides the driving forces for the formation and evolution of microstructures in solder interconnections during the life cycle of an electronic device. Contrary to thermodynamic data, the availability of kinetic data in the literature, even on the most important binary systems, is very limited. Therefore the kinetic analyses often remain qualitative in nature. However, the kinetic considerations can still provide useful information about the time scales of the reactions. Information on the formation and the evolution of solder interconnection microstructures in the most important metal systems has been reviewed in Chapters 3 and 4.

By utilising the experimental information obtained from solid-liquid reaction couples between liquid Sn/Sn-rich solders and the most common base metals, the formation mechanisms of the interfacial intermetallic compounds were presented. It was shown that Ni alloyed either to solder or Cu metallisation has a strong effect on the interfacial reactions between Sn and Cu. Cu(Ni) alloys with about 10 at-% Ni exhibited the fastest reaction rate with liquid tin and the rate was many times higher than those obtained with pure copper or with pure nickel. In addition, the reaction zone was composed of two different morphologies: i) a continuous uniform layer of the intermetallic compound (uniphase), and ii) the two-phase layer containing $[Cu,Ni]_6Sn_5$ tubes and fibres in the tin matrix. When the effect of Ni on the solid-state interfacial reactions between Sn and Cu(Ni) alloys was investigated, the most important results were as follows: (i) the addition of 0.1 at-% of Ni to Cu reduced the total thickness of the intermetallic compound layers (by reducing especially the thickness of Cu_3Sn) to about half of that in the pure

Cu/Sn diffusion couple used as a reference; (ii) the addition of 1 to 2.5 at-% of Ni to Cu continued the previous trend, produced a significant amount of pores at the Cu/Cu_3Sn interface, and increased the thickness of Cu_6Sn_5 in comparison with that in the pure Cu/Sn couple, and (iii) the addition of up to 5 at-% Ni increased the total thickness of the IMC layers to about twice that in the Cu/Sn diffusion couple and caused Cu_3Sn to disappear and, finally, the addition of 10 at-% of Ni to Cu caused pores to disappear and diminished the total IMC thickness again to close to that of the Cu/Sn diffusion couple.

Further, it was shown that the additional elements, such as P, Au, Fe, Zn, and Ti, when present in the solder interconnections, changed the interfacial microstructure significantly. These elements can: i) increase or reduce the reaction/growth rates; ii) change the physical properties of the phases formed, and iii) form additional reaction products or displace the binary equilibrium phases by forming new reaction products.

In this thesis it was demonstrated that the thermodynamic calculations supported by kinetic considerations together with detailed microstructural observations can provide a very useful method for studying chemical reactions at solder-metallisation interfaces, as well as their influence on the reliability of high-density lead-free solder interconnections.

REFERENCES

1. J. K. Kivilahti, JOM 54 (12) (2002) 52.
2. J. Kivilahti, IEEE Trans. Compon. Packaging Manuf. Technol. 18 (1995) 326.
3. K. Rönkä, F. van Loo, and J. Kivilahti, Scripta Mater. 37 (10) (1997) 1575.
4. L. S. Darken and R. W. Gurry, Physical Chemistry of Metals, McGraw-Hill, 1953.
5. "IPMA, The Thermodynamic Databank for Interconnection and Packaging Materials", Helsinki University of Technology, Helsinki (2000).
6. N. A. Gokcen, Thermodynamics, Techscience incorporated, 1975.
7. J. Philibert, Atom movements Diffusion and mass transport in solids, Les Editions de Physique, 1991.
8. T. Massalski, Binary Alloy Phase Diagrams, ASM, 1996.
9. P. Shewmon, Diffusion in Solids, 2nd edition, TMS, 1989.
10. C. Wagner, Acta Metall. 17 (1969) 99.
11. J. K. Kivilahti and K. Kulojärvi, in: Proceedings of Design and Reliability of Solders and Solder Interconnections, TMS, 1997.
12. R. Gagliano, G. Ghosh, and M. Fine, J. Electr. Mater., 31 (11) (2002) 1195.
13. T. Mattila, V. Vuorinen, and J.K. Kivilahti, J. of Mater. Res. 19 (11) (2004), 3214.
14. T. Chiu, K. Zeng, R. Stierman, D. Edwards, and K. Ano, in: Proceedings of Electronics Components and Technology Conference, IEEE, 2004.
15. C. Kao, Mater. Sci. Eng. A238 (1997) 196.
16. A. Hayashi, C. Kao, and Y. Chang, Scr. Mater., 37 (4) (1997) 393.
17. J. Bernal, Nature, 122 (3063) (1928) 54.
18. A. Gangulee, C. Das, and M. Bever, Metall. Trans., 4 (1973) 2063.
19. A-K. Larsson, L. Stenberg, and S. Lidin, Acta Crystal., B50 (1994) 636.
20. N. Saunders and A. P. Miodownik, Bull. Alloy Phase Diag. 11 (3) (1990) 278.
21. T. Laurila, V. Vuorinen, and J. K. Kivilahti, Mater. Sci. Eng. R49 (1-2) (2005) 1.
22. K. N. Tu, Acta Metall., 21 (1973) 347.
23. K. N. Tu, Mater. Chem. Phys., 46 (1996) 217.

24. K. N. Tu and R. Thompson, Acta Metall., 30 (1982) 947.

25. H. Bhedwar, K. Ray, S. Kulkarni, and V. Balasubramanian, Scr. Metall., 6 (1972) 919.

26. L. Revay, Surf. Tech., 5 (1977) 57.

27. M. Onishi and H. Fujibuchi, Trans. Jap. Inst. Metals, 16 (1975) 539.

28. Z. Mei, A. Sunwoo, and J. Morris, Metall. Trans., 23A (1992) 857.

29. M. Oh, Doctoral Dissertation, Leigh University, 1994.

30. K. Zeng, R. Stierman, T-C. Chiu, D. Edwards, K. Ano, and K. N. Tu, J. Appl. Phys., 97 (024508) (2005).

31. P. Nash and A. Nash, Bull. Alloy Phase Diag., 6 (1985) 350.

32. S. Bader, W. Gust, and H. Hieber, Acta Metall. Mater., 43 (1) (1995) 329.

33. G. Ghosh, Metall. Mater. Trans., 30A (1999) 1481.

34. J. Miettinen, Calphad, 27 (2003) 309.

35. H. S. Liu, J. Wang, and Z. P. Jin, Calphad, 28 (2004) 363.

36. H. Yu, V. Vuorinen, and J. K. Kivilahti, in: The Proceedings of Electronic Component and Technology Conference, IEEE, 2006.

37. H. Yu, V. Vuorinen, and J. K. Kivilahti, accepted J. Electr. Mater.

38. D. Gur and M. Bamberger, Acta Mater., 46 (14) (1998) 4917.

39. J. Haimovich, Weld. J., 68 (3) (1989) 102.

40. F. Foster, ASTM Spec. Publ., 319 (1963) 13.

41. W. Harding and H. Pressly, in: Proceedings of the 50th Annual American Electroplating Society, 1963.

42. W. Mulholland and D. Willyard, Weld. J. Res. Suppl., 54 (10) (1974) 466.

43. A. Romig, Y. Chang, J. Stephens, D. Frear, V. Marcotte, and C. Lea, in: D. Frear, W. Jones, and K. Kinsman (Eds.), EMPMD Monograph series, Vol. 1: Solder Mechanics – A State of the Art Assessment, TMS, 1994.

44. P. Kim and K. N. Tu, J. Appl. Phys., 80 (7) (1996) 3822.

45. R. J. Klein Wassink, Soldering in electronics, 2nd Ed. Electrochemical Publications Ltd., 1989.

46. P. Kim and K. N. Tu, Mater. Chem. Phys., 53 (2) (1998) 165.

47. P. Oberndorff, Doctoral Dissertation, Eindhoven University of Technology, 2001.

48. K. Zeng and J. K. Kivilahti, J. Electr. Mater., 30 (1) (2001) 35.

49. M. Robertson and M. Karnowsky, SC-TM-68-728, Sandia National Laboratories, Albuquerque, NM, December 1968.

50. S. Nakahara and R. McCoy, Appl. Phys. Lett., 37 (1) (1980) 42.

51. C. Chang, T. Callcott, and E. Arakawa, J. Appl. Phys., 53 (11) (1982) 7362.

52. L. Buene, Thin Solid Films, 47 (1977) 159.

53. L. Buene and S. Jacobson, Phys. Scr., 18 (1978) 397.

54. L. Buene, H. Falkenberg-Arell, J. Gjonnes, and J. Tafto, Thin Solid Films, 67 (1980) 95.

55. B. Hugsted, L. Buene, T. Finstand, O. Lonsjo, and T. Olsen, Thin Solid Films, 98 (1982) 81.

56. S. Nakahara, R. McCoy, L. Buene, and J. Vandenberg, Thin Solid Films, 84 (1981) 185.

57. W. Bader, Welding Journal, 48 (12) (1969) 551.

58. W. Bader, in: Proc. Conf. Physical Metall., Metal Joining, 1980.

59. C. Thwaites, Trans. Inst. Metal Finishing, 43 (1965) 143.

60. S. Ganesan and M. Pecht, Lead-free Electronics, John Wiley & Sons, 2006.

61. A. Brunson and M. Gerl, Phys. Rev., 21B (12) (1980) 5447.

62. B. Dyson, J. Appl. Phys., 37 (6) (1966) 482.

63. S. Sen, A. Ghorai, and K. Bandyopadhyay, Thin Solid Films, 155 (1987) 243.

64. Z. Marinkovic and V. Simic, Thin Solid Films, 195 (1991) 127.

65. G. Ghosh, J. Electr. Mater., 33 (10) (2004) 1080.

66. R. R. Tummala, Fundamentals of Microsystems Packaging, McGraw-Hill, 2001.

67. J. Lau, Solder Joint Reliability: Theory and applications, Van Nostrand Reinhold, 1991.

68. T. Laurila, T. Mattila, V. Vuorinen, J. Karppinen, J. Li, M. Sippola, and J. K. Kivilahti, Microelectr. Reliab. (in print).

69. K. J. Puttlitz and K.A. Stalter, Handbook of Lead-Free Solder Technology for Microelectronic Assemblies, Marcel Dekker, 2004.

70. C-H. Lin, S-W. Chen, and C-H. Wang, J. Electr. Mater., 31 (9) (2002) 907.

71. S-W. Chen and C-A. Chang, J. Electr. Mater., 33 (10) (2004) 1071.

72. W. T. Chen, C. E. Ho, and C. R. Kao, J. of Mater. Res., 17 (2) (2002) 263.

73. C. E. Ho, R. Y. Tsai, Y. L. Lin, and C. R. Kao, J. Electr. Mater., 31 (6) (2002) 584.

74. P-L. Wu, M-K. Huang, C. Lee, and S-R. Tzan, J. Electr. Mater., 33 (3) (2004) 157.

75. J. Y. Tsai, Y. C. Hu, C. M. Tsai, and C. R. Kao, J. Electr. Mater., 32 (11) (2003) 1203.

76. C. E. Ho, Y. L. Lin, S. C. Yang, C. R. Kao, and D. S. Jiang, J. Electr. Mater., 35 (5) (2006) 1017.

77. C. E. Ho, Y. L. Lin, S. C. Yang, and C. R. Kao, in: Proceedings of 10th International Symposium on Advanced Packaging Materials, IEEE, 2005.

78. W. C. Luo, C. E. Ho, J. Y. Tsai, Y. L. Lin, and C. R. Kao, Mater. Sci. Eng. A 396 (2005) 385.

79. S. C. Hsu, S. J. Wang, and C.Y. Liu, J. Electr. Mater., 32 (11) (2003) 1214.

80. S. J. Wang and C.Y. Liu, J. Electr. Mater., 32 (11) (2003) 1303.

81. K. Zeng, V. Vuorinen, and J. K. Kivilahti, IEEE Trans. Compon. Packaging Manuf. Technol., 25 (3) (2002) 162.

82. K. Zeng and K. N. Tu, Mater. Sci. Eng. R 38 (2002) 55.

83. M. O. Alam, Y. C. Chan, and K. N. Tu, Chem. Mater., 15 (2003) 4340.

84. M. Amagai in: The Proceedings of Electronic Component and Technology Conference, IEEE, 2006.

85. H. Nishikawa, J. Y. Piao, and T. Takemoto, J. Electr. Mater., 33 (5) (2006) 1127.

86. F. Gao, T. Takemoto, and H. Nishikawa, Mater. Sci. Eng. A 420 (1-2) (2006) 39.

87. M. Tanaka, T. Sasaki, T. Kobayashi, and K. Tatsumi in: The Proceedings of Electronic Component and Technology Conference, IEEE, 2006.

88. I. de Sousa, D. W. Henderson, L. Patry, S. Kang, and D-Y. Shih in: The Proceedings of Electronic Component and Technology Conference, IEEE, 2006.

89. E. K. Ohriner, Welding Research Supplement, (1987) 191.

90. A. Paul, Doctoral Dissertation, Technical University of Eindhoven, 2004.

91. M. J. H. van Dal, A. M. Gusak, C. Cserhati, A. A. Kodentsov, and F. J. J. van Loo, Phys. Rev. Lett., 86 (2001) 3352.

92. M. J. H. van Dal, A. M. Gusak, C. Cserhati, A. A. Kodentsov, and F. J. J. van Loo, Phil. Mag. A, 82 (2002) 943.

93. F. D. B. Houghton, Circuit World, 26 (2) (2000) 10.

94. V. F. Hribar, J. L. Bauer, and T. P. O'Donnell, in: Proceedings of 3rd Inter. SAMPE Electronics Conference, 1989.

95. K. Puttlitz, IEEE Trans. CHMT, 13 (4) (1990) 647.

96. E. Bradley and K. Banerji, in Proceedings of 45th Electronic Components and Technology Conference, IEEE, 1995.

97. Z. Mei, P. Callery, D. Fisher, F. Hua, and J. Glazer, in: Proceedings of Pacific Rim/ASME Inter. Intersociety Electronic and Photonic Packaging Conference, Advances in Electronic Packaging, ASME, 1997.

98. R. Ghaffarian, in: Proceedings Surface Mount International Conference and Exposition '98, SMTA, 1998.

99. R. W. Johnson, V. Wang, and M. Palmer, in Proceedings of Surface Mount International Conference and Exposition '98, SMTA, 1998.

100. Z. Mei, M. Kaufmann, A. Eslambolchi, and P. Johnson, in: Proceedings of 48th Electronic Components and Technology Conference, IEEE, 1998.

101. Z. Mei, P. Johnson, M. Kaufmann, and A. Eslambolchi, in: Proceedings of 49th Electronic Components and Technology Conference, IEEE, 1999.

102. J-W. Yoon, S-W. Kim, and S-B. Jung, J. Alloys Comp., 385 (2004) 192.

103. S. J. Hang, H. J. Kao, and C. Y. Liu, J. Electr. Mater., 33 (10) (2004) 1130.

104. S-W. Kim, J-W. Yoon, and S-B. Jung, J. Electr. Mater, 33 (10) (2004) 1182.

105. M. He, Z. Chen, and G. Qi, Acta Mater. 52 (2004) 2047.

106. M. He, Z. Chen, G. Qi, C. C. Wong, and S. G. Mhaisalkar, Thin Solid Films, 462-463 (2004) 363.

107. M. He, A. Kumar, P. T. Yeo, G. J. Qi, and Z. Chen, Thin Solid Films, 462-463 (2004) 387.

108. M. O. Alam, Y. C. Chan, and K. N. Tu, J. Appl. Phys., 94 (6) (2003) 4108.

109. B-L. Young, J-G. Duh, and G-Y. Jang, J. Electr. Mater, 32 (12) (2003) 1463.

110. M. O. Alam, Y. C. Chan, and K. C. Hung, Microel. Reliab., 42 (2002) 1065.

111. Y-D. Jeon, K-W. Paik, K-S. Bok, W-S. Choi, and C-L. Cho, J. Electr. Mater, 31 (5) (2002) 520.

112. P. L. Liu and J. K. Shang, Metall. Mater. Trans. 31A (2000) 2867.

113. J. W. Jang, P. G. Kim, K. N. Tu, D. R. Frear, and P. Thompson, J. Appl. Phys., 85 (12) (1999) 8456.

114. T. Laurila, V. Vuorinen, T. Mattila, and J.K. Kivilahti J. Electr. Mater, 34 (1) (2005) 103.

115. R. Erich, R. J. Coyle, G. M. Wenger, and A. Primavera, in: Proceedings of 24th IEEE/CPMT International Electronics Manufacturing Technology Symposium, IEEE, 1999.

116. S. C. Hung, P. J. Zheng, S. C. Lee, and J. J. Lee, in: Proceedings of 24th IEEE/CPMT International Electronics Manufacturing Technology Symposium, IEEE, 1999.

117. A. Zribi, R. R. Chromik, R. Presthus, J. Clum, K. Teed, L. Zavalij, J. DeVita, J. Tova, and E. J. Cotts, in: Proceedings of 49th Electronic Components and Technology Conference, IEEE, 1999.

118. A. Minor and J. Morris, Metall. Mater. Trans., 31A (2000) 798.

119. C. Ho, L. Shiau, and C. Kao, J. Electr. Mater., 31 (11) (2002) 1264.

120. L. Shiau, C. Ho, and C. Kao, Sold. Surf. Mount. Technol., 14 (3) (2002) 25.

121. ASM Handbook - Metallography and Microstructures, ASM,2004.

122. P. B. Hirch, A. Howie, R. B. Nicholson, D. W. Pashley, and M. J. Whelan, Electron Microscopy of Thin Crystals, Butterworth, 1965.

123. Thermo-Calc software L, Royal Institute of Technology, Sweden

124. T-M. Korhonen, Doctoral Dissertation, Helsinki University of Technology, 2001.

125. K. J. Rönkä, Doctoral Dissertation, Helsinki University of Technology, 2001.

126. Z. Huang, P. P. Conway, C. Liu, and R. C. Thomson, J. Mater. Res., 20 (3) (2005) 649.

127. P-Y. Yeh, J-M. Song, and K-L. Lin, J. Electr. Mater., 35 (5) (2006) 978.

128. M. N. Islam, Y. C. Chan, A. Sharif, and M. O. Alam, Microelectronics Reliability 43 (2003) 2031.

129. P. G. Harris and K. S. Chaggar, Sold. Surf. Mount. Technol., 10 (3) (1998) 38.

130. W. J. Boettinger, C. A. Handwerker, and U. R. Kattner, "Reactive Wetting and Intermetallic Formation", in: F. G. Yost et al. (Eds), The Mechanics of Solder Alloy Wetting and Spreading, Van Nostrand Reinhold, 1993.

131. V. Vuorinen, T. Laurila, H. Yu, and J. K. Kivilahti, J. Appl. Phys., 99 (023530) (2006).

132. S. Terashima and M. Tanaka, Mater. Trans. 45 (3) (2004) 681.

133. S. Terashima, K. Takahama, M. Nozaki, and M. Tanaka, Mater. Trans. 45 (4) (2004) 1383.

134. The SGTE databank for solutions and substances, Department of Materials Science and Engineering, The Royal Institute of Technology, Sweden, released 1992.

135. J-H. Shim, C-S. Oh, B-J. Lee, and D-N. Lee , Z. Metallkd, 87 (1996) 205.

136. H. S. Liu, J. Wang, and Z. P. Jin, CALPHAD, 28 (2004) 363.

137. S-W. Chen, S-H. Wu, and S-W. Lee, J. Electr. Mater, 32, (11) (2003) 1188.

138. G. Ghosh, Acta Mater, 49 (2002) 2609.

139. G. Ghosh, J. Electr. Mater, 33 (3) (2004) 229.

140. T. M. Korhonen, S. J. Hong, P. Su, and M. A. Korhonen, in: Proceedings of the 2000 SMTA International Conference, 2000.

141. J. S. Lee Pak and K. Mukherjee, Mater. Sci. Eng. A 117 (1989) 167.

142. CRC Handbook of Chemistry and Physics, 72nd Edition, CRC Press, 1991.

143. A. Brunson and M. Gerl, Phys. Rev., 21 (12) (1980) 5447.

144. F. J. J. van Loo, Prog. Solid St. Chem. 20 (1990) 47.

145. G. Ghosh, J. Electr. Mater, 33 (3) (2004) 229.

146. C. W. Hwang, K. Suganuma, M. Kiso, and S. Hashimoto, J. Mater. Res., 18 (11) (2003) 2540.

147. H. Matsuki, H. Ibuka, and H. Saka, Sci. Tech. Adv. Mater., 3 (2002) 261.

148. Y-D. Jeon, K-W. Paik, K-S. Bok, W-S. Choi, and C-L. Cho, in: Proceedings of Electronic Components and Technology Conference, IEEE, 2001.

149. W. J. Johnson, Prog. Mater. Sci., 30 (1986) 81.

150. M-A. Nicolet, in: H. Jain and D. Gupta (Eds.), Diffusion in Amorphous Materials, TMS, 1994.

151. M. Alajoki, L. Nguyen, and J. Kivilahti, in: Proceedings of Electronic Components and Technology Conference, IEEE, 2005.

152. T. T. Mattila and J. K. Kivilahti, J. Electr. Mater, 35 (2) (2006) 250.

153. G. Ghosh, Acta mater. 49 (2001) 2609.

154. K. P. Gupta, J. Phase Equil., 21 (5) (2000) 479.

155. L. Garner, S. Sane, D. Suh, T. Byrne, A. Dani, T. Martin, M. Mello, M. Patel, and R. Williams, Intel Technology Journal, 09 (04) (2005) 297.

156. C. E. Birchenall, Atom Movements, ASM, 1951.

157. E. Wachtel and E. Bayer, Z. Metallkd., 75 (1984) 61.

158. F. M. d'Heurle and P. Gas, J. Mater. Res., 1 (1986) 205.

159. I. Belova and G. E. Murch, Phil. Mag., A80 (9) (2000) 2073.

160. I. Belova and G. E. Murch, Phil. Mag., A82 (2) (2002) 269

161. F. J. J. van Loo, B. Pieraggi, and R. Rapp, Acta Metall. Mater., 38 (9) (1990) 1769.

162. J. Glazer, J. of Electr. Mater., 23 (8) (1994) 693.

163. A. Guy, Elements of Physical Metallurgy, Addison Wesley, 1960.

164. S. Anhock, H. Oppermann, C. Kallmayer, R. Aschenbrenner, L. Thoman, and H. Reichel, in: Proceedings of 22nd IEEE/CPMT International Electronics Manufacturing Technology Symposium, IEEE, 1998.

165. L. Zavalij, A. Zribi, R. Chromik, S. Pitely, P. Zavalij, and E. Cotts, J. Alloys Compounds., 334 (2002) 79.

166. J. Roeder, Doctoral Dissertation, Lehigh University, 1988.